



“Con fundamento en los artículos 21 y 27 de la Ley Federal del Derecho de Autor y como titular de los derechos moral y patrimonial de la obra titulada **“Gravimetría Cuántica en el mismo estado interno usando pulsos de luz Raman compuestos”**, Tesis para obtener el grado de **Maestro en Ciencias (Física)**, otorgo de manera gratuita y permanente a la Facultad de Ciencias de la Universidad Autónoma de San Luis Potosí, la autorización para que difunda la obra en cualquier medio, incluido el electrónico, y la divulgue entre sus usuarios, profesores, estudiantes o terceras personas, sin que pueda percibir por tal divulgación una contraprestación”

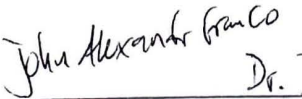
Fecha presentación: 24 de Febrero de 2020

Fecha autorización: 28 de Febrero de 2020

Nombre y Firma de AUTORES

  
Diego Alejandro Lancheros Naranjo  
Estudiante

  
Dr. Eduardo Gómez  
Asesor

  
Dr. John Alexander Franco  
Co-asesor (si aplica)

Universidad Autónoma de San Luis Potosí  
Facultad de Ciencias  
Instituto de Física Manuel Sandoval Vallarta  
Laboratorio de Átomos Fríos  
San Luis Potosí, México  
2020



**UASLP**

Universidad Autónoma  
de San Luis Potosí



# Gravimetría Cuántica en el mismo estado interno usando pulsos de luz Raman compuestos

Tesis para obtener el grado de Maestría en Ciencias (Física)  
Diego Alejandro Lancheros Naranjo

Asesor

Dr. Eduardo Gómez García

Asesor

Dr. John Alexander Franco Villafañe

QUANTUM GRAVIMETRY IN THE SAME INTERNAL STATE USING  
COMPOSITE LIGHT RAMAN PULSES.

**Diego Alejandro Lancheros Naranjo**

**Advisors:** Eduardo Gómez García, Dr. Sc.  
John Alexander Franco Villafañe, Dr. Sc.

INSTITUTO DE FÍSICA  
UNIVERSIDAD AUTÓNOMA DE SAN LUIS POTOSÍ  
February 24, 2020.

*El presente trabajo solamente puede ser dedicado a todas las personas que más que amigos, se convirtieron en mi familia a lo largo de mi estancia en México.*

*A Aarón y Cuauhtémoc.*

*A Inés y Gabriela.*

*A Paulina y René.*

*A David y Andrea.*

*A Mario.*

*A Jesús y Alejandra.*

*A Juan José y Juan Manuel.*

*Muchas gracias por estar ahí en mis horas más oscuras.  
E infinitas gracias más por estar ahí en mis horas más luminosas.*



# Contents

	1
List of Figures	5
Abstract.	9
Introduction.	11
Chapter 1. Hamiltonian for matter-radiation Interaction.	13
1. Semi-classical theory of matter-radiation interaction.	13
2. Momentum transfer in Atomic Transitions.	16
3. Raman Transitions.	18
Chapter 2. Raman Transitions driven by a modulated laser.	23
1. Doppler sensitive Raman transitions.	23
2. Experimental setup for a Composite-Light Interferometer.	25
3. Raman transitions with three lasers.	28
4. The Galilean Transformation.	33
5. Parameters in a composite-light Mach-Zehnder Interferometer.	34
Chapter 3. Time-dependent perturbation theory in detuned Raman transitions.	41
1. Composite light Interferometry.	42
2. The parameters $\eta_i$ .	45
3. Perturbative solution to the Schrödinger's Equation.	45
4. Temporal symmetry of the amplitude probability equations.	53
Chapter 4. Quantum Gravimetry in a Composite-light Interferometer.	55
1. Perturbative solution to first order of the Mach-Zehnder interferometer of seven steps.	55
2. Phases due to gravitational interaction.	61
3. Interferometric Fringes.	65
Conclusions.	71
Appendix A. The Galilean Transformation.	73
Appendix B. Numerical solutions of the Differential Equations.	79
Appendix C. Perturbative Solutions of the seven steps Interferometer.	83
1. Second Pulse.	85
2. Third Pulse.	88
3. Fourth Pulse.	91

4. Fifth Pulse.	93
5. Sixth Pulse.	96
Appendix D. The Second order coefficients.	101
1. The $a_2^\beta$ coefficient.	101
2. The $b_2^\beta$ coefficient.	104
Bibliography	107

## List of Figures

1.1 Scheme of a two level system.	17
1.2 Transition scheme for a stimulated Raman transition.	19
2.1 An optical Mach-Zehnder interferometer works by splitting the light beam through a Beam-Splitter (BS1), and letting that the phases of the light changes as they travels by their optical path, then, through a second Beam-Splitter, they are recombined to make them interfere.	23
2.2 Retro-reflected configuration for a stimulated Raman transition. Figure adapted from [1].	24
2.3 Levels scheme of an Alkali atom that are involved in the Raman transition of the experiment illustrated at Fig. (2.2). Figure adapted from [1].	25
2.4 Raman spectroscopy spectrum for an alkali atom as a function of the detuning $\delta$ . The data corresponds to a $\pi$ -pulse of 135 $\mu$ s of duration. When an atom is released to free-fall, the frequencies which this interacts suffer Doppler shift. By this mechanism, the Raman transitions become velocity-dependent. Figure adapted from [1].	26
2.5 Setup for two Raman pairs with opposite momentum transfer. AOM: acousto-optical modulator, FEOM: fiber electro-optical modulator, PBS: polarization beam splitter. The polarizations of the carrier and sidebands are also shown.	26
2.6 Scheme of the first couple of counterpropagating Raman beams.	27
2.7 Scheme of the second couple of counterpropagating Raman beams.	28
2.8 Scheme of transitions of two counter-propagating Raman beams.	28
2.9 Scheme showing the possible states of the atom and the couplings between them.	34
2.10 Bloch sphere representing Rabi Oscillations with a detuning $\delta$ .	34
2.11 Scheme to obtain the detuning due to adjacent transitions.	35
2.12 Scheme showing the possible states of the atom and the strongest couplings.	37
2.13 One of the initial conditions of our interferometer is that we have an initial momentum distribution in the state $ a, 0\rangle$ , which introduces a new detuning parameter.	38
2.14 Diagram to obtain the detuning due to the width of the initial momentum distribution.	38
3.1 The interaction of an atom with an electric field produce energy shifts of it internal states.	41
3.2 Scheme of Rb <sup>87</sup> states involved in the experimental setup	42
3.3 Scheme of the seven steps Mach-Zehnder Interferometer proposed insensible to external electromagnetic fluctuations. The colors red and green suggest the pair that is resonant in each pair. Red for $\Omega_+$ and green for $\Omega_-$ .	43



3.4 Initial configuration of the probability amplitude of the states at the beginning of the First Pulse.	43
3.5 Initial configuration of the probability amplitude of the states before we have the second pulse-step done.	44
3.6 Final configuration of the probability amplitudes of the states after we apply the second pulse-step.	44
3.7 The interaction of a modulated laser with an atom implies a multilevel coupling in momentum states. In Fig. (3.7a) is shown the coupling when we take into account one couple of side-bands of a modulated laser, where $\tilde{\Omega}_{\pm}^1 = \Omega\sqrt{1 + 4\mu^2}$ . The Fig. (3.7b) shows the case when we have multiple side-band frequencies from a modulated laser. The Fig. (3.7c) illustrates the difference between the reference [2] and the present work, because they consider the multiple sidebands pairs of just one Raman pair, neglecting the other one due to Doppler effect. We consider two Raman pairs with one pair of sidebands each one.	46
3.8 Configuration of states where $\Omega_+$ is the resonant pulse.	47
3.9 Situation when we have the pair $\Omega_+$ resonant and the Raman pair $\Omega_-$ drives a perturbative transition $ a, 0\rangle \leftrightarrow  b, -1\rangle$ . Here, we define $\tilde{\Omega}_{\pm}^n = \Omega\sqrt{1 + (2n)\mu}$	50
4.1 Initial configuration of the probability amplitude of the states at the beginning of the First Pulse. The dashed transitions denotes that is detuned by the Doppler effect.	55
4.2 Final configuration of the probability amplitude of the states at the end of the first pulse.	56
4.3 Population of state $ a, 2\rangle$ as a function of the initial velocity. The red-solid line represents the squared difference between the analytical and the numerical ( $N$ ) solution at the end of the first pulse ( $\tau_1$ ) multiplied by $10^4$ . The blue-dashed line corresponds to $\eta_1^2$ .	56
4.4 Initial configuration of the probability amplitude of the states before we apply the second pulse.	57
4.6 Error in amplitude of state $ b, 3\rangle$ as a function of the initial velocity for the second pulse. The red-solid line represents the difference between the analytical and numerical ( $N$ ) solutions at the time $t_2$ multiplied by $10^3$ . The blue-dashed line corresponds to the perturbative parameter $\eta_1^2$ .	58
4.5 Final configuration of the probability amplitudes of the states after we have the second pulse-step done.	58
4.7 Populations of the different states after the second pulse (at time $t_2 = \tau_1 + \tau_2$ ) as a function of $\mu$ with an initial velocity of $v_0 = 5$ m/s. The vertical lines indicate the special Rabi frequencies (Eq. (36)).	59
4.8 Interferometric fringes with an initial atomic cloud velocity of $v_0 = 10$ m/s as a function of $\gamma = g - g'$ . In light gray we used the first special value of the parameter $\mu$ while in dashed red line we have the case when $\mu = \sqrt{2}$ , illustrating the fact that we lose visibility when we do not use the special Rabi frequencies.	60
4.9 The state $ b, -1\rangle$ is not excited in a perturbative way in the second pulse.	60
4.10 Argument of the numerical solution and the analytical solution of the state $ b, 3\rangle$ at the time $t_{3A} + \tau_3/3$ as a function of the dark time $T$ . The range of the horizontal axis goes from $100\tau_2$ to $100\tau_2 + \pi/(\mu\Omega)$ .	63

4.11	Error in amplitude of state $ a, 0\rangle$ as a function of the initial velocity for the sixth pulse. The red-solid line represents the difference between the analytical and numerical ( $N$ ) solutions at the time $t_{6D}$ (Eq. (67)). The blue-dashed line corresponds to the perturbative parameter $\eta_1^2$ .	64
4.12	Error in amplitude of state $ b, 1\rangle$ as a function of the initial velocity for the sixth pulse. The red-solid line represents the difference between the analytical and numerical ( $N$ ) solutions at the time $t_{6D}$ (Eq. (67)). The blue-dashed line corresponds to the perturbative parameter $\eta_1^2$ .	65
4.13	Interferometric fringes obtained for the population at the state $ a\rangle$ as a function of the parameter $\gamma$ . The light gray line shows the case when we have an initial velocity of the atom cloud of $v_0 = 10$ m/s. The dashed red line shows the numerical case when we have an initial velocity of $v_0 = 0.03$ m/s while the black line is the analytical first order approximation to these fringes through the perturbative method introduced in the Chapter 3 and the present one.	68
4.14	Parameter $a_2^\beta$ (Appendix D) as function of $\gamma = g - g'$ .	69
4.15	Parameter $b_2^\beta$ (Appendix D) as function of $\gamma = g - g'$ .	69
4.16	Interference fringes as a function of $\gamma = g - g'$ with a variation of the standard deviation $\sigma_p$ of the momentum initial distribution of the state $ a, 0\rangle$ , showing that the increase of this deviation reduces the visibility of the fringes.	70
C.1	Initial configuration of the probability amplitude of the states before the second pulse is applied.	85
C.2	Final configuration of the probability amplitudes of the states after the second pulse.	85
C.3	Initial configuration of the probability amplitude of the states before the third pulse.	88
C.4	Final configuration of the probability amplitude of the states after the third pulse.	88
C.5	Initial configuration of the probability amplitude of the states before the fourth pulse.	91
C.6	Final configuration of the probability amplitude of the states after the fourth pulse.	91
C.7	Initial configuration of the probability amplitude of the states before the fifth pulse.	93
C.8	Final configuration of the probability amplitude of the states after the fifth pulse.	94
C.9	Initial configuration of the probability amplitude of the states before the sixth pulse.	96
C.10	Final configuration of the probability amplitude of the states after the sixth pulse.	97



## **Abstract.**

In the present thesis we introduce an atomic gravimetric sequence using Raman-type composite light pulses that excites a superposition of two momentum states with the same internal level. The scheme allows the suppression of common noise, making it less sensitive to external fluctuations of electromagnetic fields.

The Raman beams are generated with a fiber modulator and are capable of momentum transfer in opposite directions. We introduce an analytical method to account for perturbative transitions to spurious states and We obtain analytical expressions for the interference fringes in terms of three perturbative parameters that characterize the imperfections due to undesired frequencies introduced by the modulation process. We find special values of the Rabi frequency that improve the fringes visibility.



## Introduction.

The interference of matter-wave packets has had a huge impact in the development of applications of atom interferometry in a variety of fields involving metrology. In [3], [4] is presented an atom interferometry experiment to the measurement of the local gravitational constant  $g$  with a relative sensitivity of  $\Delta g/g = 2 \times 10^{-8}$ , that is to say, the measurement of this constant at eight significant figures. The realization of velocity-dependent Raman transitions in opposite momentum directions allowed the isolating of the Sagnac effect in a free-fall atomic sample, to the measurement of rotation rates at better uncertainties of  $6 \times 10^{-10}$  rad s<sup>-1</sup> [5], [6]. This research fields opens the potential applications in inertial navigation, oil exploration and prediction of earthquakes [7], geophysical studies and tests for general relativity [8].

The current research and applications of this quantum technology is leaning to make the apparatus portable, and making the intrinsic suppression of technical noise [9]. With these aims, it is possible to use a light modulator to introduce side-bands that work as the additional frequencies [10], with the subsequent noise reduction compared with the use of two independent lasers referenced by each other with a phase lock loop.

Another consequence of this scheme is the freedom to excite momentum states with different momentum directions. This could be used to maximize the scale factor in Mach-Zehnder interferometry, and the demonstration of immunity to non-inertial perturbations and external magnetic fluctuations [9]. Nevertheless, this also has as consequence the insertion of systematic errors due by a Raman laser generated by phase modulation which introduce an overall phase and a visibility loss in the interferometric fringes [2]. Additionally, overall systematic overall phase shifts can be introduced by the use of two pairs of counter-propagating Raman pulses due to Doppler detuning [1], modelled as light shifts in the states involved.

In the present thesis we propose a new interferometric scheme for a Mach-Zehnder interferometer different from that one proposed at [9] in the symmetry of the states that acquire gravitational phase, studying in detail the phases involved by non-resonant transitions ([?, 24]t [9]), the temperature effects in the contrast of the interferometer fringes, and most of all, the deduction of possible systematic phase shifts effects resulting from perturbative transitions due to the Doppler detuning of one counter-propagating Raman pair using an analytic method, complementing the numerical work illustrated at [2].

Finally, we propose a set of important parameters to the experimental performance of the experiment proposed and contrast the numerical values with current values for atoms of Rb<sup>87</sup> [11].



## CHAPTER 1

### Hamiltonian for matter-radiation Interaction.

The present chapter is intended as the introduction of the idea of momentum transfer in Raman transitions as an efficient mechanism compared with direct transitions between electronic states. The first section introduces the minimal coupling as the theoretical approach for the construction of the Hamiltonian that takes into account the interaction between an electromagnetic field and an atom; in the second section this approach is used to demonstrate the coupling between internal atomic states and the momentum of the atom; in the third section, these ideas are applied to the study of the Raman transitions showing that it is possible to improve the momentum transfer using two photon transitions.

#### 1. Semi-classical theory of matter-radiation interaction.

**1.1. Norm gauge in the Schrödinger's equation.** The states in quantum mechanics possess a norm gauge, that is to mean, if we transform a state under the product of an arbitrary phase (with an argument  $\Theta(\mathbf{r})$ ), the probabilities do not change:

$$\begin{aligned} |\psi\rangle &\rightarrow |\tilde{\psi}\rangle = e^{i\Theta(\mathbf{r})} |\psi\rangle, \\ |\psi(\mathbf{r}, t)|^2 &= |\tilde{\psi}(\mathbf{r}, t)|^2. \end{aligned}$$

The expected value of the position operator is invariant:

$$\begin{aligned} \langle \tilde{\psi} | \hat{x} | \tilde{\psi} \rangle &= \langle \psi | e^{-i\Theta(\mathbf{r})} \hat{x} e^{i\Theta(\mathbf{r})} | \psi \rangle \\ &= \langle \psi | \hat{x} | \psi \rangle. \end{aligned}$$

Nevertheless, for the momentum operator this doesn't hold:

$$\begin{aligned} \langle \tilde{\psi} | \hat{p} | \tilde{\psi} \rangle &= \langle \psi | e^{-i\Theta(\hat{\mathbf{r}})} \hat{p} e^{i\Theta(\hat{\mathbf{r}})} | \psi \rangle, \\ &= \langle \psi | \left( \hat{p} e^{-i\Theta(\hat{\mathbf{r}})} - \left[ \hat{p}, e^{-i\Theta(\hat{\mathbf{r}})} \right] \right) e^{i\Theta(\hat{\mathbf{r}})} | \psi \rangle, \\ &= \langle \psi | \left( \hat{p} + i\hbar \nabla e^{-i\Theta(\hat{\mathbf{r}})} \right) e^{i\Theta(\hat{\mathbf{r}})} | \psi \rangle, \\ &= \langle \psi | (\hat{p} + \hbar \nabla \Theta(\hat{\mathbf{r}})) | \psi \rangle. \end{aligned}$$

If we define the transformed operator:

$$\hat{p}_\Theta = \hat{p} + \hbar \nabla \Theta(\hat{\mathbf{r}}),$$

then the transformed wavefunction satisfies the equation:



$$i\hbar \frac{\partial}{\partial t} \tilde{\psi}(\mathbf{r}, t) = -\frac{\hbar^2}{2m} [\nabla + i\nabla\Theta(\mathbf{r})]^2 \tilde{\psi}(\mathbf{r}, t) + V(\mathbf{r})\tilde{\psi}(\mathbf{r}, t).$$

$$i\hbar \frac{\partial}{\partial t} |\tilde{\psi}\rangle = \left[ \frac{\hat{p}_\Theta}{2m} + V(\hat{\mathbf{r}}) \right] |\tilde{\psi}\rangle.$$

**1.2. The minimal coupling.** We are going to consider the Lagrangian of a charged particle in an electromagnetic field.

By the definition of the scalar  $\phi$  and vector  $\mathbf{A}$  potentials in classical electrodynamics, we have that:

$$\mathbf{E} = -\nabla\phi - \frac{\partial\mathbf{A}}{\partial t} \quad \mathbf{B} = \nabla \times \mathbf{A}.$$

where  $\mathbf{E}$  is the electric field,  $\mathbf{B}$  is the magnetic field. Also, the Lorentz force has the form:

$$\mathbf{F} = q(\mathbf{E} + \mathbf{v} \times \mathbf{B}),$$

$$\mathbf{F} = q \left[ -\nabla\phi - \frac{\partial\mathbf{A}}{\partial t} + \mathbf{v} \times (\nabla \times \mathbf{A}) \right]$$

with  $\mathbf{v}(t)$  the velocity of the charged particle of charge  $q$  at time  $t$ . It can be demonstrated [12] that:

$$[\mathbf{v} \times (\nabla \times \mathbf{A})]_x = \frac{\partial}{\partial x} (\mathbf{v} \cdot \mathbf{A}) - \frac{dA_x}{dt} + \frac{\partial A_x}{\partial t},$$

from which the  $x$ -component of the force can be written as:

$$F_x = q \left[ -\frac{\partial}{\partial x} (\phi - \mathbf{A} \cdot \mathbf{v}) - \frac{d}{dt} \left( \frac{\partial}{\partial v_x} (\mathbf{A} \cdot \mathbf{v}) \right) \right].$$

This allows us to express the Lorentz force in a very specific form and to define a generalized potential  $U$  in the following form:

$$F_x = -\frac{\partial U}{\partial x} + \frac{d}{dt} \frac{\partial U}{\partial v_x}$$

$$U = q\phi - q\mathbf{A} \cdot \mathbf{v}.$$

And also allows us to define the Lagrangian of the system as:

$$\mathcal{L} = \frac{p^2}{2m} - q\phi + q\mathbf{A} \cdot \mathbf{v},$$

Through this Lagrangian we are able to determine the canonical conjugate momentum to be:

$$\mathbf{p}_r = \mathbf{p} + q\mathbf{A}$$

From this canonical conjugate momentum we have that the Hamiltonian of the system through the Equation (8-19) of [12] is:

$$H = \frac{1}{2m} (\mathbf{p} - q\mathbf{A})^2 + q\phi.$$

In general, we define the minimal coupling between a charged particle and an electromagnetic field by the replacement of the quantities:

$$\begin{aligned} p_i &\rightarrow p_i - qA_i \\ V(\mathbf{r}) &\rightarrow V(\mathbf{r}) + q\phi. \end{aligned}$$

These equations determine the dynamics of the particle and we can apply them in the Schrödinger's picture to get the differential equation of the dynamics of the wave-function of an electron in an electromagnetic field.

**1.3. The Dipolar Approximation.** The dipolar approximation is used in the case where the wavelength of the electromagnetic field is greater than the atomic dimensions. Under this condition, we have that:

$$\begin{aligned} \mathbf{A}(\mathbf{r}_0 + \mathbf{r}, t) &= \mathbf{A}(t) \exp[i\mathbf{k} \cdot (\mathbf{r}_0 + \mathbf{r})], \\ &= \mathbf{A}(t) \exp(i\mathbf{k} \cdot \mathbf{r}_0) (1 + i\mathbf{k} \cdot \mathbf{r} + \dots), \\ &\approx \mathbf{A}(t) \exp(i\mathbf{k} \cdot \mathbf{r}_0), \end{aligned}$$

where  $\mathbf{k}$  is the wavevector of the electromagnetic field and  $\mathbf{r}_0$  is the center of mass position of the atom. What we have done is to neglect the term of the form  $\mathbf{k} \cdot \mathbf{r}$  and all its greater powers, since we have that:

$$\mathbf{k} \cdot \mathbf{r} = \frac{2\pi}{\lambda} (\hat{\mathbf{k}} \cdot \mathbf{r}),$$

with  $\lambda$  the wavelength of the field. Essentially we are supposing that the  $\mathbf{r}$  dimensions relevant for the atom (units of Å) are several orders of magnitude smaller than the wavelength  $\lambda$  (of several nm), which means that the atom is subjected to the same intensity of the field. From this, the electromagnetic field that interacts with the atom is dependent of the time and the fixed atomic center of mass position  $\mathbf{r}_0$ . Then, the Schrödinger's equation takes the form:

$$\left\{ -\frac{\hbar^2}{2m} \left[ \nabla - \frac{ie}{\hbar} \mathbf{A}(\mathbf{r}_0, t) \right]^2 + V(r) \right\} \psi(\mathbf{r}, t) = i\hbar \frac{\partial \psi}{\partial t}(\mathbf{r}, t), \quad (1)$$

where  $e$  is the electron charge. If we take the wave function under the norm gauge:

$$\psi(\mathbf{r}, t) = \exp \left[ \frac{ie}{\hbar} \mathbf{A}(\mathbf{r}_0, t) \cdot \mathbf{r} \right] \phi(\mathbf{r}, t),$$

we have that:

$$\nabla^2 \psi(\mathbf{r}, t) = \exp \left[ \frac{ie}{\hbar} \mathbf{A}(\mathbf{r}_0, t) \cdot \mathbf{r} \right] \left\{ \nabla^2 + \frac{2ie}{\hbar} \mathbf{A}(\mathbf{r}_0, t) \cdot \nabla - \frac{e^2}{\hbar^2} |\mathbf{A}(\mathbf{r}_0, t)|^2 \right\} \phi(\mathbf{r}, t).$$

As a consequence:

$$\begin{aligned} \left[ \nabla - \frac{ie}{\hbar} \mathbf{A}(\mathbf{r}_0, t) \right]^2 \psi(\mathbf{r}, t) &= \left\{ \nabla^2 - \frac{2ie}{\hbar} \mathbf{A}(\mathbf{r}_0, t) \cdot \nabla - \frac{e^2}{\hbar^2} |\mathbf{A}(\mathbf{r}_0, t)|^2 \right\} \exp \left[ \frac{ie}{\hbar} \mathbf{A}(\mathbf{r}_0, t) \cdot \mathbf{r} \right] \phi(\mathbf{r}, t) \\ &= \nabla^2 \psi(\mathbf{r}, t) + \exp \left[ \frac{ie}{\hbar} \mathbf{A}(\mathbf{r}_0, t) \cdot \mathbf{r} \right] \left\{ -\frac{2ie}{\hbar} \mathbf{A}(\mathbf{r}_0, t) + \frac{e^2}{\hbar^2} |\mathbf{A}(\mathbf{r}_0, t)|^2 \right\} \phi(\mathbf{r}, t). \end{aligned}$$

From these results, the equation for  $\phi(\mathbf{r}, t)$  is:

$$\begin{aligned}
-\frac{\hbar^2}{2m}\nabla^2\phi(\mathbf{r},t) + V(r)\phi(\mathbf{r},t) &= i\hbar\left[\frac{ie}{\hbar}\frac{\partial\mathbf{A}}{\partial t}(\mathbf{r}_0,t)\cdot\mathbf{r}\right]\phi(\mathbf{r},t) + i\hbar\frac{\partial\phi}{\partial t}(\mathbf{r},t) \\
\left[\frac{p^2}{2m} + V(r) + e\frac{\partial\mathbf{A}}{\partial t}(\mathbf{r}_0,t)\cdot\mathbf{r}\right]\phi(\mathbf{r},t) &= i\hbar\frac{\partial\phi}{\partial t}(\mathbf{r},t).
\end{aligned} \tag{2}$$

Remembering that under the Coulomb's gauge:

$$\mathbf{E}(\mathbf{r},t) = -\frac{\partial\mathbf{A}}{\partial t}(\mathbf{r},t),$$

and also,

$$\mathbf{d} = e\mathbf{r},$$

where  $E(\mathbf{r},t)$  is the electromagnetic field and  $\mathbf{d}$  is the dipolar moment of the atom. Replacing these quantities in the obtained equation (2):

$$\begin{aligned}
\left[\frac{p^2}{2m} + V(r) - \mathbf{d}\cdot\mathbf{E}(\mathbf{r},t)\right]\phi(\mathbf{r},t) &= i\hbar\frac{\partial\phi}{\partial t}(\mathbf{r},t), \\
[H_0 + H_I]\phi(\mathbf{r},t) &= i\hbar\frac{\partial\phi}{\partial t}(\mathbf{r},t).
\end{aligned}$$

This last equation indicates that the interaction between the electromagnetic field with the atom can be modeled through the interaction Hamiltonian:

$$H_I = -\mathbf{d}\cdot\mathbf{E}(\mathbf{r},t). \tag{3}$$

From here, we have deduced that this dipolar term is what dominates the radiation-matter interaction in the atomic case. [13].

## 2. Momentum transfer in Atomic Transitions.

The electronic transitions driven by electromagnetic fields between atomic states are subject to the principles of energy and momentum conservation principles. When a photon is absorbed through a transition of an electron between two states, the photon momentum is transferred to the atom, as illustrated in Fig. (1.1) .

The photon momentum recoil  $p$  is related to the wave number  $k$  of the electromagnetic wave by the relation

$$p = \hbar k,$$

where  $\hbar$  is the reduced Planck's constant.

The internal atomic states are coupled with external degrees of freedom of the atom, from which the Hilbert space  $\mathcal{H}$  of the state is a tensor product between the Hilbert space of internal states  $\mathcal{H}_i$  and the Hilbert space of the external states  $\mathcal{H}_e$ :

$$\mathcal{H} = \mathcal{H}_i \otimes \mathcal{H}_e.$$

Let's consider a two-level system, as is illustrated in Fig. (1.1). Under the dipolar approximation, the Hamiltonian of this system has the form:

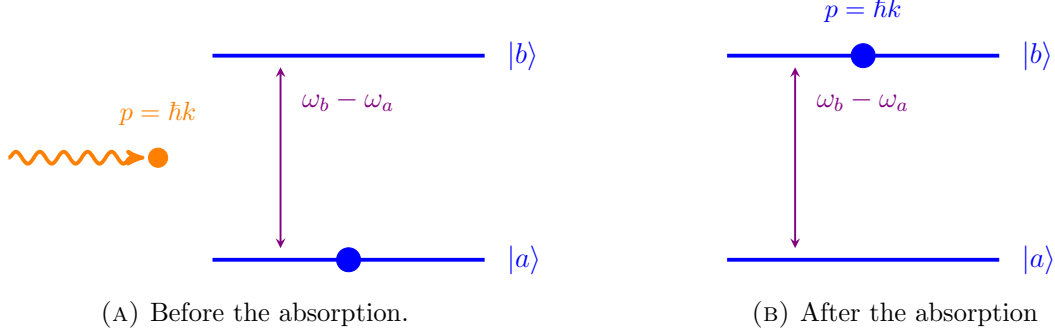


FIGURE 1.1. Scheme of a two level system.

$$H = \frac{p^2}{2m} + \hbar\omega_b |b\rangle \langle b| + \hbar\omega_a |a\rangle \langle a| - e\mathbf{r} \cdot \mathbf{E}(\mathbf{r}, t), \quad (4)$$

where  $e$  is the electron charge and  $\mathbf{E}(\mathbf{r}, t)$  is the electromagnetic field which interacts with the atom, having the form:

$$\mathbf{E}(\mathbf{r}, t) = \mathbf{E}_0 \cos(\mathbf{k} \cdot \mathbf{r} - \omega t + \phi), \quad (5)$$

with  $\mathbf{E}_0$  the amplitude vector (which carries the information of the polarization and intensity of the wave),  $\mathbf{k}$  is the wavevector,  $\omega$  is its angular frequency, and  $\phi$  is its characteristic initial phase. Let's suppose that we can express the initial state of the atomic system in the interaction picture of the non-perturbed hamiltonian  $\hat{H}_0$ :

$$\hat{H}_0 = \frac{p^2}{2m} + \hbar\omega_b |b\rangle \langle b| + \hbar\omega_a |a\rangle \langle a|,$$

and in a specific momentum state  $|\mathbf{p}\rangle$ :

$$|\Psi(t)\rangle = C_{a,\mathbf{p}}(t) |a, \mathbf{p}\rangle \exp \left[ -i \left( \omega_a + \frac{|\mathbf{p}|^2}{2m\hbar} \right) t \right].$$

With the aim to solve the Schrödinger's Equation using the Hamiltonian of Eq. (4), we let the coefficients  $C_{b,\mathbf{p}}$  and  $C_{a,\mathbf{p}}$  be time-dependent, which now represent probability amplitudes that vary much slower than the corresponding phases in time. The interaction term  $H_I = -e\mathbf{r} \cdot \mathbf{E}(\mathbf{r}, t)$  provokes transitions between our base states, both in the Hilbert space of internal states, and in the Hilbert space of external states, in this last case due to the terms  $e^{\pm i\mathbf{k} \cdot \mathbf{r}}$  involved in the functional form of the electromagnetic wave Eq. (5). Since  $e^{\pm i\mathbf{k} \cdot \mathbf{r}}$  is the momentum translation operator, we have that:

$$e^{\pm i\mathbf{k} \cdot \mathbf{r}} = \int d\mathbf{p} |\mathbf{p} \pm \hbar\mathbf{k}\rangle \langle \mathbf{p}|.$$

This equation means that the term of the field dependence of the position apart from making transitions between the internal states of the atom, it also makes transitions between momentum states with a difference of  $\pm \hbar\mathbf{k}$ . From here we can establish that when we have a superposition of the internal states  $|a\rangle$  and  $|b\rangle$ , its wavefunctions are separating in time at a velocity  $\mathbf{v} = \hbar\mathbf{k}/m$ , and from this, we can make the expansion of the state in the following form:

$$|\Psi(t)\rangle = C_{b,\mathbf{p}+\hbar\mathbf{k}}(t) |b, \mathbf{p} + \hbar\mathbf{k}\rangle \exp \left[ -i \left( \omega_b + \frac{|\mathbf{p} + \hbar\mathbf{k}|^2}{2m\hbar} \right) t \right] + C_{a,\mathbf{p}}(t) |a, \mathbf{p}\rangle \exp \left[ -i \left( \omega_a + \frac{|\mathbf{p}|^2}{2m\hbar} \right) t \right].$$

If we take this state and we replace it into the time-dependent Schrödinger's Equation, we obtain the differential equations for the time-dependent amplitudes  $C_{a,\mathbf{p}}$  and  $C_{b,\mathbf{p}+\hbar\mathbf{k}}$ :

$$\begin{aligned} i\hbar\dot{C}_{b,\mathbf{p}+\hbar\mathbf{k}}(t) &= -e \langle b, \mathbf{p} + \hbar\mathbf{k} | \mathbf{r} \cdot \mathbf{E} | a, \mathbf{p} \rangle \exp [i(\omega_{ba} + \omega_p)t] C_{a,\mathbf{p}}(t), \\ i\hbar\dot{C}_{a,\mathbf{p}}(t) &= -e \langle a, \mathbf{p} | \mathbf{r} \cdot \mathbf{E} | b, \mathbf{p} + \hbar\mathbf{k} \rangle \exp [-i(\omega_{ba} + \omega_p)t] C_{b,\mathbf{p}+\hbar\mathbf{k}}(t), \end{aligned}$$

where  $\omega_{ba} = \omega_b - \omega_a$ , and the dot means time derivative, also:

$$\begin{aligned} \omega_p &= \frac{|\mathbf{p} + \hbar\mathbf{k}|}{2m\hbar} - \frac{|\mathbf{p}|^2}{2m\hbar}, \\ \omega_p &= \underbrace{\frac{\mathbf{k} \cdot \mathbf{p}}{m}}_{\text{Doppler shift}} + \underbrace{\frac{\hbar k^2}{2m}}_{\text{photon recoil}}. \end{aligned}$$

The detuning due to momentum  $\omega_p$  finally is the fingerprint of the change of the momentum in the wave-functions associated with the internal states. As the eigenstates of momentum are delocalized in the coordinate space, in general to account to overlapping and interference of these wave-functions, we should consider wave-packets in momentum space, as we will do in the next chapters. The important thing we want to stress in the present section is that the transitions between internal states imply also momentum-state transitions and detunings dependent of the momentum [14].

### 3. Raman Transitions.

The last introduction has served as a base to show that when it is considered interactions radiation-matter the phases of the probability amplitudes and from this, the atomic transitions, begin to be dependent of the momentum states, that is to say, of external degrees of freedom of the atom. Let's consider a system formed by three levels, where two of them,  $|a\rangle$  and  $|b\rangle$  are ground hyperfine states, which transition is electric dipolar forbidden, whilst the third one, denoted as  $|e\rangle$ , is an intermediate state of greater energy than  $|a\rangle$  and  $|b\rangle$ , as shown in Fig. (1.2). In the figure is suggested that the frequency of a first laser  $\omega_1$  is used to couple the states  $|a\rangle$  and  $|e\rangle$ , but that there exists a detuning between this frequency and the transition frequency  $\omega_{ea}$ , denoted as  $\Delta$ . In the same fashion,  $\omega_2$  couples the states  $|b\rangle$  and  $|e\rangle$  also with a detuning  $\Delta$ .

Our aim in this section is to give the conditions needed so that the transitions of this system occur between the states  $|a\rangle$  and  $|b\rangle$ , providing an effective system of two levels. Due to the existence of detunings between the lasers and the electronic transition frequencies that the emission from the level  $|e\rangle$  only can be stimulated, and therefore, we can neglect the spontaneous emission in our system [15]. This process is called stimulated Raman transitions.

Let's begin the study of these transitions with the initial Hamiltonian of the system of three levels, in which we take as zero of energy the excited state  $|e\rangle$ :

$$H_0 = \frac{p^2}{2m} - \hbar\omega_{ae} |a\rangle \langle a| - \hbar\omega_{be} |b\rangle \langle b|. \quad (6)$$

The electromagnetic field that interacts with this system is modeled through:

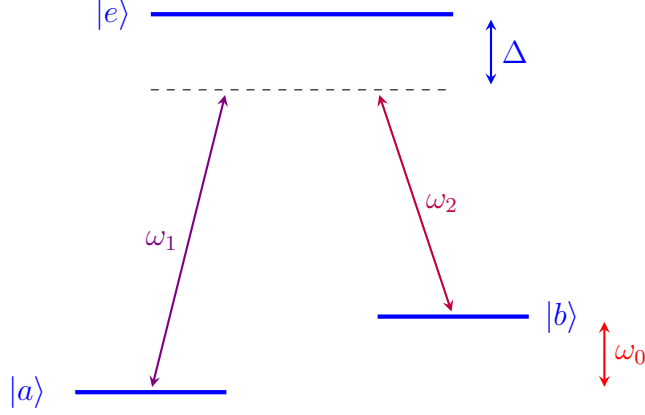


FIGURE 1.2. Transition scheme for a stimulated Raman transition.

$$\mathbf{E}(\mathbf{r}, t) = \mathbf{E}_1 \cos(\mathbf{k}_1 \cdot \mathbf{r} - \omega_1 t) + \mathbf{E}_2 \cos(\mathbf{k}_2 \cdot \mathbf{r} - \omega_2 t),$$

where the amplitude vectors  $\mathbf{E}_1$  and  $\mathbf{E}_2$  determine the polarization and amplitude of the incident waves, while  $\omega_1$  and  $\omega_2$  are the frequencies of the lasers and  $\mathbf{k}_1$  and  $\mathbf{k}_2$  are the corresponding wave-vectors. We express this field in the following form:

$$\begin{aligned} \mathbf{E}(\mathbf{r}, t) &= \mathbf{E}^{(+)}(\mathbf{r}, t) + \mathbf{E}^{(-)}(\mathbf{r}, t), \\ \mathbf{E}^{(\pm)}(\mathbf{r}, t) &= \frac{1}{2} \left( \mathbf{E}_1 e^{\pm i(\mathbf{k}_1 \cdot \mathbf{r} - \omega_1 t)} + \mathbf{E}_2 e^{\pm i(\mathbf{k}_2 \cdot \mathbf{r} - \omega_2 t)} \right) \end{aligned}$$

In general, we want to express the interaction Hamiltonian  $H_I = -e\mathbf{r} \cdot \mathbf{E}$  in terms of the base  $|a\rangle$ ,  $|b\rangle$  and  $|e\rangle$ . Nevertheless, due to the selection rules, we have that the terms  $\langle a| \langle a|$ ,  $\langle b| \langle b|$  and  $\langle e| \langle e|$  are zero. Additionally, we consider that there are no transitions between  $|a\rangle$  and  $|b\rangle$  but only through the intermediate state  $|e\rangle$ , in such a way that the term  $\langle a| \langle b|$  is also zero. From these suppositions, we can express the dipolar momentum operator in the form,

$$\begin{aligned} \mathbf{d} &= \mathbf{d}^{(+)} + \mathbf{d}^{(-)}, \\ \mathbf{d}^{(+)} &= \langle a| \mathbf{d} |e\rangle \sigma_1 + \langle b| \mathbf{d} |e\rangle \sigma_2, \\ \mathbf{d}^{(-)} &= \langle a| \mathbf{d} |e\rangle^* \sigma_1^\dagger + \langle b| \mathbf{d} |e\rangle^* \sigma_2^\dagger, \end{aligned}$$

where we have denoted  $\sigma_1 = |a\rangle \langle e|$  and  $\sigma_2 = |b\rangle \langle e|$ . Also, we consider that  $\omega_1$  only can couple the states  $|a\rangle$  and  $|e\rangle$ , and not the states  $|b\rangle$  and  $|e\rangle$ , due to the detunings involved, and also that  $\omega_2$  only can couple the states  $|b\rangle$  and  $|e\rangle$  but not the states  $|a\rangle$  and  $|e\rangle$ ; then, at the moment to calculate the matrix elements of the interaction hamiltonian, we neglect elements that involve states and wave-vectors crossed, as instance, the term  $\langle e| e^{-i(\mathbf{k}_1 \cdot \mathbf{r} - \omega_1 t)}$ . From here, we can express the interaction hamiltonian as follows:

$$H_I = -\frac{1}{2} \langle a | \mathbf{d} \cdot \mathbf{E}_1 | e \rangle \left( \sigma_1 e^{-i\mathbf{k}_1 \cdot \mathbf{r}} e^{i\omega_1 t} + \sigma_1^\dagger e^{i\mathbf{k}_1 \cdot \mathbf{r}} e^{-i\omega_1 t} \right) - \frac{1}{2} \langle b | \mathbf{d} \cdot \mathbf{E}_2 | e \rangle \left( \sigma_2 e^{-i\mathbf{k}_2 \cdot \mathbf{r}} e^{i\omega_2 t} + \sigma_2^\dagger e^{i\mathbf{k}_2 \cdot \mathbf{r}} e^{-i\omega_2 t} \right).$$

From which we can define the Rabi frequencies:

$$\Omega_1 = -\frac{\langle a | \mathbf{d} \cdot \mathbf{E}_1 | e \rangle}{\hbar},$$

$$\Omega_2 = -\frac{\langle b | \mathbf{d} \cdot \mathbf{E}_2 | e \rangle}{\hbar},$$

we can express finally the interaction hamiltonian as:

$$H_I = \frac{\hbar\Omega_1}{2} \left( \sigma_1 e^{-i\mathbf{k}_1 \cdot \mathbf{r}} e^{i\omega_1 t} + \sigma_1^\dagger e^{i\mathbf{k}_1 \cdot \mathbf{r}} e^{-i\omega_1 t} \right) + \frac{\hbar\Omega_2}{2} \left( \sigma_2 e^{-i\mathbf{k}_2 \cdot \mathbf{r}} e^{i\omega_2 t} + \sigma_2^\dagger e^{i\mathbf{k}_2 \cdot \mathbf{r}} e^{-i\omega_2 t} \right). \quad (7)$$

Our next step is to transform our Hamiltonian to a reference system that rotates with the frequencies of the lasers. With that aim, we transform the probability amplitudes of the states expressed in terms of the base  $|a\rangle$ ,  $|b\rangle$  and  $|e\rangle$ :

$$|\psi(t)\rangle = \psi_a(t) e^{-i\omega_1 t} |a\rangle + \psi_b(t) e^{-i\omega_2 t} |b\rangle + \psi_e(t) |e\rangle$$

Writing the Hamiltonian taking into account these extra terms, an energy recalibration is performed to eliminate the phases dependent of the frequencies of the lasers [11]:

$$H_0 = \frac{p^2}{2m} + \hbar\Delta |a\rangle \langle a| + \hbar\Delta |b\rangle \langle b|,$$

$$H_I = \frac{\hbar\Omega_1}{2} \left( \sigma_1 e^{-i\mathbf{k}_1 \cdot \mathbf{r}} + \sigma_1^\dagger e^{i\mathbf{k}_1 \cdot \mathbf{r}} \right) + \frac{\hbar\Omega_2}{2} \left( \sigma_2 e^{-i\mathbf{k}_2 \cdot \mathbf{r}} + \sigma_2^\dagger e^{i\mathbf{k}_2 \cdot \mathbf{r}} \right),$$

where  $\Delta = \omega_1 - \omega_{ae} = \omega_2 - \omega_{be}$ . Through the transformation:

$$|\psi\rangle \rightarrow e^{-i\Delta t} |\psi\rangle,$$

we can introduce energy recalibrations to the system. Using this, we can deduce the equations of evolution for the three states:

$$i\hbar\partial_t \psi_e(\mathbf{r}, t) = \frac{p^2}{2m} \psi_e(\mathbf{r}, t) + \frac{\hbar\Omega_1}{2} e^{i\mathbf{k}_1 \cdot \mathbf{r}} \psi_a(\mathbf{r}, t) + \frac{\hbar\Omega_2}{2} e^{i\mathbf{k}_2 \cdot \mathbf{r}} \psi_b(\mathbf{r}, t) - \hbar\Delta \psi_e(\mathbf{r}, t), \quad (8)$$

$$i\hbar\partial_t \psi_a(\mathbf{r}, t) = \frac{p^2}{2m} \psi_a(\mathbf{r}, t) + \frac{\hbar\Omega_1}{2} e^{-i\mathbf{k}_1 \cdot \mathbf{r}} \psi_e(\mathbf{r}, t) \quad (9)$$

$$i\hbar\partial_t \psi_b(\mathbf{r}, t) = \frac{p^2}{2m} \psi_b(\mathbf{r}, t) + \frac{\hbar\Omega_2}{2} e^{-i\mathbf{k}_2 \cdot \mathbf{r}} \psi_e(\mathbf{r}, t), \quad (10)$$

where we recalibrate the energy of the system by  $\Delta$ . Due to the great detuning of the intermediate state  $|e\rangle$ , this state is barely populated unless it has an initial population [16]. We have that  $|\Delta| \gg \Gamma$ , where  $1/\Gamma$  is the lifetime of the excited state; as we are interested in time scales of the dynamics greater than  $1/\Gamma$ , and by the Eq. (8) the oscillations of the state  $|e\rangle$  are faster than  $1/\Gamma$ , we can consider that the amplitude of this state becomes stationary instantaneously [11].

The consideration of the different time scales allows us to perform the Adiabatic approximation. The scale times where the excitation and stimulated decaying of the state  $|e\rangle$  are so short that we can make in Eq. (8)  $\partial_t \psi_e(\mathbf{r}, t) = 0$ . Also, the time variations in the transitions due to the term  $p^2/2m$  in Eq. (8) corresponds to the order of kHz, whilst the same time variations due to the internal dynamics of the atom, measured by the Rabi frequencies  $\Omega_1$  and  $\Omega_2$  corresponds to MHz, so we also neglect the contribution of  $p^2/2m$  in the Eq. (8) [11]. This converts the Eq. (8) in:

$$\psi_e(\mathbf{r}, t) = \frac{\Omega_1}{2\Delta} e^{i\mathbf{k}_1 \cdot \mathbf{r}} \psi_a(\mathbf{r}, t) + \frac{\Omega_2}{2\Delta} e^{i\mathbf{k}_2 \cdot \mathbf{r}} \psi_b(\mathbf{r}, t). \quad (11)$$

Replacing the Eq. (11) into the Eqs (9) and (10) we obtain:

$$\begin{aligned} i\hbar\partial_t \psi_a(\mathbf{r}, t) &= \frac{p^2}{2m} \psi_a(\mathbf{r}, t) + \hbar\omega_1^{AC} \psi_a(\mathbf{r}, t) + \frac{\hbar\Omega_R}{2} e^{i(\mathbf{k}_2 - \mathbf{k}_1) \cdot \mathbf{r}} \psi_b(\mathbf{r}, t) \\ i\hbar\partial_t \psi_b(\mathbf{r}, t) &= \frac{p^2}{2m} \psi_b(\mathbf{r}, t) + \hbar\omega_2^{AC} \psi_b(\mathbf{r}, t) + \frac{\hbar\Omega_R}{2} e^{i(\mathbf{k}_1 - \mathbf{k}_2) \cdot \mathbf{r}} \psi_a(\mathbf{r}, t), \end{aligned}$$

where we have defined the Raman-Rabi frequency  $\Omega_R$  as:

$$\Omega_R = \frac{\Omega_1 \Omega_2}{2\Delta},$$

and also,

$$\begin{aligned} \omega_1^{AC} &= \frac{\Omega_1^2}{4\Delta}, \\ \omega_2^{AC} &= \frac{\Omega_2^2}{4\Delta}, \end{aligned}$$

The effective hamiltonian for this system is then:

$$H_R = \frac{p^2}{2m} + \hbar\omega_1^{AC} |a\rangle \langle a| + \hbar\omega_2^{AC} |b\rangle \langle b| + \frac{\hbar\Omega_R}{2} \left( \sigma_R e^{i(\mathbf{k}_2 - \mathbf{k}_1) \cdot \mathbf{r}} + \sigma_R^\dagger e^{-i(\mathbf{k}_2 - \mathbf{k}_1) \cdot \mathbf{r}} \right),$$

with  $\sigma_R = |a\rangle \langle b|$  the lowering ladder operator between the ground states. This hamiltonian implies that at any time a transition is carried on between these states, there will be at the same time a change in the momentum state with a magnitude given by the difference of the wave-vectors given by  $\Delta p = \hbar\Delta k$  with  $\Delta k = |k_1 - k_2|$  [11]. This result is very important in atom interferometry, because it is possible spatially separate wave functions of the two state effective system to resolve them using the frequencies of the involved counter-propagating lasers.





## Raman Transitions driven by a modulated laser.

### 1. Doppler sensitive Raman transitions.

The coherent manipulation of the atomic wave-function in different momentum states, as was illustrated in the past chapter, opens the possibility to realize beam splitters and mirrors in an atom interferometer [14], in special, the implementation of Mach-Zehnder interferometers, this is illustrated in Fig.(2.1).

In the same fashion, through the use of Stimulated Raman transitions we can split the wave-function of an atom through  $\pi/2$ -pulses, and, interchange the populations of different states, the analog to mirrors, through  $\pi$ -pulses. Additionally, the relative motion of the atomic samples with respect to the phases of the lasers involved in the transition can be measured, which means the realization of a very accurate ruler due to the fact that the wave-lengths of the lasers is in the optical range (hundreds of nm of precision) [1].

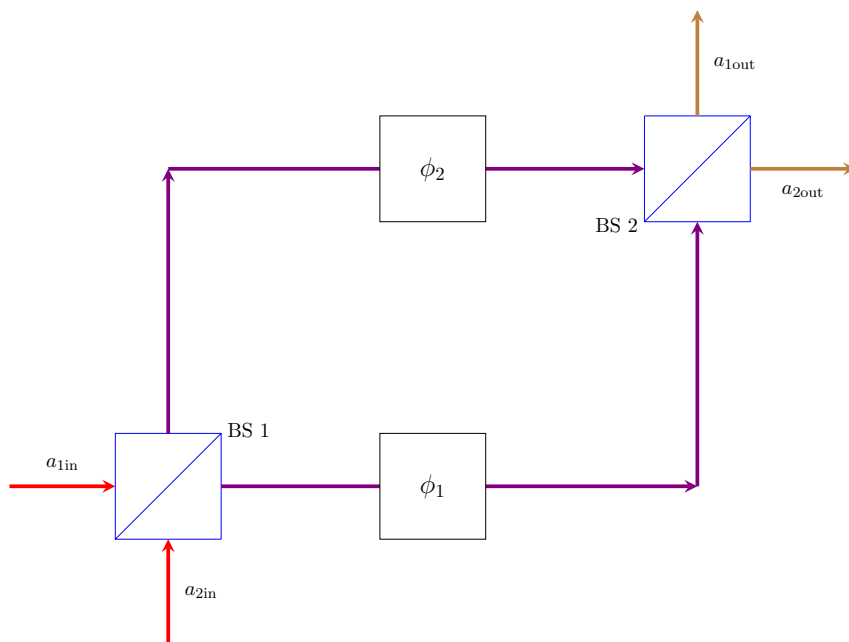


FIGURE 2.1. An optical Mach-Zehnder interferometer works by splitting the light beam through a Beam-Splitter (BS1), and letting that the phases of the light changes as they travels by their optical path, then, through a second Beam-Splitter, they are recombined to make them interfere.

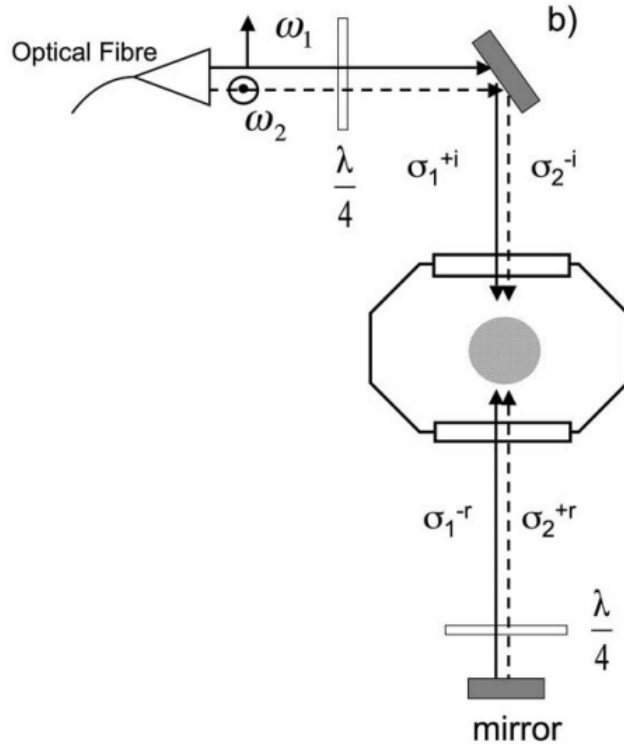


FIGURE 2.2. Retro-reflected configuration for a stimulated Raman transition. Figure adapted from [1].

This level of precision is what enables the determination, for example, of the local gravitational constant  $g$  with nine significant digits [3]. The main sources of error come from the path that the atoms follow, then is required a high control in the form of the laser wave-front, the velocity and the temperature of the atomic sample.

The Fig. (2.2) illustrates the experimental setup for counterpropagating Raman transitions implemented by [1] with the following features:

- (1) We have two Raman lasers with orthogonal polarizations traveling through the same polarization-maintaining fiber. Each beam is denoted by a continuous and a dashed line
- (2) The polarizations of the beams are changed by a first plate of  $\lambda/4$ .
- (3) The beams crossed the chamber where the alkali atoms are, in this case,  $\text{Rb}^{87}$  and then are reflected by a mirror, crossing a second  $\lambda/4$  plate twice.

The Fig. (2.3) shows the  $\Lambda$ -configuration in an alkali atom,  $\text{Rb}^{87}$  for gravimetry experiments. As was said in the previous chapter, the intermediate transitions are dipolar, as consequence, the selection rules are dependent of the polarization of the lasers [13]. The Rabi frequency of the Raman transition is given by [10],

$$\Omega_R = [\mathbf{E}_1 \times \mathbf{E}_2^*] \cdot \mathbf{M}, \quad (12)$$

with,

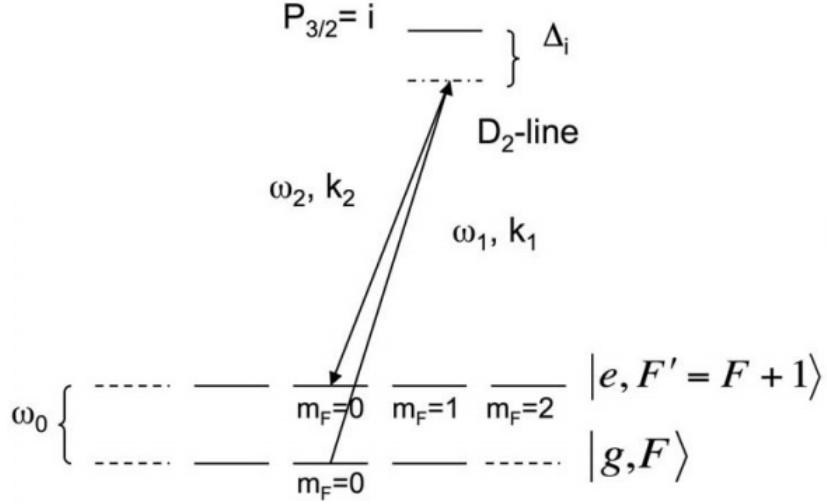


FIGURE 2.3. Levels scheme of an Alkali atom that are involved in the Raman transition of the experiment illustrated at Fig. (2.2). Figure adapted from [1].

$$\mathbf{M} = \frac{e^2}{4\hbar^2\Delta} \sum_n \langle a | \mathbf{r} | n \rangle \times \langle b | \mathbf{r} | n \rangle^*,$$

where  $a$  and  $b$  are the hyperfine ground states that couples through the Raman transition and  $n$  runs over all the intermediate states. The Eq. (12) implies that to maximize the transition between the ground states we should have  $\mathbf{E}_1$  and  $\mathbf{E}_2^*$  orthogonal, and contrapropagating to get the Doppler sensitive transitions required for gravimetry and applications in the measurement of inertial forces [10].

In the case of Fig. (2.2) we obtain two counter-propagating Raman pairs, the first one composed by those beams denoted as  $\sigma_1^{+i}$  and  $\sigma_2^{+r}$  and the second composed by  $\sigma_1^{-i}$  and  $\sigma_2^{-r}$ . Each Raman pair can be used to transfeere momentum to the atom in opposite directions. This is demonstrated through Raman spectroscopy, as illustrated by the spectrum of Fig. (2.4), where is shown the population at state  $|e, F' = F + 1\rangle$  of Fig. (2.3) after a  $\pi$ -pulse. The authors in reference [1] chose a fall time for the atomic sample in the vacuum chamber to make the transition, and they do a sweep in the two photon detuning frequency  $\delta = \omega_0 - (\omega_1 - \omega_2)$  based in Fig. (2.3). The peaks denoted as 1 and 1' correspond to Doppler-shifted resonances, with momentum transference in opposite directions. As the detuning is reduced, there appears co-propagating transitions without momentum transference, denoted as 2, and 3 and 3' denote transitions between states of the magnetic manifold illustrated at Fig. (2.3).

## 2. Experimental setup for a Composite-Light Interferometer.

The Fig. (2.5) shows the experimental setup proposed to perform counter-propagating Raman-transitions in an atomic cloud.

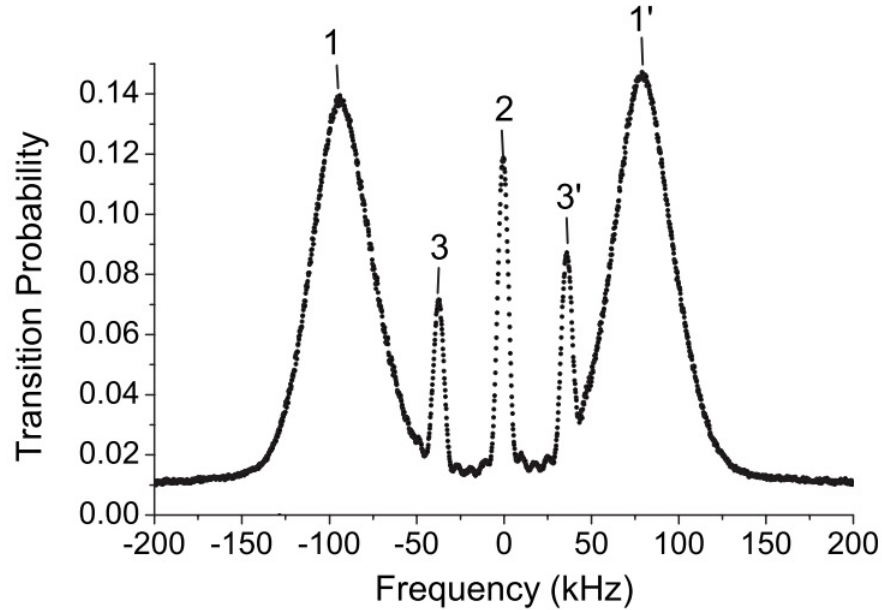


FIGURE 2.4. Raman spectroscopy spectrum for an alkali atom as a function of the detuning  $\delta$ . The data corresponds to a  $\pi$ -pulse of  $135 \mu\text{s}$  of duration. When an atom is released to free-fall, the frequencies which this interacts suffer Doppler shift. By this mechanism, the Raman transitions become velocity-dependent. Figure adapted from [1].

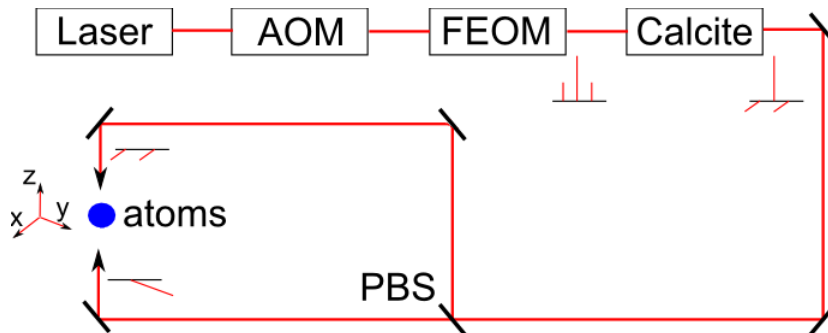


FIGURE 2.5. Setup for two Raman pairs with opposite momentum transfer. AOM: acousto-optical modulator, FEOM: fiber electro-optical modulator, PBS: polarization beam splitter. The polarizations of the carrier and sidebands are also shown.

- (1) The light from a Ti-Sapphire laser pass through an acousto-optical modulator AOM, used with the aim to make the pulses of light, that is to mean, its function is to generate pulses of rectangular form with a customized time interval  $\tau$ .
- (2) When the light goes through the Fiber Electro-optical modulator FEOM, the light frequency is phase modulated and as consequence is splitted into multiple bands [2]. Nevertheless, as increasing orders of the sidebands have decreasing amplitudes [10], in this thesis we consider

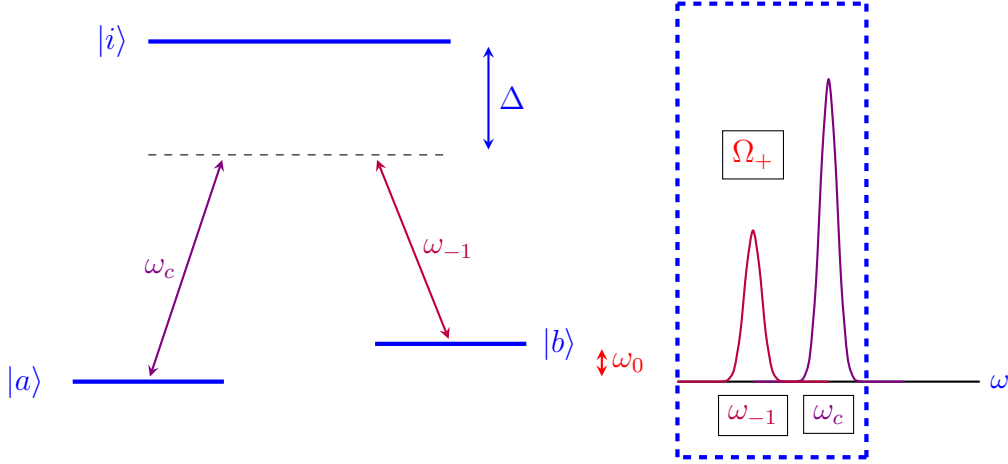


FIGURE 2.6. Scheme of the first couple of counterpropagating Raman beams.

just three frequencies: the carrier, denoted as  $\omega_0$  (with the same frequency of the laser at the input of FEOM), and the sidebands of first order, denoted as  $\omega_{-1}$  (of lower frequency than the carrier) and  $\omega_1$  (of greater frequency than the carrier).

- (3) Then the carrier and the sidebands are passed through a calcite crystal. This material has the characteristic of being birefringent, which means that has two refractive indexes that allow the manipulation of the polarization of the incident light-pulses. When the crystal is cutted at a specific long length (compared to the wave-length of the beams, for the experiment involved it is 13.13 cm), it becomes highly dispersive, which gives to the experimenter the possibility of leaving the polarizations of the sidebands equal and orthogonal to the polarization of the carrier, maximizing the value of the Raman frequencies of the pairs when these have linear polarizations [10].
- (4) Finally, the carrier and the sidebands are separated in path through a Polarizing Beam-Splitter PBS with the aim that the sidebands and the carrier incide into the atom in a counterpropagating form.

The Figs. (2.6) and (2.7) illustrate the action of the two counterpropagating Raman pairs. Let us suppose that the carrier photon with frequency  $\omega_{-1}$  incidés downwards in the Fig. (2.6), as illustrated at Fig. (2.5). Then at the end of the two photon process, the emitted photon must to have momentum  $\mathbf{p} = \hbar\mathbf{k}_{-1} = -\hbar k_{-1}\hat{\mathbf{z}}$ , where  $\mathbf{k}_i$  is the wave vector of the  $i = -1, c, 1$  for the  $-1$  sideband, the carrier and the  $+1$  sideband, respectively. From here, we obtain that the atomic recoil momentum is  $\mathbf{p} = (\hbar/c)(\omega_{-1} + \omega_c)\hat{\mathbf{z}}$ , that is to mean, in the opposite direction as gravity as illustrated in Fig. (2.5). For this reason, we denote the associated Raman frequency for this process  $\Omega_-$ .

The Fig. (2.7) illustrates the action of the second pair. A photon of frequency  $\omega_{+1}$  incidés over the atom with momentum  $\mathbf{p} = \hbar\mathbf{k}_{+1}$  and also the emitted one has momentum  $\mathbf{p} = \hbar\mathbf{k}_c = \hbar k_c\hat{\mathbf{z}}$ . By the momentum conservation principle, the atom must gain a recoil momentum of  $\mathbf{p} = -(\hbar/c)(\omega_c + \omega_{+1})\hat{\mathbf{z}}$ , that is to mean, in the same direction of the gravity acceleration. To the two-photon Raman frequency associated with this transition we will denoted as  $\Omega_+$ .

As an additional approximation to our system, and just to purposes of momentum transfer, we will consider that  $\omega_c \approx \omega_{-1} \approx \omega_{+1}$ , so that  $k = \omega/c$ , from which the atomic momentum transfer has a magnitude of  $p = 2\hbar k$ . We will denote  $k_e = 2k$ .

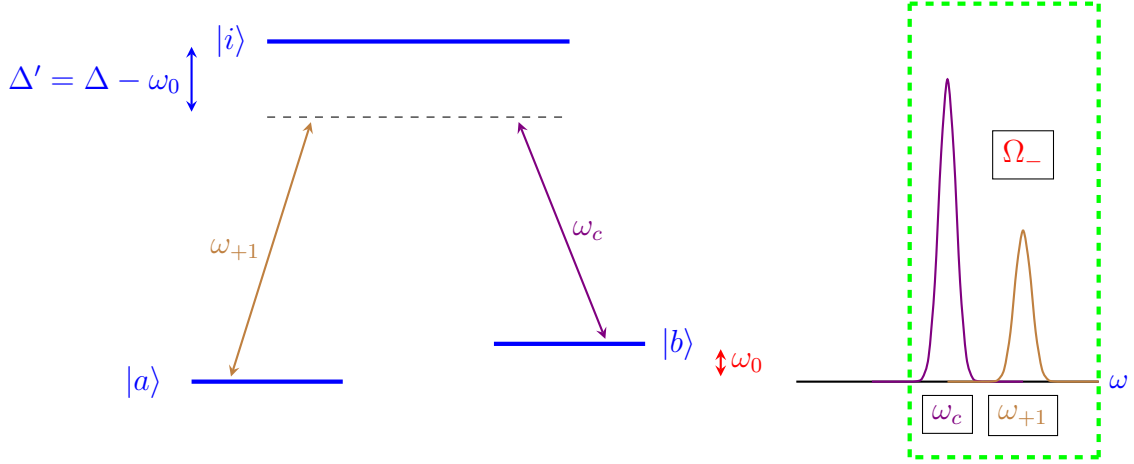


FIGURE 2.7. Scheme of the second couple of counterpropagating Raman beams.

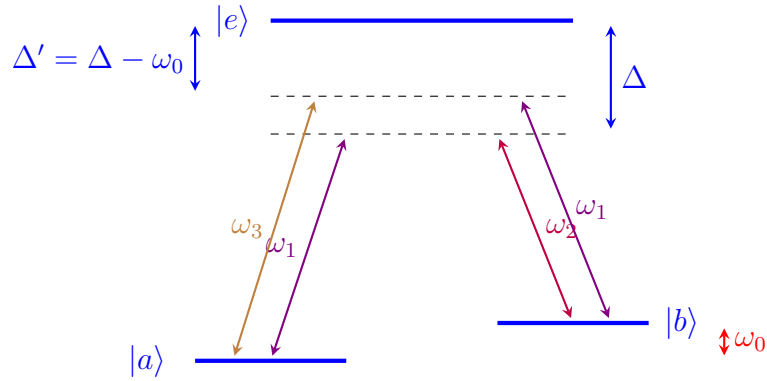


FIGURE 2.8. Scheme of transitions of two counter-propagating Raman beams.

### 3. Raman transitions with three lasers.

In the past section we encountered that if we change the detuning of a Raman transition we can excite momentum transference in the atom in opposite directions when we have a retro-reflected experimental setup as such as shown in Fig. (2.2). In the same fashion, we can maintain fixed the detuning of the Raman transition and introduce a second Raman pair with the aim to make Raman transitions again in opposite directions in an analogous way as shown in the proposition of Fig. (2.2). To perform such opposite momentum transitions, we need to compensate the detuning due to the Doppler effect according with the atomic free falling, which can be done shifting continuously the frequency of the lasers, process that we refer to as frequency chirping.

In this section we introduce the system of a  $\Lambda$  configuration with three lasers. Let us consider the scheme presented at Fig. (2.8) where we have a system of three lasers with frequencies  $\omega_1$ ,  $\omega_2$  and  $\omega_3$  interacting with a three level atom in  $\Lambda$  configuration. We are going to follow a mechanism exposed at the Chapter 1 to obtain the equations that determines the dynamics of the probability amplitudes  $C_a(p, t)$  and  $C_b(p, t)$ .

In this case, we assume that the form of the field involved has the following form:

$$\begin{aligned}\mathbf{E}(\mathbf{r}, t) &= \mathbf{E}^{(+)}(\mathbf{r}, t) + \mathbf{E}^{(-)}(\mathbf{r}, t), \\ \mathbf{E}^{(+)}(\mathbf{r}, t) &= \frac{1}{2}\hat{\epsilon}_1 E_1 e^{i(\mathbf{k}_1 \cdot \mathbf{r} - \omega_1 t)} + \frac{1}{2}\hat{\epsilon}_2 E_2 e^{i(\mathbf{k}_2 \cdot \mathbf{r} - \omega_2 t + \phi_2)} + \frac{1}{2}\hat{\epsilon}_3 E_3 e^{i(\mathbf{k}_3 \cdot \mathbf{r} - \omega_3 t + \phi_3)}, \\ \mathbf{E}^{(-)}(\mathbf{r}, t) &= \frac{1}{2}\hat{\epsilon}_1 E_1 e^{-i(\mathbf{k}_1 \cdot \mathbf{r} - \omega_1 t)} + \frac{1}{2}\hat{\epsilon}_2 E_2 e^{-i(\mathbf{k}_2 \cdot \mathbf{r} - \omega_2 t + \phi_2)} + \frac{1}{2}\hat{\epsilon}_3 E_3 e^{-i(\mathbf{k}_3 \cdot \mathbf{r} - \omega_3 t + \phi_3)},\end{aligned}$$

where  $\mathbf{k}_i$ ,  $\omega_i$ ,  $E_i$  and  $\hat{\epsilon}_i$  represent the wave-vector, the frequency, the magnitude and the polarization vector of the three fields with  $i = 1, 2, 3$ , as corresponds, and  $\phi_2$  and  $\phi_3$  corresponds to the relative phases of the fields 2 and 3 with respect to the first one. We follow the next steps in order to get the dynamics of the involved states:

- (1) We express the state of the atom as a superposition of the states  $|a\rangle$ ,  $|b\rangle$  and  $|e\rangle$ , whose dynamics is given by the corresponding amplitude probabilities  $C_a(t)$ ,  $C_b(t)$  and  $C_e(t)$ :

$$|\Psi(\mathbf{r}, t)\rangle = c_a(t)e^{i\omega_{ea}t} |a\rangle + c_b(t)e^{i\omega_{eb}t} |b\rangle + c_e(t) |e\rangle. \quad (13)$$

- (2) We replace the state Eq. (13) into the time-dependent Schrödinger equation:

$$i\hbar \frac{\partial |\Psi\rangle}{\partial t} = (\hat{H}_0 + \hat{H}_I) |\Psi\rangle, \quad (14)$$

where  $\hat{H}_0$  is as given by Eq. (6) and where  $\hat{H}_I$  is given by Eq. (3) under the dipole approximation to obtain:

$$\begin{aligned}i\hbar \dot{c}_a(t) &= c_e(t)e^{-i(\omega_e - \omega_a)t} \langle a | H_I | e \rangle \\ i\hbar \dot{c}_b(t) &= c_e(t)e^{-i(\omega_e - \omega_b)t} \langle b | H_I | e \rangle \\ i\hbar \dot{c}_e(t) &= c_a(t)e^{i(\omega_e - \omega_a)t} \langle e | H_I | a \rangle + c_b(t)e^{i(\omega_e - \omega_b)t} \langle e | H_I | b \rangle.\end{aligned}$$

Here again we assume that the transitions only can be done through the intermediate state  $|e\rangle$ .

- (3) In general,  $\mathbf{E}^{(+)}(\mathbf{r}, t)$  oscillates with complex exponentials dependent on  $-\omega_i$  with  $i = 1, 2, 3$ , while in the same fashion,  $\mathbf{E}^{(-)}(\mathbf{r}, t)$  oscillates with complex exponentials dependent on  $\omega_i$  with  $i = 1, 2, 3$ . As an example, when we calculate the matrix element  $\langle a | H_I | e \rangle$ , this depends on the exponentials  $\exp[-i(\omega_{ea} + \omega_i)]$  associated with  $\mathbf{E}^{(+)}(\mathbf{r}, t)$  and  $\exp[-i(\omega_{ea} - \omega_i)]$  associated with  $\mathbf{E}^{(-)}(\mathbf{r}, t)$ . Nevertheless, a phase given by  $\omega_{ea} + \omega_i$  oscillates faster than one given by  $\omega_{ea} - \omega_i$ , so in general the contribution from the first oscillation is much smaller than an oscillation given by the second one.

This observation allows us to neglect contributions from phases that oscillates faster comparative with others, this approximation is called *Rotating Wave Approximation* [17]. This approximation is based in the Lemma of Riemman-Lebesgue [18], which states that:

$$\lim_{x \rightarrow \infty} \int_a^b f(t)e^{ixt} dt = 0 \quad (15)$$

where  $f(t)$  is an integrable function defined on a closed interval  $[a, b]$ . To solve the differential equations we need to integrate them, in this form, the Riemann-Lebesgue lemma guarantees us that the contributions from fast oscillating terms can be neglected.



- (4) We neglect couplings between the states that do not correspond to the scheme shown in Fig. (2.8). For instance, we neglect contributions from phases like  $e^{\pm i(\omega_{eb}-\omega_3)t}$  because the transition  $|b\rangle \leftrightarrow |e\rangle$  driven by  $\omega_3$  is far-detuned in comparison with the transitions driven by the fields  $\omega_1$  and  $\omega_2$ , and as a consequence, it can not complete a Raman transition with none of these beams. A similar argument holds for the phase  $e^{\pm i(\omega_{ea}-\omega_2)t}$ . The interaction hamiltonian under this approximation has the form:

$$\begin{aligned}
H_I = & \frac{\hbar\Omega_1^{ea}}{2}\sigma_a e^{-i\mathbf{k}_1\cdot\mathbf{r}} e^{-i(\omega_{ea}-\omega_1)t} + \frac{\hbar\Omega_3^{ea}}{2}\sigma_a e^{-i\mathbf{k}_3\cdot\mathbf{r}} e^{-i(\omega_{ea}-\omega_3)t} \\
& + \frac{\hbar\Omega_1^{ea*}}{2}\sigma_a^\dagger e^{i\mathbf{k}_1\cdot\mathbf{r}} e^{i(\omega_{ea}-\omega_1)t} + \frac{\hbar\Omega_3^{ea*}}{2}\sigma_a^\dagger e^{i\mathbf{k}_3\cdot\mathbf{r}} e^{i(\omega_{ea}-\omega_3)t} \\
& + \frac{\hbar\Omega_2^{eb}}{2}\sigma_b e^{-i\mathbf{k}_2\cdot\mathbf{r}} e^{-i(\omega_{eb}-\omega_2)t} + \frac{\hbar\Omega_1^{eb}}{2}\sigma_b e^{-i\mathbf{k}_1\cdot\mathbf{r}} e^{-i(\omega_{eb}-\omega_1)t} \\
& + \frac{\hbar\Omega_2^{eb*}}{2}\sigma_b^\dagger e^{i\mathbf{k}_2\cdot\mathbf{r}} e^{i(\omega_{eb}-\omega_2)t} + \frac{\hbar\Omega_1^{eb*}}{2}\sigma_b^\dagger e^{i\mathbf{k}_1\cdot\mathbf{r}} e^{i(\omega_{eb}-\omega_1)t},
\end{aligned} \tag{16}$$

where,

$$\begin{aligned}
\Omega_1^{ea} &= -\frac{\langle a|\mathbf{d}\cdot\mathbf{E}_{01}|e\rangle}{\hbar} & \Omega_3^{ea} &= -\frac{\langle a|\mathbf{d}\cdot\mathbf{E}_{03}|e\rangle}{\hbar} \\
\Omega_1^{eb} &= -\frac{\langle b|\mathbf{d}\cdot\mathbf{E}_{01}|e\rangle}{\hbar} & \Omega_2^{eb} &= -\frac{\langle b|\mathbf{d}\cdot\mathbf{E}_{02}|e\rangle}{\hbar}
\end{aligned}$$

- (5) We denote the wave-functions of the system as  $C_a(\mathbf{r}, t) = \langle a|\Psi(\mathbf{r}, t)\rangle$ ,  $C_b(\mathbf{r}, t) = \langle b|\Psi(\mathbf{r}, t)\rangle$  and  $C_e(\mathbf{r}, t) = \langle e|\Psi(\mathbf{r}, t)\rangle$ . Using the Eqs. (16) and Eq. (14) the differential equations for the dynamics of the wave-functions are

$$\begin{aligned}
i\hbar\partial_t C_a(\mathbf{r}, t) &= \frac{p^2}{2m} C_a(\mathbf{r}, t) \\
&+ \frac{\hbar\Omega_1^{ea}}{2} e^{-i\mathbf{k}_1\cdot\mathbf{r}} e^{-i(\omega_{ea}-\omega_1)t} C_e(\mathbf{r}, t) + \frac{\hbar\Omega_3^{ea}}{2} e^{-i\mathbf{k}_3\cdot\mathbf{r}} e^{-i(\omega_{ea}-\omega_3)t} C_e(\mathbf{r}, t)
\end{aligned} \tag{17}$$

$$\begin{aligned}
i\hbar\partial_t C_b(\mathbf{r}, t) &= \frac{p^2}{2m} C_b(\mathbf{r}, t) \\
&+ \frac{\hbar\Omega_2^{eb}}{2} e^{-i\mathbf{k}_2\cdot\mathbf{r}} e^{-i(\omega_{eb}-\omega_2)t} C_e(\mathbf{r}, t) + \frac{\hbar\Omega_1^{eb}}{2} e^{-i\mathbf{k}_1\cdot\mathbf{r}} e^{-i(\omega_{eb}-\omega_1)t} C_e(\mathbf{r}, t)
\end{aligned} \tag{18}$$

$$\begin{aligned}
i\hbar\partial_t C_e(\mathbf{r}, t) &= \frac{p^2}{2m} C_e(\mathbf{r}, t) + \frac{\hbar\Omega_1^{ea*}}{2} e^{i\mathbf{k}_1\cdot\mathbf{r}} e^{i(\omega_{ea}-\omega_1)t} C_a(\mathbf{r}, t) + \frac{\hbar\Omega_3^{ea*}}{2} e^{i\mathbf{k}_3\cdot\mathbf{r}} e^{i(\omega_{ea}-\omega_3)t} C_a(\mathbf{r}, t) \\
&+ \frac{\hbar\Omega_2^{eb*}}{2} e^{i\mathbf{k}_2\cdot\mathbf{r}} e^{i(\omega_{eb}-\omega_2)t} C_b(\mathbf{r}, t) + \frac{\hbar\Omega_1^{eb*}}{2} e^{i\mathbf{k}_1\cdot\mathbf{r}} e^{i(\omega_{eb}-\omega_1)t} C_b(\mathbf{r}, t).
\end{aligned} \tag{19}$$

- (6) We can now perform the elimination of the intermediate state  $|e\rangle$  in a similar manner as we did in Chapter 1. We neglect the contribution of the term of kinetic energy for this state, so we can determine that the corresponding wave function is under the adiabatic approximation since  $p^2/2m \ll \hbar|\Omega|$  in general for any Rabi frequency [11]. Then, integrating the Eq. (19) with respect time, we get:

$$\begin{aligned}
C_e(\mathbf{r}, t) = & -\frac{\Omega_1^{ea*}}{2} e^{i\mathbf{k}_1 \cdot \mathbf{r}} C_a(\mathbf{r}, t) \frac{e^{i(\omega_{ea}-\omega_1)t} - 1}{(\omega_{ea} - \omega_1)} - \frac{\Omega_3^{ea*}}{2} e^{i\mathbf{k}_3 \cdot \mathbf{r}} C_a(\mathbf{r}, t) \frac{e^{i(\omega_{ea}-\omega_3)t} - 1}{(\omega_{ea} - \omega_3)} \\
& - \frac{\Omega_2^{eb*}}{2} e^{i\mathbf{k}_2 \cdot \mathbf{r}} C_b(\mathbf{r}, t) \frac{e^{i(\omega_{eb}-\omega_2)t} - 1}{(\omega_{eb} - \omega_2)} - \frac{\Omega_1^{eb*}}{2} e^{i\mathbf{k}_1 \cdot \mathbf{r}} C_b(\mathbf{r}, t) \frac{e^{i(\omega_{eb}-\omega_1)t} - 1}{(\omega_{eb} - \omega_1)}.
\end{aligned} \tag{20}$$

Replacing the Eq. (20) in the dynamical equations for the states  $|a\rangle$  and  $|b\rangle$  we obtain:

$$\begin{aligned}
i\hbar\partial_t C_a(\mathbf{r}, t) = & \frac{p^2}{2m} C_a(\mathbf{r}, t) \\
& - \frac{\hbar|\Omega_1^{ea}|^2}{4} C_a(\mathbf{r}, t) e^{-i(\omega_{ea}-\omega_1)t} \frac{e^{i(\omega_{ea}-\omega_1)t} - 1}{\omega_{ea} - \omega_1} \\
& - \frac{\hbar\Omega_1^{ea}\Omega_3^{ea*}}{4} e^{-i(\mathbf{k}_1-\mathbf{k}_3) \cdot \mathbf{r}} C_a(\mathbf{r}, t) e^{-i(\omega_{ea}-\omega_1)t} \frac{e^{i(\omega_{ea}-\omega_3)t} - 1}{\omega_{ea} - \omega_3} \\
& - \frac{\hbar\Omega_1^{ea}\Omega_2^{eb*}}{4} C_b(\mathbf{r}, t) e^{-i(\mathbf{k}_1-\mathbf{k}_2) \cdot \mathbf{r}} e^{-i(\omega_{ea}-\omega_1)t} \frac{e^{i(\omega_{eb}-\omega_2)t} - 1}{\omega_{eb} - \omega_2} \\
& - \frac{\hbar\Omega_1^{ea}\Omega_1^{eb*}}{4} C_b(\mathbf{r}, t) e^{-i(\omega_{ea}-\omega_1)t} \frac{e^{i(\omega_{eb}-\omega_1)t} - 1}{\omega_{eb} - \omega_1} \\
& - \frac{\hbar\Omega_1^{ea*}\Omega_3^{ea}}{4} C_a(\mathbf{r}, t) e^{i(\mathbf{k}_1-\mathbf{k}_3) \cdot \mathbf{r}} e^{-i(\omega_{ea}-\omega_3)t} \frac{e^{i(\omega_{ea}-\omega_1)t} - 1}{\omega_{ea} - \omega_1} \\
& - \frac{\hbar|\Omega_3^{ea}|^2}{4} C_a(\mathbf{r}, t) e^{-i(\omega_{ea}-\omega_3)t} \frac{e^{i(\omega_{ea}-\omega_3)t} - 1}{\omega_{ea} - \omega_3} \\
& - \frac{\hbar\Omega_2^{eb*}\Omega_3^{ea}}{4} C_b(\mathbf{r}, t) e^{i(\mathbf{k}_2-\mathbf{k}_3) \cdot \mathbf{r}} e^{-i(\omega_{ea}-\omega_3)t} \frac{e^{i(\omega_{eb}-\omega_2)t} - 1}{\omega_{eb} - \omega_2} \\
& - \frac{\hbar\Omega_1^{eb*}\Omega_3^{ea}}{4} C_b(\mathbf{r}, t) e^{i(\mathbf{k}_1-\mathbf{k}_3) \cdot \mathbf{r}} e^{-i(\omega_{ea}-\omega_3)t} \frac{e^{i(\omega_{eb}-\omega_1)t} - 1}{\omega_{eb} - \omega_1}
\end{aligned} \tag{21}$$

$$\begin{aligned}
i\hbar\partial_t C_b(\mathbf{r}, t) &= \frac{p^2}{2m} C_b(\mathbf{r}, t) \\
&- \frac{\hbar\Omega_1^{ea*}\Omega_2^{eb}}{4} C_a(\mathbf{r}, t) e^{i(\mathbf{k}_1-\mathbf{k}_2)\cdot\mathbf{r}} e^{-i(\omega_{eb}-\omega_2)t} \frac{e^{i(\omega_{ea}-\omega_1)t} - 1}{\omega_{ea} - \omega_1} \\
&- \frac{\hbar\Omega_2^{eb}\Omega_3^{ea*}}{4} C_a(\mathbf{r}, t) e^{-i(\mathbf{k}_2-\mathbf{k}_3)\cdot\mathbf{r}} e^{-i(\omega_{eb}-\omega_2)t} \frac{e^{i(\omega_{ea}-\omega_3)t} - 1}{\omega_{ea} - \omega_3} \\
&- \frac{\hbar|\Omega_2^{eb*}|^2}{4} C_b(\mathbf{r}, t) e^{-i(\omega_{eb}-\omega_2)t} \frac{e^{i(\omega_{eb}-\omega_2)t} - 1}{\omega_{eb} - \omega_2} \\
&- \frac{\hbar\Omega_1^{eb*}\Omega_2^{eb}}{4} C_b(\mathbf{r}, t) e^{i(\mathbf{k}_1-\mathbf{k}_2)\cdot\mathbf{r}} e^{-i(\omega_{eb}-\omega_2)t} \frac{e^{i(\omega_{eb}-\omega_1)t} - 1}{\omega_{eb} - \omega_1} \\
&- \frac{\hbar\Omega_1^{ea*}\Omega_1^{eb}}{4} C_a(\mathbf{r}, t) e^{-i(\omega_{eb}-\omega_1)t} \frac{e^{i(\omega_{ea}-\omega_1)t} - 1}{\omega_{ea} - \omega_1} \\
&- \frac{\hbar\Omega_1^{eb}\Omega_3^{ea*}}{4} C_a(\mathbf{r}, t) e^{-i(\mathbf{k}_1-\mathbf{k}_3)\cdot\mathbf{r}} e^{-i(\omega_{eb}-\omega_1)t} \frac{e^{i(\omega_{ea}-\omega_3)t} - 1}{\omega_{ea} - \omega_3} \\
&- \frac{\hbar\Omega_1^{eb}\Omega_2^{eb*}}{4} C_b(\mathbf{r}, t) e^{-i(\mathbf{k}_1-\mathbf{k}_2)\cdot\mathbf{r}} e^{-i(\omega_{eb}-\omega_1)t} \frac{e^{i(\omega_{eb}-\omega_2)t} - 1}{\omega_{eb} - \omega_2} \\
&- \frac{\hbar|\Omega_1^{eb}|^2}{4} C_b(\mathbf{r}, t) e^{-i(\omega_{eb}-\omega_1)t} \frac{e^{i(\omega_{eb}-\omega_1)t} - 1}{\omega_{eb} - \omega_1}
\end{aligned} \tag{22}$$

(7) We are going to introduce a series of approximations to the Eq. (21) and Eq. (22):

- (a) The Raman transitions  $|a\rangle \leftrightarrow |b\rangle$  are determined by the effective Rabi frequencies  $\Omega_R^2$  and  $\Omega_R^3$ , which are sensible to the polarization of the fields involved. We can express these effective frequencies (Raman frequencies) as [10]:

$$\Omega_R^2 = [\mathbf{E}_1 \times \mathbf{E}_2^*] \cdot \frac{e^2}{4\hbar^2\Delta} \{ \langle a | \mathbf{r} | e \rangle \times \langle b | \mathbf{r} | e \rangle \}, \tag{23}$$

$$\Omega_R^3 = [\mathbf{E}_3 \times \mathbf{E}_1^*] \cdot \frac{e^2}{4\hbar^2\Delta'} \{ \langle a | \mathbf{r} | e \rangle \times \langle b | \mathbf{r} | e \rangle \}. \tag{24}$$

where  $\Delta = \omega_0 - (\omega_1 - \omega_2)$  is the detuning between the states  $|a\rangle$  and  $|b\rangle$  with the level  $|e\rangle$  by the pair  $\omega_1$  and  $\omega_2$ ,  $\Delta' = \omega_0 - (\omega_3 - \omega_1)$  is the detuning between the same states driven by the pair  $\omega_1$  and  $\omega_3$  (Fig. (2.8)), and  $e$  is the electron charge. From the Eqs. (23) and (24) we have that, in general, if we have the Raman frequencies that involve fields with the same linear polarization, their values are much smaller in comparison with those ones that involve orthogonal polarization.

In our configuration Fig. (2.5), we suppose that the field  $\mathbf{E}_1$  (the carrier) has an orthogonal linear polarization to the fields  $\mathbf{E}_2$  and  $\mathbf{E}_3$  (sidebands), and therefore, in the Eq. (21) we discard terms proportional to  $|\Omega_1^{ea}|^2$ ,  $\Omega_1^{ea}\Omega_1^{eb*}$ ,  $|\Omega_3^{ea}|^2$  and  $\Omega_2^{eb*}\Omega_3^{ea}$ , whilst in the Eq. (22) we discard terms proportional to  $\Omega_2^{eb}\Omega_3^{ea*}$ ,  $|\Omega_2^{eb*}|^2$ ,  $\Omega_1^{eb*}\Omega_1^{eb}$  and  $|\Omega_1^{eb}|^2$ .

- (b) In the Eqs. (21) and (22) there exist phases of two types: one photon transition (like  $e^{\pm i(\omega_{ea}-\omega_1)t}$ ) and two photon transition (like  $e^{\pm i[(\omega_{ea}-\omega_1)-(\omega_{eb}-\omega_2)]t}$ ). While the detunings of the first type are of the order of GHz, of the second type are of the order of MHz.

Then, in this point we also invoke the argument of the rotating wave approximation to neglect all the terms proportional to the phases of the first type.

- (c) We also impose the resonance condition. For the Eqs. (21) and (22) we have that the frequencies involved are obtained through phase modulation, from which:

$$\omega_1 - \omega_2 = \omega_3 - \omega_1.$$

- (d) Additionally, we will make an approximation to the wave-vectors, to simplify the explicit dependence with respect of the position of the differential Eqs. (21) and (22). We will suppose that  $k_1 \approx k_2 \approx k_3$ , and we will denote the corresponding wave-vectors as  $\mathbf{k}_1 = \mathbf{k}$  and  $\mathbf{k}_2 = \mathbf{k}_3 = -\mathbf{k}$ . From here we have that  $\mathbf{k}_1 - \mathbf{k}_2 = 2\mathbf{k}$ , and  $\mathbf{k}_1 - \mathbf{k}_3 = 2\mathbf{k}$ .

Under these approximations, the dynamical equations for  $|a\rangle$  and  $|b\rangle$  take the form:

$$i\hbar\partial_t C_a(\mathbf{r}, t) = \frac{p^2}{2m} C_a(\mathbf{r}, t) - \hbar\Omega_R^1 e^{-2i\mathbf{k}\cdot\mathbf{r}} C_b(\mathbf{r}, t) - \hbar\Omega_R^{2*} e^{2i\mathbf{k}\cdot\mathbf{r}} C_b(\mathbf{r}, t), \quad (25)$$

$$i\hbar\partial_t C_b(\mathbf{r}, t) = \frac{p^2}{2m} C_b(\mathbf{r}, t) - \hbar\Omega_R^{1*} e^{2i\mathbf{k}\cdot\mathbf{r}} C_a(\mathbf{r}, t) - \hbar\Omega_R^2 e^{-2i\mathbf{k}\cdot\mathbf{r}} C_a(\mathbf{r}, t). \quad (26)$$

The Eqs. (25) and (26) define the interaction of the atoms with the three electromagnetic fields. Nevertheless, we need to include also the interaction of the atoms with the gravitational field, step which is done replacing the kinetic energy in each state with the total mechanical energy of the atom in each state, obtaining then,

$$i\hbar\partial_t C_a(\mathbf{r}, t) = \left( \frac{p^2}{2m} + mgz \right) C_a(\mathbf{r}, t) - \hbar\Omega_R^1 e^{-2i\mathbf{k}\cdot\mathbf{r}} C_b(\mathbf{r}, t) - \hbar\Omega_R^{2*} e^{2i\mathbf{k}\cdot\mathbf{r}} C_b(\mathbf{r}, t), \quad (27)$$

$$i\hbar\partial_t C_b(\mathbf{r}, t) = \left( \frac{p^2}{2m} + mgz \right) C_b(\mathbf{r}, t) - \hbar\Omega_R^{1*} e^{2i\mathbf{k}\cdot\mathbf{r}} C_a(\mathbf{r}, t) - \hbar\Omega_R^2 e^{-2i\mathbf{k}\cdot\mathbf{r}} C_a(\mathbf{r}, t); \quad (28)$$

where  $g$  is the gravitational acceleration, while  $z$  is the position operator of the atom. Finally, the Eqs. (27) and (28) constitute the equations that define the dynamics of the wave-functions of the states  $|a\rangle$  and  $|b\rangle$ , from which the performing of the atom interferometer is based.

#### 4. The Galilean Transformation.

With the aim to simplify the Eqs. (27) and (28), we perform a unitary transformation to treat the differential equations in the center of mass moving frame of the atom. The procedure is developed with detail in Appendix A. In synthesis, we obtain the differential equations of the probability amplitudes as a function of time in the momentum space:

$$\begin{aligned} i\dot{C}_p^b(t) &= \left[ \Omega_+ e^{ik_e z_c(t) + i(2\beta - \mu)(\Omega t)} C_{p - \hbar k_e}^a(t) + \Omega_- e^{-ik_e z_c(t) - i(2\beta + \mu)(\Omega t)} C_{p + \hbar k_e}^a(t) \right] e^{i\alpha(t)} \\ i\dot{C}_p^a(t) &= \left[ \Omega_+^* e^{-ik_e z_c(t) - i(2\beta + \mu)(\Omega t)} C_{p + \hbar k_e}^b(t) + \Omega_-^* e^{ik_e z_c(t) + i(2\beta - \mu)(\Omega t)} C_{p - \hbar k_e}^b(t) \right] e^{-i\alpha(t)} \end{aligned} \quad (29)$$

where we have defined,

$$\beta = \frac{k_e p}{2m\Omega} \quad (30)$$

$$\mu = \frac{\hbar k_e^2}{2m\Omega} \quad (31)$$

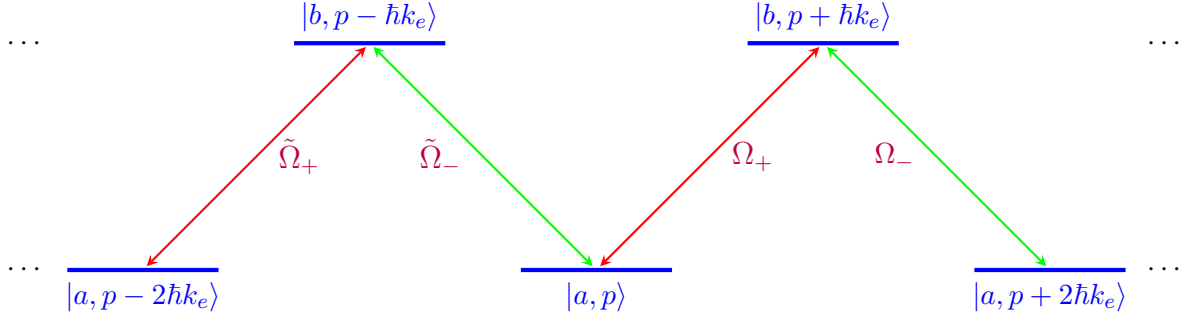


FIGURE 2.9. Scheme showing the possible states of the atom and the couplings between them.

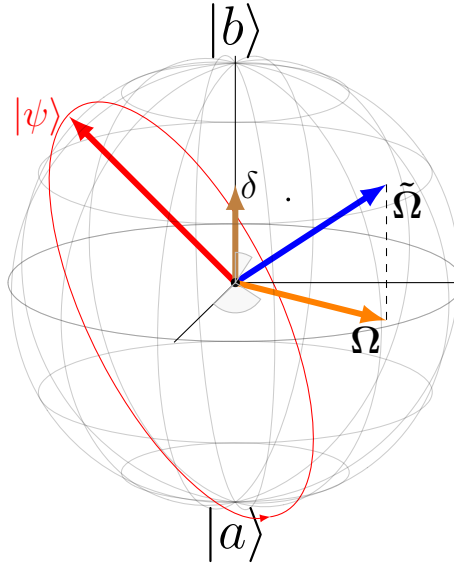


FIGURE 2.10. Bloch sphere representing Rabi Oscillations with a detuning  $\delta$ .

### 5. Parameters in a composite-light Mach-Zehnder Interferometer.

The fact that through the Raman transitions we can change the momentum state of an atom implies that now we have a new degree of freedom to work with. From this, instead of considering a system of two levels, as in Fig. (1.1), we have an array of infinite states, as illustrated at Fig. (2.9). The aim in this section is the definition of two of the three parameters that we consider to characterize the performance of the proposed Mach-Zehnder interferometer. The introduction of these parameters is done in an intuitive way, with the intention to compare our statements with numerical simulations given in the Chapter 3.

The dynamics of matter-radiation in a two level system can be visualized in the Bloch sphere [17]. In the Bloch sphere, any possible state  $|\psi\rangle$  of a two-level system is represented as a vector that lies in its surface, as illustrated at Fig. (2.10). In general, the dynamics of the state  $|\psi\rangle$  is described as a precession with respect to the Rabi vector, represented as  $\tilde{\Omega}$ , as illustrated in Fig. (2.10).

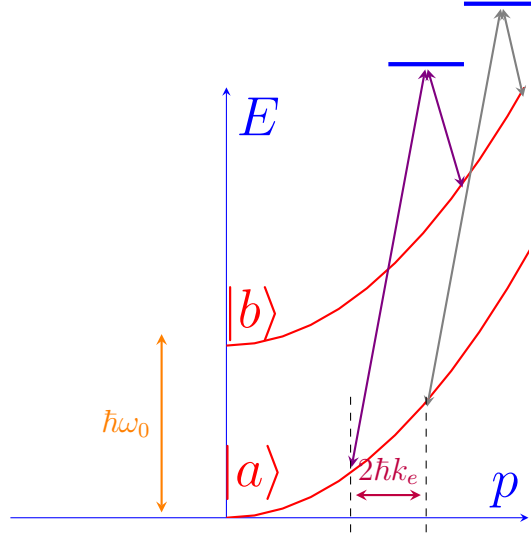


FIGURE 2.11. Scheme to obtain the detuning due to adjacent transitions.

Let's consider the situation where the laser frequency  $\omega_L$  is at resonance with the energy splitting of the two-level system  $\hbar\omega_{ab}$ , that is to say,  $\omega_{ab}$  and that as an initial condition the total population is at the ground state  $|a\rangle$ . In these conditions, the precession axis would lie in the equator of the Bloch's sphere, represented as the vector  $\Omega$  in Fig. (2.10). Then we can populate the state  $|b\rangle$  at a Rabi frequency  $\Omega$ .

If we now consider that there is a difference between the laser frequency and the transition energy then the precession axis lies outside the equatorial plane, because now it has a vertical component proportional to  $\delta$ , the value of the detuning frequency [17]. This has as a consequence that we cannot populate perfectly the excited state  $|b\rangle$ , as illustrated at Fig. 2.10 by the red path in the surface of the Bloch sphere, because it cannot pass through the north pole.

In this case, the angular frequency of the vector state  $|\psi\rangle$  in its dynamics is given by:

$$\begin{aligned}\tilde{\Omega} &= \sqrt{\Omega^2 + \delta^2}, \\ \tilde{\Omega} &\approx \Omega \left[ 1 + \frac{1}{2} \left( \frac{\delta}{\Omega} \right)^2 \right].\end{aligned}$$

This allows us to use the ratio between the Rabi frequency and the detuning as a parameter that quantifies the efficiency of the population from the ground state to the excited state in the case when the ratio  $\delta/\Omega < 1$ .

**5.1. The parameter  $\mu$ .** In the moment that the transition between the states  $|a, 0\rangle \leftrightarrow |b, 1\rangle$  is resonant through the correct frequency chirping (using the  $\alpha_+$  one), we also perform transitions between the states  $|a, -2\rangle \leftrightarrow |b, -1\rangle$  or between the states  $|a, 2\rangle \leftrightarrow |b, 3\rangle$ , and so on, as indicated schematically in the Fig. (2.9). The aim of this section is to determine a parameter that counts this detuning in the situation when we execute momentum jumps to the right with the Raman pair  $\Omega_+$ . The Fig. (2.11) represents a scheme of the situation described. The dispersion relation of a free particle is given by:

$$E = \frac{p^2}{2m}, \quad (32)$$

where  $E$  is the energy of the atom and  $p$  its momentum. This dispersion relation is represented by the red parabolas shown in Fig. (2.11), where the energy difference between them is precisely the hyperfine splitting  $\hbar\omega_0$ . The change in energy due to the transition  $|a, 0\rangle \leftrightarrow |b, 1\rangle$  is given by:

$$\begin{aligned} |a, 0\rangle &\leftrightarrow |b, 1\rangle, \\ \Delta E_1 &= \frac{(p + \hbar k_e)^2}{2m} - \frac{p^2}{2m}. \end{aligned}$$

In the other hand, the change in energy due to the adjacent transition  $|a, 2\rangle \leftrightarrow |b, 3\rangle$  is given by:

$$\begin{aligned} |a, 2\rangle &\leftrightarrow |b, 3\rangle, \\ \Delta E_2 &= \frac{(p + 3\hbar k_e)^2}{2m} - \frac{(p + 2\hbar k_e)^2}{2m}. \end{aligned}$$

The change in energy in these transitions is then:

$$\begin{aligned} \Delta E_\mu &= \Delta E_2 - \Delta E_1, \\ \Delta E_\mu &= 4\frac{\hbar^2 k_e^2}{2m}. \end{aligned}$$

From here, the detuning frequency  $\delta_\mu$  has the form:

$$\delta_\mu = 4\frac{\hbar k_e^2}{2m}.$$

Then, the ratio between the Rabi frequency and the detuning of the transition has the form:

$$\frac{\Omega}{\delta_\mu} = \frac{1}{4\mu}.$$

This implies that the population transition between the states  $|a, 2\rangle \leftrightarrow |b, 3\rangle$ , when the transition  $|a, 0\rangle \leftrightarrow |b, 1\rangle$  resonant is determined by the previously defined parameter  $\mu$ .

In the performance of our interferometer we want to minimize the transition between the states  $|a, 2\rangle \leftrightarrow |b, 3\rangle$  in the case when our frequency chirping makes the transition  $|a, 0\rangle \leftrightarrow |b, 1\rangle$  is resonant. For this reason we would want to make the ratio  $\Omega/\delta_\mu$  as small as possible. That is to say, we want the situation where:

$$\mu \gg 1. \quad (33)$$

Nevertheless, a simple observation would make this condition to change achieving the same aim with the choice of specific Rabi frequencies  $\Omega_n$  as is shown in the next subsection.

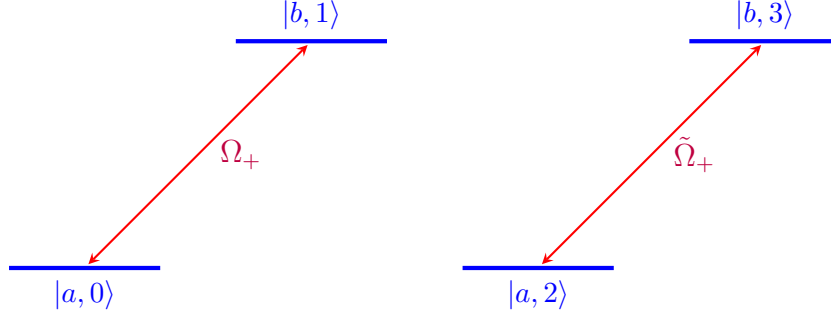


FIGURE 2.12. Scheme showing the possible states of the atom and the strongest couplings.

5.1.1. *Special Rabi Frequencies.* The Fig. (2.12) represents the situation where the transition  $|a, 0\rangle \leftrightarrow |b, 1\rangle$  is resonant. At the same time, we have that the states  $|a, 2\rangle \leftrightarrow |b, 3\rangle$  are coupled, but this transition is detuned with a Rabi frequency  $\tilde{\Omega}_+$  given by:

$$\begin{aligned}\tilde{\Omega}_+ &= \sqrt{\Omega^2 + 4 \left( \frac{\hbar k_e^2}{2m} \right)^2} \\ \tilde{\Omega}_\pm &= \Omega \sqrt{1 + 4\mu^2}.\end{aligned}\quad (34)$$

Now, let's suppose we want to perform a  $\pi$ -pulse between the states  $|a, 0\rangle \rightarrow |b, 1\rangle$ , and let us suppose that we also have initial population in the state  $|a, 2\rangle$ . From here, the probability of transition to the state  $|b, 3\rangle$  is proportional to  $\sin\left(\pi/2\tilde{\Omega}_+\right)$  [19]:

$$C_3^b(\tau_\pi) \propto \sin\left(\frac{\pi}{2}\sqrt{1 + 4\mu^2}\right).$$

We can establish the condition under which this quantity is always equal to zero making that:

$$\begin{aligned}\frac{\pi}{2}\sqrt{1 + 4\mu_n^2} &= n\pi \quad n = 1, 2, \dots \\ \mu_n^2 &= \frac{1}{4}(4n^2 - 1) \quad n = 1, 2, \dots\end{aligned}\quad (35)$$

This is a condition for the Rabi frequency, that is to mean, if we state that:

$$\begin{aligned}\frac{\Omega_n}{\tilde{\omega}_R} &= \frac{2}{\sqrt{3}}, \frac{2}{\sqrt{15}}, \frac{2}{\sqrt{35}}, \dots, \\ \tilde{\omega}_R &= \frac{\hbar k_e^2}{2m} = 4 \frac{\hbar k^2}{2m} = 4\omega_R,\end{aligned}\quad (36)$$

where  $\omega_R$  is the photon recoil frequency. We can perform  $2\pi$ -transitions between the states  $|a, 2\rangle \leftrightarrow |b, 3\rangle$  while at the same time we perform  $\pi$ -transitions between the states  $|a, 0\rangle \leftrightarrow |b, 1\rangle$ .

**5.2. The parameter  $\beta$ .** In the present subsection, we consider the fact that we begin in the realization of the Mach-Zehnder interferometer with an initial momentum distribution of the atomic cloud, as is illustrated in the Fig. (2.13).



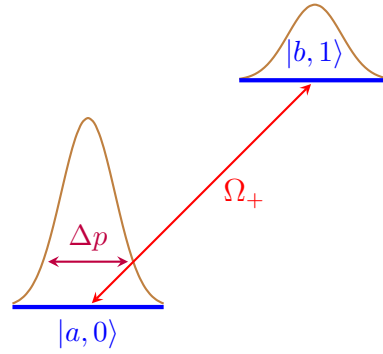


FIGURE 2.13. One of the initial conditions of our interferometer is that we have an initial momentum distribution in the state  $|a, 0\rangle$ , which introduces a new detuning parameter.

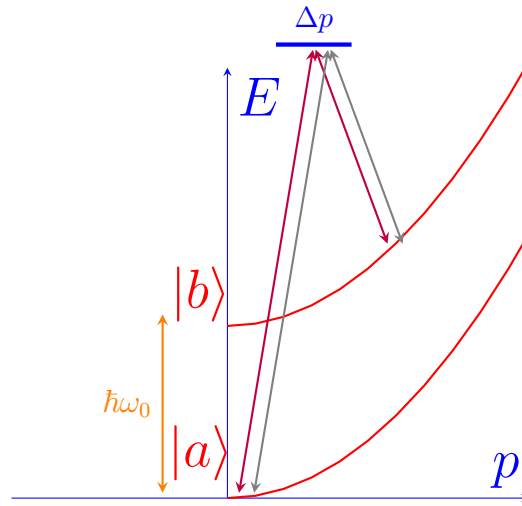


FIGURE 2.14. Diagram to obtain the detuning due to the width of the initial momentum distribution.

The energy diagram that illustrates this situation is depicted in the Fig. (2.14). Here again we have a situation where we want to make a transition from the state  $|a, 0\rangle$  to the state  $|b, 1\rangle$ , and we compare this with another transition from the state  $|a, \Delta\rangle = |a, p + \Delta p\rangle$  to the state  $|b, 1 + \Delta\rangle = |b, p + \hbar k_e + \Delta p\rangle$ .

In the transition  $|a, 0\rangle \leftrightarrow |b, 1\rangle$  the change in energy is given by  $\Delta E_1$ :

$$\begin{aligned} |a, 0\rangle &\leftrightarrow |b, 1\rangle \\ \Delta E_1 &= \frac{\hbar^2 k_e^2}{2m}. \end{aligned}$$

In the same direction, the difference in energy between the possible states  $|a, p + \Delta\rangle$  and  $|b, p + \Delta\rangle$  is given by  $\Delta E_2$ :

$$\begin{aligned} |a, p + \Delta\rangle &\leftrightarrow |b, p + \Delta\rangle \\ E_2 &= \frac{(\Delta p + \hbar k_e)^2}{2m} - \frac{(\Delta p)^2}{2m} \end{aligned}$$

The change in energy in this case,  $\Delta E_\beta$  is given by the expression:

$$\begin{aligned} \Delta E_\beta &= \Delta E_2 - \Delta E_1, \\ \Delta E_\beta &= 2 \left( \hbar \frac{k_e \Delta p}{2m} \right). \end{aligned}$$

The detuning frequency in this case  $\delta_\beta$  is given by:

$$\delta_\beta = \frac{k_e \Delta p}{m},$$

which indicates that is a detuning momentum-dependent, that is to say, if we have an initial momentum distribution, the different parts of the wave-function experiment Rabi oscillations with different Rabi frequencies, this explains the width of the peaks 1 and 1' in Fig. (2.4), due to this Doppler effect detuning. As consequence, the ratio between the Rabi frequency and the detuning has the value:

$$\frac{\Omega}{\delta_\beta} = \frac{1}{2\beta},$$

with  $\beta$  as defined in Eq. (30). To improve the interferometer performance, we establish that this ratio must be as great as possible, for which we establish the condition:

$$\beta \ll 1. \tag{37}$$

This implies that  $\beta$  is a perturbative parameter for our interferometer performance.



## CHAPTER 3

### Time-dependent perturbation theory in detuned Raman transitions.

The interaction of an atom with electric and magnetic fields changes the energy of the internal states. In the case of an electric field, in the situation when the detuning is much greater than the Rabi frequency  $\Omega \ll |\delta|$ , the energy shift for the ground state  $|a\rangle$  is [19]

$$\Delta E_a = \frac{\hbar\Omega^2}{4\delta},$$

and for the excited state  $|b\rangle$  is

$$\Delta E_b = -\frac{\hbar\Omega^2}{4\delta},$$

this has as consequence that the energy shifts are proportional to the intensity of the electric field that interacts with the atom. For instance, we would have a position dependent shift in energy if the atom interacts with a stationary wave and this energy gradient at the same time produces a net force in the atom, known as the dipole force [19].

The magnetic fields also can introduce energy shifts in the internal states of the atoms depending on the magnetic quantum number  $m_F$ . In the case of small magnetic field  $B$  the energy shift is given by the expression [11]

$$\Delta E_B = \mu_B g_F m_F B, \tag{38}$$

with  $\mu_B$  is the Bohr magneton and  $g_F$  is the Landé factor. The Eq. (38) implies that the energy shift is proportional to the magnitude of the magnetic field. The Fig. (3.2) represents the level scheme in

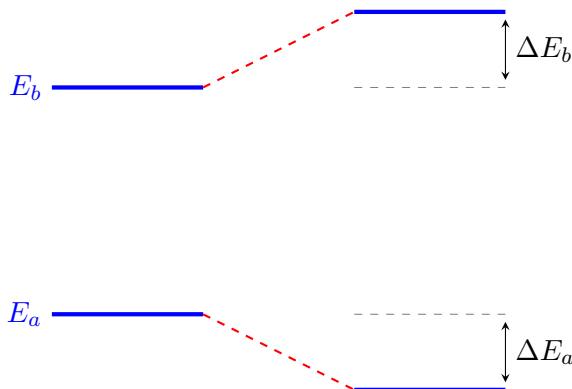


FIGURE 3.1. The interaction of an atom with an electric field produce energy shifts of it internal states.

$$\begin{aligned}
 |e\rangle &= \underline{|5P_{1/2}, F = 1, 2; m_F\rangle} \\
 |b\rangle &= \overline{|5S_{1/2}, F = 2, m_F = 0\rangle} \\
 |a\rangle &= \overline{|5S_{1/2}, F = 1, m_F = 0\rangle}
 \end{aligned}$$

FIGURE 3.2. Scheme of Rb<sup>87</sup> states involved in the experimental setup

Rb<sup>87</sup> used in atomic interferometry. The states  $|a\rangle$  and  $|b\rangle$  are insensible to magnetic fields. As in the next section will be shown, the accumulation of phase due to the gravitational interaction occurs in the the superposition between state  $|a\rangle$  and  $|b\rangle$ , from which there is no energy shift due to external magnetic fields in this interferometric design.

The fluctuations in amplitude of electromagnetic fields produce energy shifts in internal atomic states, which implies phase difference fluctuations between the states  $|a\rangle$  and  $|b\rangle$ . These phase fluctuations introduce systematic errors in the fringes of atomic interferometers. In this chapter, using the momentum degree of freedom, we propose a Mach-Zehnder interferometer that corrects this issue through the phase accumulation in just one internal atomic level. Nevertheless, the interferometer proposed has multiple couplings between the states that must be accounted in the determination of the gravitational phase. We present an analytical method based in time-dependent perturbation theory to quantify the error involved in the detuned Raman transitions due to the Doppler effect.

## 1. Composite light Interferometry.

**1.1. Seven steps Interferometer.** With the aim that the phase accumulation due to the gravitational acceleration be insensible to external electromagnetic fields, it is proposed a seven-steps interferometer. The Fig. (3.3) shows a scheme that illustrates the steps of the interferometer. We introduce a change in the notation of the momentum states in the following form:

$$|j, n\rangle = |j, p + n\hbar k_e\rangle \quad \text{with } j = a, b.$$

Let us consider the first two steps done in it:

- (1) The initial condition is that the whole population of the interferometer is in the state  $|a, 0\rangle$ . The Fig. (3.4) shows this situation, and we configure the chirping in frequency to make the transition  $|a, 0\rangle \leftrightarrow |b, 1\rangle$  resonant driven by the laser pair represented by  $\Omega_+$ .

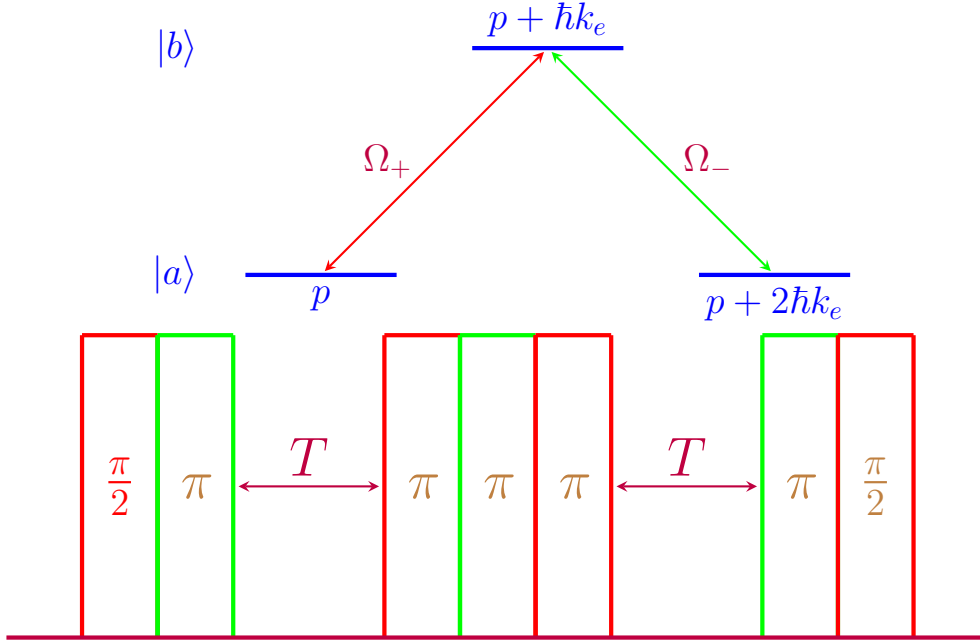


FIGURE 3.3. Scheme of the seven steps Mach-Zehnder Interferometer proposed insensitive to external electromagnetic fluctuations. The colors red and green suggest the pair that is resonant in each pair. Red for  $\Omega_+$  and green for  $\Omega_-$ .

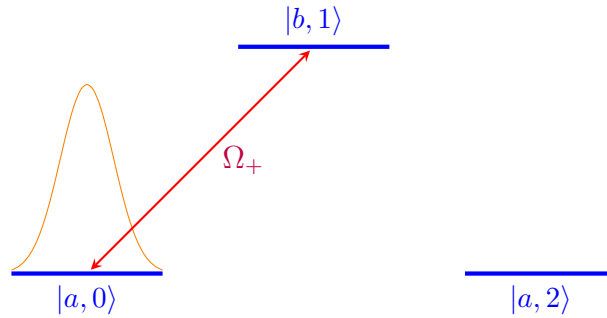


FIGURE 3.4. Initial configuration of the probability amplitude of the states at the beginning of the First Pulse.

This pulse, according to Fig. (3.3) corresponds to a  $\pi/2$  pulse, from here, at the end of this first interferometric step we get a superposition of the states  $|a, 0\rangle$  and  $|b, 1\rangle$ .

- (2) To perform the second pulse, now we make the pair  $\Omega_-$  resonant with the transition  $|b, 1\rangle \leftrightarrow |a, 2\rangle$ , as shown in the Fig. (3.5).

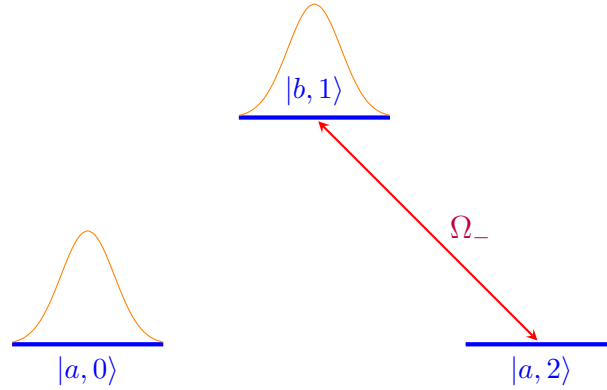


FIGURE 3.5. Initial configuration of the probability amplitude of the states before we have the second pulse-step done.

For this case, we perform a  $\pi$ -pulse that transfers the population from the state  $|b, 1\rangle$  to the state  $|a, 2\rangle$ . If we use one of the special Rabi frequencies deduced in the Chapter 2, we guarantee that the population of the state  $|a, 0\rangle$  remains the same, and its amplitude gains a phase proportional to the parameter  $\mu$  (this will be developed in the next sections). At the end, we obtain a superposition between the states  $|a, 0\rangle$  and  $|a, 2\rangle$ , as is illustrated in Fig. (3.6).

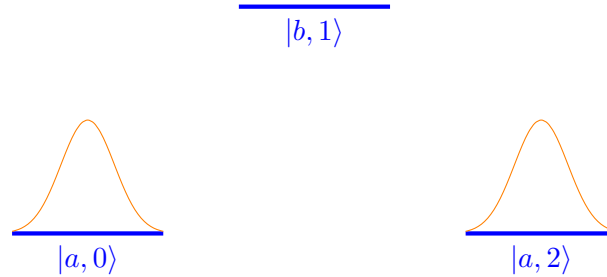


FIGURE 3.6. Final configuration of the probability amplitudes of the states after we apply the second pulse-step.

- (3) It is in this point that the gravitational phase accumulation occurs. As the superposition obtained is in the same internal atomic state, then the energy shifts are the same in both states,  $|a, 0\rangle$  and  $|a, 2\rangle$ , and the associated phase shifts are not printed in the final phase of the interferometer.

**1.2. Spurious transitions in the interferometer.** The schematic of a Mach-Zehnder atomic interferometer of composite light pulses presented at Fig. (3.3) only considers resonant transitions between the momentum states. Nevertheless, in the experiment proposed it is not possible to turn off a Raman pair when the other is turned on, that is to mean, if we have resonant the pair  $\Omega_+$  using the correct frequency tuning, also we have turned on the pair  $\Omega_-$ , and this fact introduces another transitions in our seven-steps interferometer.

This has as a consequence that there exists additional couplings between the states besides the adjacent ones produced by the resonant transitions driven by  $\Omega_+$  and  $\Omega_-$ . In fact, this problem is much more general now, in the sense that as we have now an infinite array of states, now all of them get coupled by the interactions with the Raman pairs  $\Omega_+$  and  $\Omega_-$ , as is shown in Fig. (3.7).

## 2. The parameters $\eta_i$ .

**2.1. The detuning due to the Doppler Effect.** Let us consider the first step of our seven-step interferometer, where we have the pair  $\Omega_+$  resonant with the transition  $|a, 0\rangle \leftrightarrow |b, 1\rangle$  by the use of the chirping frequency  $\alpha_+(t)$  Eq. (41). The situation is illustrated at Fig. (3.8).

In this first step, additionally to have the pair  $\Omega_+$  resonant, we have a coupling between the states  $|a, 0\rangle \leftrightarrow |b, -1\rangle$  due to the fact that we also have the Raman pair  $\Omega_-$  turned on but with the chirping frequency resonant to  $\Omega_+$ . From the application of

which means that the chirping introduces a phase given by  $e^{-ik_e z_c(t)}$ . From this, we deduce that there exists a Doppler detuning between these transitions (the first one resonant to the pair  $\Omega_+$  and the second driven by the second pair  $\Omega_-$  with a detuned Rabi frequency  $\tilde{\Omega}_-^1 = \Omega\sqrt{1 + \mu^2}$ ) given by:

$$\delta_\eta = 2k_e v(t). \quad (39)$$

This allows us to determine the ratio  $\Omega/\delta_\eta$  that quantifies the efficiency of the transition  $|a, 0\rangle \leftrightarrow |b, -1\rangle$ . And from here, we can define a new perturbative parameter  $\eta$  for the performance of our interferometer:

$$\begin{aligned} \eta &= \frac{\Omega}{\delta_\eta}, \\ \eta &= \frac{\Omega}{2k_e v_c(t)}. \end{aligned}$$

In general, the introduction of these spurious states to our resonant evolution can in general generate additional phases to our Mach-Zehnder Interferometer that we must take into account. Nevertheless, we can define  $\eta$  as a perturbative parameter with the aim to minimize these non-desired transitions, so from an experimental viewpoint, we need to establish:

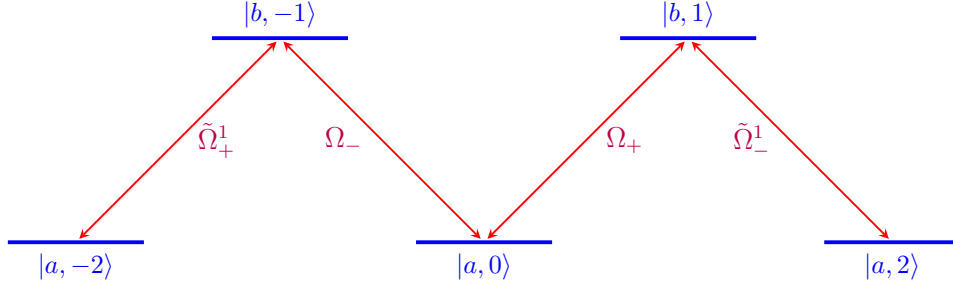
$$\eta \ll 1.$$

## 3. Perturbative solution to the Schrödinger's Equation.

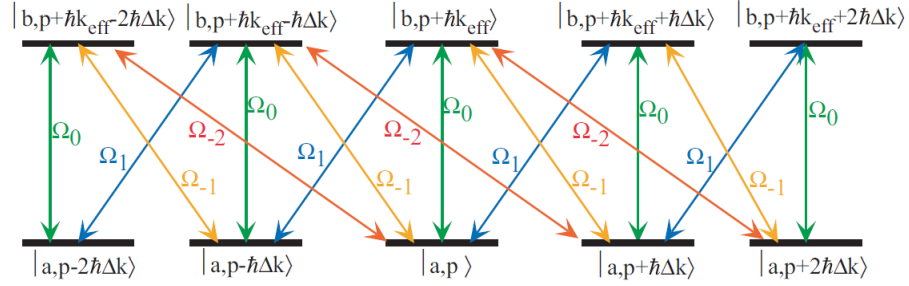
The Eqs. (29) determine the dynamics of the states  $|a, 0\rangle$  and  $|b, 0\rangle$  which depends on adjacent momentum states of the contrary internal state. That is to mean, for instance, the evolution for  $|a, 0\rangle$  depends on the dynamics of the states  $|b, -1\rangle$  and  $|b, 1\rangle$ , and so on. This has as consequence that in fact, all the states of the array of momentum states get coupled, but in different hyperfine levels. The aim of the present section is to determine the hierarchy of the couplings using a time-dependent perturbative approach.

**3.1. The Dynamical Equations.** We can generalize the Eqs. (29) with the objective to describe the evolution of any momentum-internal state:





(A) Scheme of a coupling between all the states of the momentum degree of freedom.



(B) Coupling between the momentum states due to a modulated laser, as shown by [2].

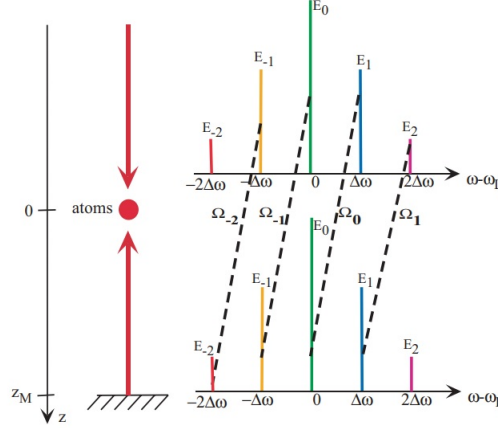
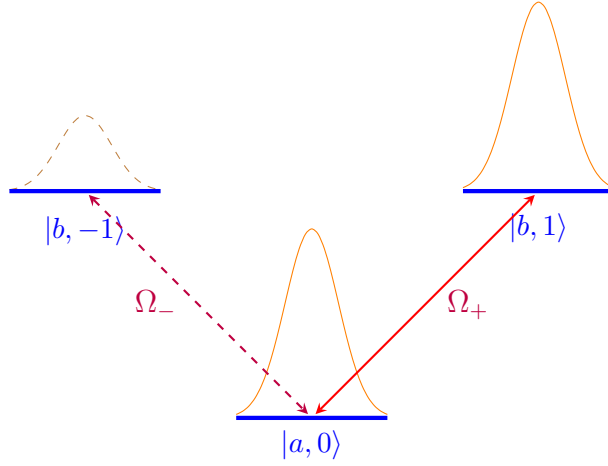
(C) In the situation presented by [2], there exist multiple counterpropagating Raman pairs, the dashed lines represent each pair. In this case, for instance, we have the coupling between the states  $|a, p\rangle \leftrightarrow |b, p + \hbar k_{\text{eff}} + n\hbar\Delta k\rangle$  with  $k_{\text{eff}} = (2\Omega_L + \Delta\omega)/c$  and  $\Delta k = 2\Delta\omega/c$ .

FIGURE 3.7. The interaction of a modulated laser with an atom implies a multilevel coupling in momentum states. In Fig. (3.7a) is shown the coupling when we take into account one couple of side-bands of a modulated laser, where  $\tilde{\Omega}_{\pm}^1 = \Omega\sqrt{1 + 4\mu^2}$ . The Fig. (3.7b) shows the case when we have multiple side-band frequencies from a modulated laser. The Fig. (3.7c) illustrates the difference between the reference [2] and the present work, because they consider the multiple sidebands pairs of just one Raman pair, neglecting the other one due to Doppler effect. We consider two Raman pairs with one pair of sidebands each one.

FIGURE 3.8. Configuration of states where  $\Omega_+$  is the resonant pulse.

$$\begin{aligned}
i\dot{C}_{p+n\hbar k_e}^{b} &= \left[ \Omega_+ e^{ik_e z_c(t) + i[2\beta + (2n-1)\mu](\Omega t)} C_{p+(n-1)\hbar k_e}^a(t) \right. \\
&\quad \left. + \Omega_- e^{-ik_e z_c(t) - i[2\beta + (2n+1)\mu](\Omega t)} C_{p+(n+1)\hbar k_e}^a(t) \right] e^{i\alpha(t)}, \\
i\dot{C}_{p+n\hbar k_e}^a &= \left[ \Omega_+^* e^{-ik_e z_c(t) - i[2\beta + (2n+1)\mu](\Omega t)} C_{p+(n+1)\hbar k_e}^b(t) \right. \\
&\quad \left. + \Omega_-^* e^{ik_e z_c(t) + i[2\beta + (2n-1)\mu](\Omega t)} C_{p+(n-1)\hbar k_e}^b(t) \right] e^{-i\alpha(t)}.
\end{aligned} \tag{40}$$

There is a very important feature about Eqs. (40), and that is the use of the chirping frequency  $\alpha(t)$ . In the experiment, we use this chirping to have resonant one of the pairs  $\Omega_+$  or  $\Omega_-$ , depending which step of the Mach-Zehnder interferometer we want to perform Fig. (3.3). We separate two chirping frequencies  $\alpha_+(t)$  and  $\alpha_-(t)$  depending if we make the pair  $\Omega_+$  or  $\Omega_-$  to be resonant:

$$\alpha_+(t) = -k_e z_c(t) - \mu(\Omega t), \tag{41}$$

$$\alpha_-(t) = k_e z_c(t) + 3\mu(\Omega t). \tag{42}$$

The chirping  $\alpha_+(t)$  Eq. (41) makes the transition  $|a, 0\rangle \leftrightarrow |b, 1\rangle$  resonant, while the second chirping  $\alpha_-(t)$  Eq. (42) makes the transition  $|a, 2\rangle \leftrightarrow |b, 1\rangle$  resonant. Below, we define the next matrices in the corresponding basis:

$$\hat{H}_0(t) = \begin{bmatrix} & |a, -2\rangle & |b, -1\rangle & |a, 0\rangle & |b, 1\rangle & |a, 2\rangle & \\ \cdots & \vdots & \vdots & \vdots & \vdots & \vdots & \ddots \\ \cdots & 0 & D_{-4} & 0 & 0 & 0 & \cdots \langle a, -2| \\ \cdots & D_{-4}^* & 0 & I_{-2}^* & 0 & 0 & \cdots \langle b, -1| \\ \cdots & 0 & I_{-2} & 0 & D_0 & 0 & \cdots \langle a, 0| \\ \cdots & 0 & 0 & D_0^* & 0 & I_2^* & \cdots \langle b, 1| \\ \cdots & 0 & 0 & 0 & I_2 & 0 & \cdots \langle a, 2| \\ \cdots & \vdots & \vdots & \vdots & \vdots & \vdots & \ddots \end{bmatrix} \quad (43)$$

$$D_n = \Omega_+^* e^{-2i(\beta+n\mu)(\Omega t)},$$

$$I_n = \Omega_-^* e^{2i[\beta+(n-2)\mu](\Omega t)}.$$

$$\hat{V}(t) = \begin{bmatrix} & |a, -2\rangle & |b, -1\rangle & |a, 0\rangle & |b, 1\rangle & |a, 2\rangle & \\ \cdots & \vdots & \vdots & \vdots & \vdots & \vdots & \ddots \\ \cdots & 0 & R_{-2} & 0 & 0 & 0 & \cdots \langle a, -2| \\ \cdots & R_{-2}^* & 0 & L_{-2}^* & 0 & 0 & \cdots \langle b, -1| \\ \cdots & 0 & L_{-2} & 0 & R_0 & 0 & \cdots \langle a, 0| \\ \cdots & 0 & 0 & R_0^* & 0 & L_0^* & \cdots \langle b, 1| \\ \cdots & 0 & 0 & 0 & L_0 & 0 & \cdots \langle a, 2| \\ \cdots & \vdots & \vdots & \vdots & \vdots & \vdots & \ddots \end{bmatrix} \quad (44)$$

$$L_n = \Omega_-^* e^{2ik_e z_c(t) + 2i[\beta+(n+2)\mu](\Omega t)},$$

$$R_n = \Omega_+^* e^{-2ik_e z_c(t) - 2i[\beta+(n+2)\mu](\Omega t)}.$$

The situation that we are considering is presented in Fig. (3.7a). Based on the Eqs. (40), we can express the dynamics of the vector of amplitude probabilities  $\mathbf{C}(t)$ :

$$i\dot{\mathbf{C}}(t) = \hat{H}(t)\mathbf{C}(t), \quad (45)$$

where we have:

$$\hat{H}(t) = \hat{H}_0(t) + \hat{V}(t), \quad (46)$$

where the matrices  $\hat{H}_0$  and  $\hat{V}(t)$  are defined according to Eqs. (43) and (44), with the convention that when we apply the chirping frequency  $\alpha_+(t)$  we have the orange entries in both matrices and the remaining entries are zero, and equivalently, when we apply the chirping frequency  $\alpha_-(t)$  we have the purple entries in both matrices and the remaining entries are zero.

$$\alpha_+(t) \rightarrow \text{orange}$$

$$\alpha_-(t) \rightarrow \text{purple}$$

**3.2. The Dyson series.** The solution of the Eq. (45) takes into account the causality expressed in the non-commutativity of the Hamiltonian  $\hat{H}(t)$  at different times  $t_1$  and  $t_2$ . The solution to Eq. (45) can be expressed in its corresponding time evolution operator  $\hat{U}(t, t_0)$  as [13]:

$$\hat{U}(t, t_0) = \hat{1} + (-i) \int_{t_0}^t dt_1 \hat{H}(t_1) + (-i)^2 \int_{t_0}^t dt_1 \int_{t_0}^{t_1} dt_2 \hat{H}(t_1) \hat{H}(t_2) + \dots \quad (47)$$

where  $t_0$  is the initial time. The Eq. (47) is known as the Dyson series and is commonly known as the time dependent perturbation theory. We can replace the decomposition of Eq. (46) into the Eq. (47) to get:

$$\begin{aligned} \hat{U}(t, t_0) = & \hat{1} + (-i) \int_{t_0}^t dt_1 \left( \hat{H}_0(t_1) + \hat{V}(t_1) \right) \\ & + (-i)^2 \int_{t_0}^t dt_1 \int_{t_0}^{t_1} dt_2 \left( \hat{H}_0(t_1) + \hat{V}(t_1) \right) \left( \hat{H}_0(t_2) + \hat{V}(t_2) \right) + \dots \end{aligned} \quad (48)$$

From Eq. (48), we make the next reordenation in the Dyson series to re-write the solution:

- (1) We take all the products that only have the identity and the matrix  $\hat{H}_0(t)$ , and we call the resultant operator  $\hat{U}_0(t, t_0)$ :

$$\hat{U}_0(t, t_0) = \hat{1} + (-i) \int_{t_0}^t dt_1 \hat{H}_0(t_1) + (-i)^2 \int_{t_0}^t dt_1 \int_{t_0}^{t_1} dt_2 \hat{H}_0(t_1) \hat{H}_0(t_2) + \dots \quad (49)$$

- (2) We take all the products where  $\hat{V}(t)$  is evaluated only in the time  $t_1$ :

$$\begin{aligned} & (-i) \int_{t_0}^t dt_1 \hat{V}(t_1) + (-i)^2 \int_{t_0}^t dt_1 \int_{t_0}^{t_1} dt_2 \hat{V}(t_1) \hat{H}_0(t_2) + \dots \\ = & (-i) \int_{t_0}^t dt_1 \hat{V}(t_1) \left\{ \hat{1} + (-i) \int_{t_0}^{t_1} dt_2 \hat{H}_0(t_2) \dots \right\} \\ = & (-i) \int_{t_0}^t dt_1 \hat{V}(t_1) \hat{U}_0(t_1, t_0) \end{aligned}$$

- (3) we can follow the same procedure taking  $\hat{V}(t)$  evaluated at different progressive times  $t_2, t_3$  successively.

$$\begin{aligned} & (-i)^2 \int_{t_0}^t dt_1 \int_{t_0}^{t_1} dt_2 \hat{H}_0(t_1) \hat{V}(t_2) \hat{U}_0(t_2, t_0) \\ & (-i)^3 \int_{t_0}^t dt_1 \int_{t_0}^{t_1} dt_2 \int_{t_0}^{t_2} dt_3 \hat{H}_0(t_1) \hat{H}_0(t_2) \hat{V}(t_3) \hat{U}_0(t_3, t_0) \end{aligned}$$

This reordenation allows us to express the time-evolution operator as:

$$\begin{aligned} \hat{U}(t, t_0) = & \hat{U}_0(t, t_0) + (-i) \int_{t_0}^t dt_1 \hat{V}(t_1) \hat{U}_0(t_1, t_0) \\ & + \sum_{n=2}^{\infty} (-i)^n \int_{t_0}^t dt_1 \dots \int_{t_0}^{t_{n-1}} dt_n \prod_{k=1}^{n-1} \left[ \hat{H}_0(t_k) + \hat{V}(t_k) \right] \hat{V}(t_n) \hat{U}_0(t_n, t_0). \end{aligned} \quad (50)$$

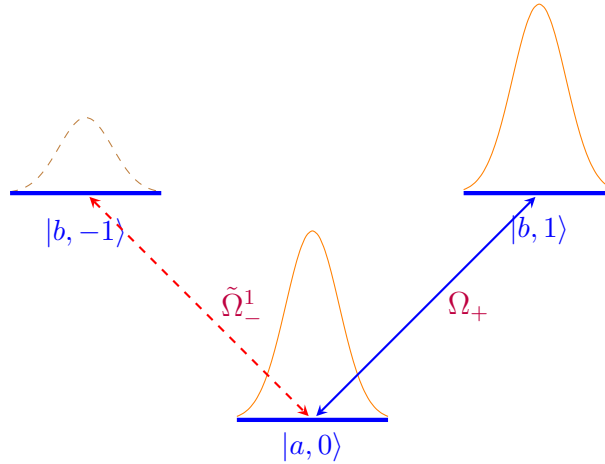


FIGURE 3.9. Situation when we have the pair  $\Omega_+$  resonant and the Raman pair  $\Omega_-$  drives a perturbative transition  $|a, 0\rangle \leftrightarrow |b, -1\rangle$ . Here, we define  $\tilde{\Omega}_{\pm}^n = \Omega \sqrt{1 + (2n)\mu}$

The reordering of the Dyson series Eq. (50) has an important feature that shares with the time-independent perturbation theory, that is, the expansion in power series of a perturbative parameter  $\lambda$ . That is to mean, each term in the series is proportional to this perturbative parameter. This fact will be illustrated at the next section.

**3.3. Stationary Phase Approximation.** The stationary phase approximation is a method to solve integrals when the integrand functions have a prominent oscillatory behavior [20]. The method is based in the observation that when we weight a given function  $f(t)$  with a sinusoidal function, in average we get zero. Then, we can consider the integral only in regions where the phase of the sinusoidal function is most flat, or in other words, when it takes a stationary behavior. Under the approximation, we have:

$$\int_a^b f(x) e^{ikg(x)} dx \approx \frac{1}{ik} \left[ \frac{f(b)}{g'(b)} e^{ikg(b)} - \frac{f(a)}{g'(a)} e^{ikg(a)} \right]. \quad (51)$$

With the aim to illustrate the perturbative expansion, let us suppose that we take the initial state  $|a, 0\rangle$  and we study the perturbative coupling  $|a, 0\rangle \leftrightarrow |b, -1\rangle$ . In this situation, we can monitor the coupling  $|a, 0\rangle \leftrightarrow |b, -1\rangle$  through calculating the probability transition  $\langle b, -1 | \hat{U}(t, 0) | a, 0 \rangle$ :

- (1) **zeroth order of approximation.** From the Eq. (50) the first term of the series would have the value:

$$\langle b, -1 | \hat{U}_0(t, 0) | a, 0 \rangle = 0,$$

because as we have that  $\hat{U}_0(t, 0)$  counts for the resonant couplings and in this case the pair  $\Omega_+$  doesn't couple the states  $|a, 0\rangle \leftrightarrow |b, -1\rangle$ , this term must be zero.

- (2) **First order approximation.** In the first order approximation, we would have that the coupling is:

$$\begin{aligned}
& (-i) \langle b, -1 | \int_{t_0}^t dt_1 \hat{V}(t_1) \hat{U}_0(t_1, t_0) | a, 0 \rangle \\
& (-i) \int_{t_0}^t dt_1 \langle b, -1 | \hat{V}(t_1) \hat{U}_0(t_1, t_0) | a, 0 \rangle \\
& (-i) \int_{t_0}^t dt_1 \langle b, -1 | \hat{V}(t_1) \left( \sum_n |a, n\rangle \langle a, n| + \sum_m |b, m\rangle \langle b, m| \right) \hat{U}_0(t_1, t_0) | a, 0 \rangle,
\end{aligned}$$

nevertheless, as it is shown by the orange part of the Eq. (44),  $\hat{V}(t)$  only can couple the states  $|b, -1\rangle \leftrightarrow |a, 0\rangle$ , then, from this summation, only the term  $n = 0$  can survive, and the remaining are zero. From here, we have that at the first order approximation:

$$(-i) \int_{t_0}^t dt_1 \langle b, -1 | \hat{V}(t_1) | a, 0 \rangle \langle a, 0 | \hat{U}_0(t_1, t_0) | a, 0 \rangle,$$

in this case, we have:

$$\begin{aligned}
\langle b, -1 | \hat{V}(t_1) | a, 0 \rangle &= L_{-2}^* \\
\langle b, -1 | \hat{V}(t_1) | a, 0 \rangle &= \Omega_- e^{-2ik_e z_c(t_1) - 2i\beta(\Omega t_1)}
\end{aligned}$$

$$\langle a, 0 | \hat{U}_0(t_1, t_0) | a, 0 \rangle = e^{-i\beta(\Omega t_1)} [\cos(\Omega t_1) + i\beta \sin(\Omega t_1)]$$

Then, we have:

$$\begin{aligned}
& (-i) \int_{t_0}^t dt_1 \Omega_- e^{-2ik_e z_c(t_1) - 2i\beta(\Omega t_1)} e^{-i\beta(\Omega t_1)} [\cos(\Omega t_1) + i\beta \sin(\Omega t_1)] \\
& = (-i) \Omega_- \int_{t_0}^t dt_1 e^{-2ik_e z_c(t_1) - 3i\beta(\Omega t_1)} [\cos(\Omega t_1) + i\beta \sin(\Omega t_1)]
\end{aligned}$$

Applying the stationary phase approximation, we obtain for the integral:

$$\begin{aligned}
& (-i)\Omega_- \left\{ \frac{1}{ik_e} \left[ \frac{\cos(\Omega t) + i\beta \sin(\Omega t)}{-2v_c(t) - \frac{3\beta\Omega}{k_e}} e^{-2ik_e z_c(t) - 3i\beta(\Omega t)} \right. \right. \\
& \quad \left. \left. - \frac{\cos(\Omega t_0) + i\beta \sin(\Omega t_0)}{-2v_c(t_0) - \frac{3\beta\Omega}{k_e}} e^{-2ik_e z_c(t_0) - 3i\beta(\Omega t_0)} \right] \right\} \\
&= \frac{\Omega_-}{2k_e v_c(t)} \left\{ \frac{\cos(\Omega t) + i\beta \sin(\Omega t)}{1 + 3\beta \frac{\Omega}{2k_e v_c(t)}} e^{-2ik_e z_c(t) - 3i\beta(\Omega t)} \right. \\
& \quad \left. - \frac{\cos(\Omega t_0) + i\beta \sin(\Omega t_0)}{\frac{v_c(t_0)}{v_c(t)} + 3\beta \frac{\Omega}{2k_e v_c(t)}} e^{-2ik_e z_c(t_0) - 3i\beta(\Omega t_0)} \right\} \\
&= \eta(t) \left\{ \frac{\cos(\Omega t) + i\beta \sin(\Omega t)}{1 + 3\beta\eta(t)} e^{-2ik_e z_c(t) - 3i\beta(\Omega t)} \right. \\
& \quad \left. - \frac{\cos(\Omega t_0) + i\beta \sin(\Omega t_0)}{\frac{v_c(t_0)}{v_c(t)} + 3\beta\eta(t)} e^{-2ik_e z_c(t_0) - 3i\beta(\Omega t_0)} \right\}.
\end{aligned}$$

Eliminating perturbative terms of second order  $\eta(t)\beta$  and making the approximation  $v_c(t_0)/v_c(t) \approx 1^1$ , our approximation gives the result for the first order in  $\eta(t)$ :

$$\begin{aligned}
& \eta(t) \left\{ \cos(\Omega t) e^{-2ik_e z_c(t) - 3i\beta(\Omega t)} - \cos(\Omega t_0) e^{-2ik_e z_c(t_0) - 3i\beta(\Omega t_0)} \right\} \\
& \approx \eta(t) e^{-2ik_e z_c(t) - 3i\beta(\Omega t)} \{ \cos(\Omega t) - \cos(\Omega t_0) \}, \tag{52}
\end{aligned}$$

assuming that  $z_c(t) \approx z_c(t_0)$  and  $t \approx t_0$ . This result allows us to conclude that the transition from the state  $|a, 0\rangle$  to the state  $|b, -1\rangle$  is proportional (at first order) to the perturbative parameter  $\eta(t)$ , and that if we want to minimize this transition, we should have the center of mass velocity  $v_c(t)$  as great as possible. Additionally, we stress out that under these approximations, we obtain the term

$$\eta(t) e^{-2ik_e z_c(t) - 3i\beta(\Omega t)}.$$

proportional to the solution of the integration at time  $t_1$ .

This last observation has an important implication because, if we consider the greatest of the second order approximation according to Eq. (50):

$$(-i)^2 \int_{t_0}^t dt_1 \hat{H}_0(t_1) \underbrace{\int_{t_0}^{t_1} dt_2 \hat{V}(t_2) \hat{U}(t_2, t_0)}_{\propto \eta(t_1) e^{\pm 2ik_e z_c(t_1)}}$$

Then, making the integration with respect to the variable  $t_1$  we obtain only terms of second order:

$$\eta(t)\eta(t_0) \quad \text{or} \quad \eta^2(t).$$

---

<sup>1</sup>This approximation is valid in the time intervals of duration of a  $\pi$ - or  $\pi/2$ -pulse.

which means that the order of the perturbative parameter  $\eta$  depends on how much we integrate any entry of the matrix  $\hat{V}(t)$ . In synthesis, the order of the approximation (measured as the number of times that the perturbative parameter  $\eta$  appears at the end of the integration) will be given by the nearest time  $t_n$  to  $t_0$  in the reordenation made of the Dyson series given by Eq. (50), because we have explicitly to integrate the term  $\hat{V}(t_n)$ .

#### 4. Temporal symmetry of the amplitude probability equations.

In the present section we study temporal translations of the amplitude probability equations as a general mechanism of determination of additional phases given by the application of the frequency chirps and the dark times  $T$  in the Mach-Zehnder interferometer given in Fig. (3.3). Let us consider the amplitude probability Eqs. (40). There is involved a phase with  $z_c(t)$ . We define:

$$z_c(v_0, t) = v_0 t + \frac{1}{2} g t^2.$$

If we perform a temporal translation:

$$t \rightarrow t' + T,$$

where  $t'$  is the new temporal variable and  $T$  is a constant. If we apply this temporal shift to the quantities involved in Eq. (40), we have:

$$\begin{aligned} \dot{C}_{p+n\hbar k_e}^b &= \frac{dC_{p+n\hbar k_e}^b}{dt} \rightarrow \dot{C}_{p+n\hbar k_e}^b = \frac{dC_{p+n\hbar k_e}^b}{dt'}, \\ \dot{C}_{p+n\hbar k_e}^a &= \frac{dC_{p+n\hbar k_e}^a}{dt} \rightarrow \dot{C}_{p+n\hbar k_e}^a = \frac{dC_{p+n\hbar k_e}^a}{dt'}, \\ z_c(v_0, t) &\rightarrow z_c(v_0, t' + T), \\ &\rightarrow v_0(t' + T) + \frac{1}{2} g(t' + T)^2, \\ &\rightarrow v_0 T + \frac{1}{2} g T^2 + (v_0 + gT)t' + \frac{1}{2} g t'^2, \\ z_c(v_0, t) &\rightarrow z_c(v_0, T) + z_c(v_0 + gT, t'). \end{aligned} \quad (53)$$

The Eq. (53) tells us that the transformation of the position can be separated into a term that is independent of the variable  $t'$  and one that is the position at time  $t'$  with the corresponding velocity recalibration  $v_0 \rightarrow v_0 + gT$ . Consequently, for the frequency chirping  $\alpha_{\pm}$ , we have that:

$$\alpha_{\pm}(t) = \mp k_e \tilde{z}_c(t) + m\mu(\Omega t),$$

where,

$$\tilde{z}_c(t) = v_0 t + \frac{1}{2} g' t^2$$

and.

$$m = \begin{cases} -1, & \text{for } \alpha_+, \\ +3, & \text{for } \alpha_-. \end{cases}$$



Under the transformation, we obtain that

$$\begin{aligned}
\alpha_{\pm}(t) &\rightarrow \alpha_{\pm}(t' + T) \\
\alpha_{\pm}(t' + T) &= \mp k_e \tilde{z}_c(t' + T) + m\mu [\Omega(t' + T)] \\
\alpha_{\pm}(t' + T) &= \mp k_e \tilde{z}_c(v_0, T) + m\mu(\Omega T) \mp k_e \tilde{z}_c(v_0 + g'T, t') + m\mu(\Omega t') \\
\alpha_{\pm}(t' + T) &= \alpha_{\pm}(v_0, T) + \alpha_{\pm}(v_0 + g'T, t')
\end{aligned} \tag{54}$$

Again for this case, we obtain that we can decomposed the transformed chirping frequency into two terms, the first one, independent of the variation parameter  $t'$  and another dependent of it. Here,  $g'$  represents the ramp value of gravitational acceleration, which can be changed by the experimenter. From Eqs. (53) and (54), we are ready to assign all the terms independent to the variable  $t'$  to the Rabi pairs, defining a transformation of these in the following way:

$$\begin{aligned}
\Omega_+ &\rightarrow \Omega_+(n, T) \\
\Omega_+(n, T) &= \Omega_+ e^{ik_e z_c(v_0, T) + i[2\beta + (2n-1)\mu](\Omega T) + i\alpha_{\pm}(v_0, T)}
\end{aligned} \tag{55}$$

And also,

$$\begin{aligned}
\Omega_- &\rightarrow \Omega_-(n, T) \\
\Omega_-(n, T) &= \Omega_- e^{-ik_e z_c(v_0, T) - i[2\beta + (2n+1)\mu](\Omega T) + i\alpha_{\pm}(v_0, T)}.
\end{aligned} \tag{56}$$

With this notation, the Eqs. (40) are transformed to the expressions:

$$\begin{aligned}
i\dot{C}_{p+n\hbar k_e}^{b} &= \left[ \Omega_+(n, T) e^{ik_e z_c(v_0 + gT, t') + i[2\beta + (2n-1)\mu](\Omega t')} C_{p+(n-1)\hbar k_e}^a(t' + T) \right. \\
&\quad \left. + \Omega_-(n, T) e^{-ik_e z_c(v_0 + gT, t') - i[2\beta + (2n+1)\mu](\Omega t')} C_{p+(n+1)\hbar k_e}^a(t' + T) \right] e^{i\alpha_{\pm}(v_0 + g'T, t')}, \\
i\dot{C}_{p+n\hbar k_e}^{a} &= \left[ \Omega_+^*(n, T) e^{-ik_e z_c(v_0 + gT, t') - i[2\beta + (2n+1)\mu](\Omega t')} C_{p+(n+1)\hbar k_e}^b(t' + T) \right. \\
&\quad \left. + \Omega_-^*(n, T) e^{ik_e z_c(v_0 + gT, t') + i[2\beta + (2n-1)\mu](\Omega t')} C_{p+(n-1)\hbar k_e}^b(t' + T) \right] e^{-i\alpha_{\pm}(v_0 + g'T, t')}.
\end{aligned} \tag{57}$$

The transformed Eqs. (57) have the same form as the Eqs. (40). This allows us to establish an invariance of the amplitude equations under time-translation, with the recalibration of the phases as in the dynamical part (dependent of  $t'$ ) as in the Rabi frequencies  $\Omega_+$  and  $\Omega_-$ . In the next chapter we will use these recalibrations to state additional approximations in the solution of the amplitude probability equations and most important, determining analytically the resultant phases of the seven steps Mach-Zehnder Interferometer.

## Quantum Gravimetry in a Composite-light Interferometer.

### 1. Perturbative solution to first order of the Mach-Zehnder interferometer of seven steps.

In the present section we apply the perturbative series solution (Eq. (50)) found in the last chapter to the seven steps of the Mach-Zehnder interferometer (Fig. (3.3)) to first order in the parameter  $\eta$ . Until this order, we have that the time-evolution operator  $\hat{U}(t, t_0)$  takes the form:

$$\hat{U}(t, t_0) = \hat{U}_0(t, t_0) + (-i) \int_{t_0}^t dt_1 \hat{V}(t_1) \hat{U}_0(t_1, t_0). \quad (58)$$

**1.1. First Pulse.** In the configuration of the seven steps Mach-Zehnder interferometer, as is shown in Fig. (3.3), the first step is a  $\pi/2$ -pulse having the Raman pair  $\Omega_+$  resonant, and the Raman pair  $\Omega_-$  detuned by the Doppler effect. The initial state for the interferometer is  $|a, 0\rangle$  and the initial situation is sketched in Fig. (4.1).

The resonant interaction given by the Raman pair  $\Omega_+$  couples the states  $|a, 0\rangle \leftrightarrow |b, 1\rangle$ , while the detuned Raman pair  $\Omega_-$  couples the states  $|b, -1\rangle \leftrightarrow |a, 0\rangle$  and  $|b, 1\rangle \leftrightarrow |a, 2\rangle$ . This has as consequence that, from Eq. (58), to first order we have perturbative populations at states  $|b, -1\rangle$  and  $|a, 2\rangle$ . Finally, at the end of the first pulse we have non-perturbative populations at states  $|a, 0\rangle$  and  $|b, 1\rangle$  and at the same time perturbative populations at states  $|b, -1\rangle$  and  $|a, 2\rangle$ , as illustrated at Fig. (4.2).

The probability amplitudes related to the perturbative states are determined by the corresponding quantites:

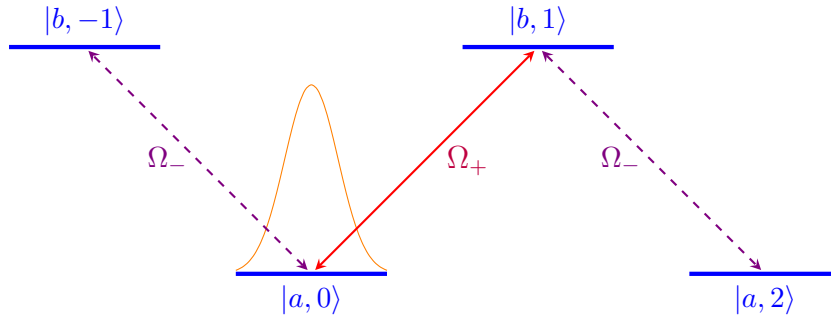


FIGURE 4.1. Initial configuration of the probability amplitude of the states at the beginning of the First Pulse. The dashed transitions denotes that is detuned by the Doppler effect.

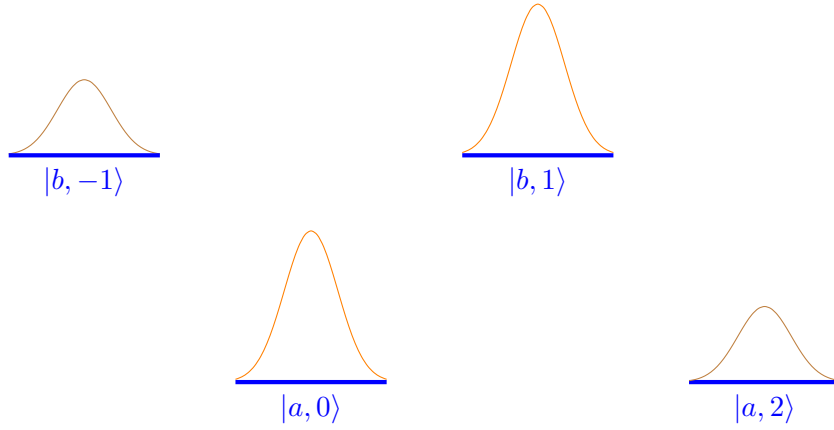


FIGURE 4.2. Final configuration of the probability amplitude of the states at the end of the first pulse.

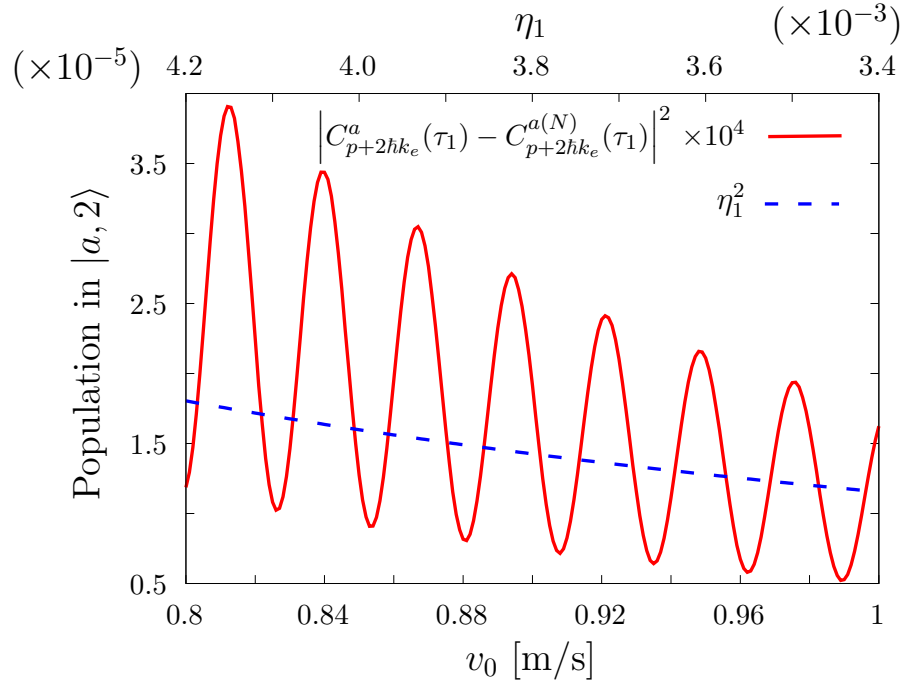


FIGURE 4.3. Population of state  $|a, 2\rangle$  as a function of the initial velocity. The red-solid line represents the squared difference between the analytical and the numerical ( $N$ ) solution at the end of the first pulse ( $\tau_1$ ) multiplied by  $10^4$ . The blue-dashed line corresponds to  $\eta_1^2$ .

$$\begin{aligned} C_{p-\hbar k_e}^b(\tau_1) &= \langle b, -1 | \hat{U}(\tau_1) | a, 0 \rangle, \\ C_{p+2\hbar k_e}^a(\tau_1) &= \langle a, 2 | \hat{U}(\tau_1) | a, 0 \rangle, \end{aligned}$$

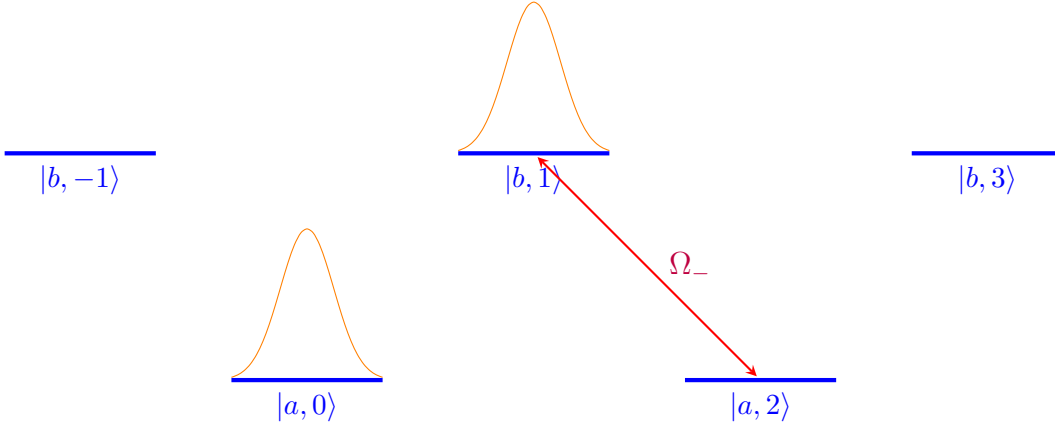


FIGURE 4.4. Initial configuration of the probability amplitude of the states before we apply the second pulse.

where  $\tau_1 = \pi/4\Omega$  for a  $\pi/2$ -pulse. We illustrated the result for  $C_{p-\hbar k_e}^b(\tau_1)$  in Eq. (52), which gives us the result:

$$C_{p-\hbar k_e}^b(\tau_1) = \eta_1 e^{-2ik_e z_c(\tau_1) - 3i\beta(\Omega\tau_1)} [\cos(\Omega\tau_1) - 1], \quad (59)$$

where we have defined  $\eta_1 = \eta(\tau_1)$ . Following a similar procedure for the amplitude probability  $C_{p+2\hbar k_e}^a(\tau_1)$  we deduce that:

$$C_{p+2\hbar k_e}^a(\tau_1) = i\eta_1 e^{2ik_e z_c(\tau_1) + i(3\beta+4\mu)(\Omega\tau_1)} \sin(\Omega\tau_1). \quad (60)$$

The Fig. (4.3) illustrates the error between the numerical solution (Appendix B) of the Eqs. (40) compared with our perturbative method according to Eq. (60), as a function of the initial velocity  $v_0$  of the atomic cloud for the case of the state  $|a, 2\rangle$ , and a very similar behavior resulted for the same comparison for the state  $|b, -1\rangle$ .

In general, from such figures we can check that the error decreases when we increase the initial velocity of the atomic cloud, which means that our approximation is better as  $\eta_1$  decreases. As our method is perturbative, it means that we suppose a power series solution of the form

$$\sum_n a_n \eta_1^n,$$

where  $a_n$  are constants. The Fig. (4.3) also shows the perturbative parameter  $\eta_1^2$  as a function of the initial velocity  $v_0$  of the atomic cloud. The error is well bounded by this parameter  $\eta_1^2$  (in four orders of magnitude), from which we conclude that the convergence of the series follows a behavior similar to a geometric series, as is expected from a perturbative expansion.<sup>1</sup>

<sup>1</sup>Los programas utilizados para ésta subsección se encuentran en la carpeta `First_Pulse`.

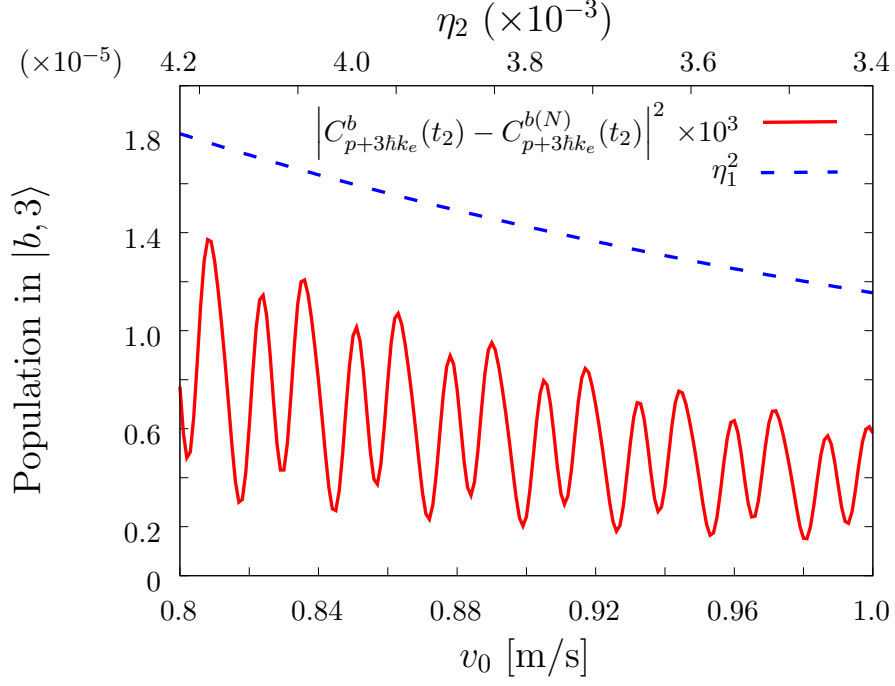


FIGURE 4.6. Error in amplitude of state  $|b, 3\rangle$  as a function of the initial velocity for the second pulse. The red-solid line represents the difference between the analytical and numerical ( $N$ ) solutions at the time  $t_2$  multiplied by  $10^3$ . The blue-dashed line corresponds to the perturbative parameter  $\eta_1^2$ .

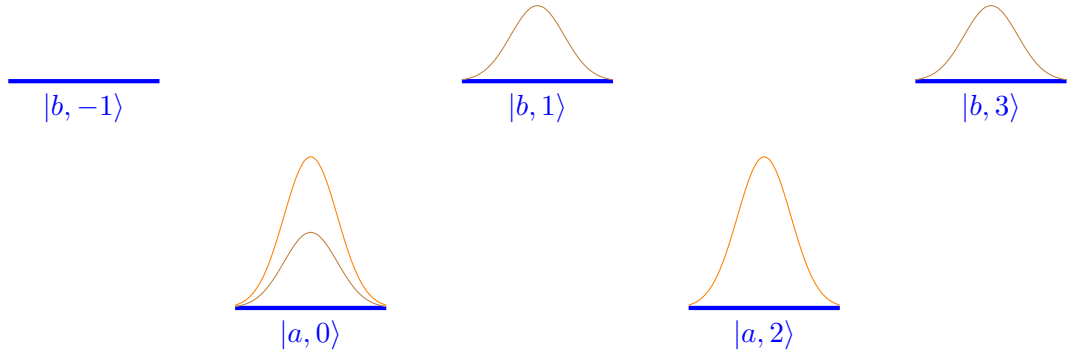


FIGURE 4.5. Final configuration of the probability amplitudes of the states after we have the second pulse-step done.

**1.2. Second Pulse.** The Figs. (4.4) and (4.5) shows the initial conditions and the final amplitudes, respectively, when the second pulse is performed in the interferometer sequence. The calculations to obtain the amplitudes of the states  $|a, 0\rangle$ ,  $|a, 2\rangle$  and  $|b, 3\rangle$  are in the Appendix C, along with the other perturbative amplitudes for the remaining pulses.

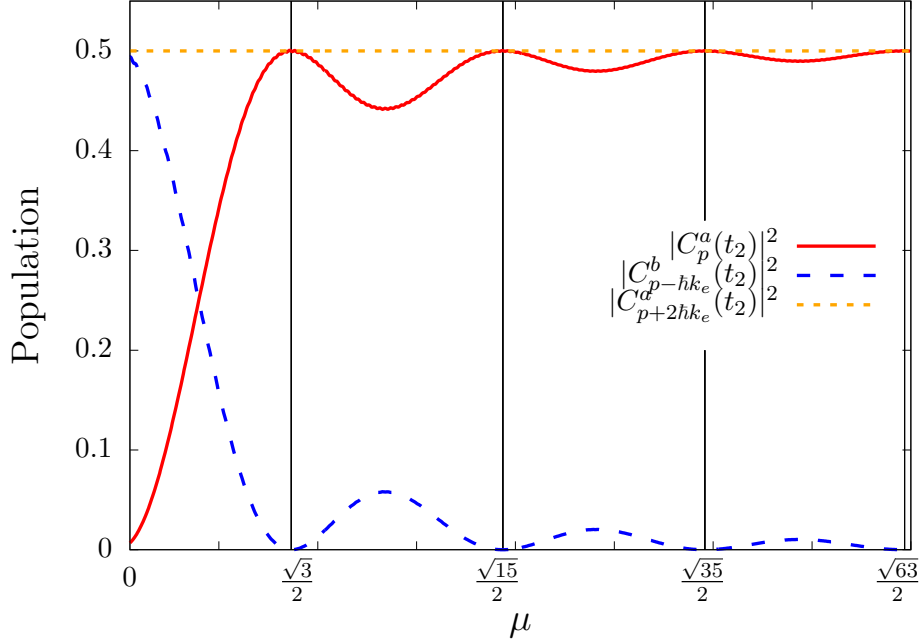


FIGURE 4.7. Populations of the different states after the second pulse (at time  $t_2 = \tau_1 + \tau_2$ ) as a function of  $\mu$  with an initial velocity of  $v_0 = 5$  m/s. The vertical lines indicate the special Rabi frequencies (Eq. (36)).

Figure (4.6) illustrates the error at the time  $t_2 = \tau_1 + \tau_2$  when the second pulse is performed (Appendix C) for the state  $|b, 3\rangle$ . In this case, we can see that again the error is well bounded by the parameter  $\eta_1^2$  when the initial velocity  $v_0$  is increased, as the perturbative solution requires.

Nevertheless, for this pulse we have an additional situation with respect to the first one. While the resonant transition  $|b, 1\rangle \leftrightarrow |a, 2\rangle$  is resonant and performs a  $\pi$ -pulse, the transition  $|b, -1\rangle \leftrightarrow |a, 0\rangle$  is detuned with a Rabi frequency  $\tilde{\Omega}_1 = \Omega\sqrt{1 + 4\mu_m^2}$  (Eq. (35)), which performs a  $2\pi$ -transition of the state  $|a, 0\rangle$  onto itself, with the gain of a corresponding phase of  $e^{-i\mu\pi}$ .

1.2.1. *Variation of the parameter  $\mu$ .* We study the variation of the parameter  $\mu$  through the populations obtained at the end of the second pulse. Figure (4.7) shows these populations in general as a function of  $\mu$  and in the special values of  $\mu$  given in Eq. (36). We can provide three conclusions from this plot.

- (1) The population of the state  $|a, 0\rangle$  is maximized at the special values of the parameter  $\mu$ . This illustrates our idea presented at Chapter 2 that we can make resonant  $2\pi$ -transitions in adjacent pairs of states to the ones that make resonant  $\pi$ -transitions through the election of an adequate Rabi frequency  $\Omega$ .
- (2) Also when the special values of the parameter  $\mu$  is used, the perturbative state  $|b, -1\rangle$  becomes negligible, as is expected from the conservation of probability, then, the use of the special Rabi frequencies also allows the minimization of the spurious populations of another states.
- (3) The second pulse does not introduce new perturbative population for the state  $|b, -1\rangle$ . Figure (4.9) illustrates the situation. In the beginning of the second pulse, the non-perturbative state  $|b, 1\rangle$  is coupled to the state  $|a, 0\rangle$  by the Doppler-detuned Rabi frequency  $\Omega_+$  and  $|a, 0\rangle$

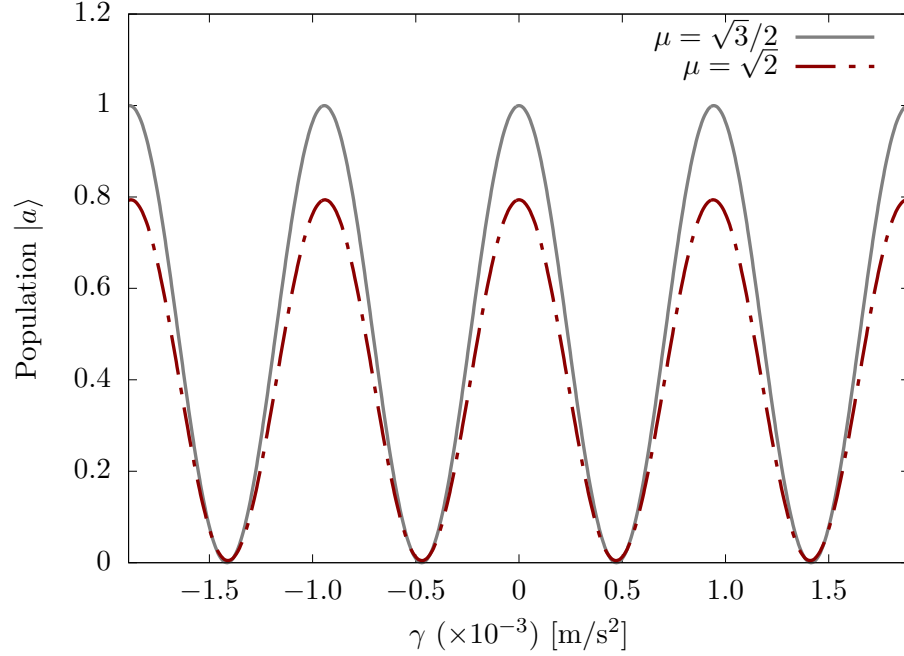


FIGURE 4.8. Interferometric fringes with an initial atomic cloud velocity of  $v_0 = 10$  m/s as a function of  $\gamma = g - g'$ . In light gray we used the first special value of the parameter  $\mu$  while in dashed red line we have the case when  $\mu = \sqrt{2}$ , illustrating the fact that we lose visibility when we do not use the special Rabi frequencies.

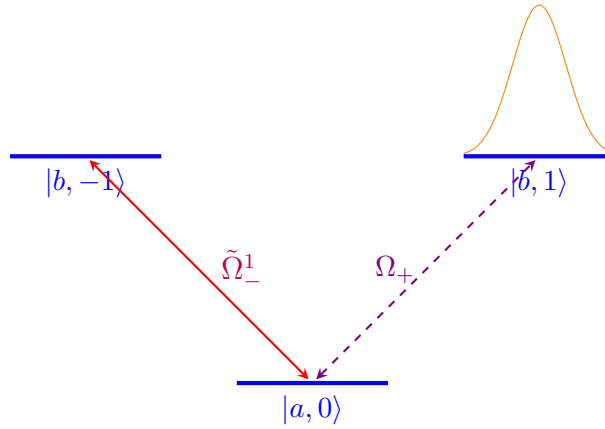


FIGURE 4.9. The state  $|b, -1\rangle$  is not excited in a perturbative way in the second pulse.

is coupled by the frequency  $\tilde{\Omega}_-$  (Eq. (34)) to the state  $|b, -1\rangle$ . In this way, the coupling between  $|b, 1\rangle$  and  $|b, -1\rangle$  through this path is quantified in the perturbative series by the term:

$$C_{p-\hbar k_e}^b(t_2) = (-i)^2 \int_{\tau_1}^{\tau_1+\tau_2} dt_1 \langle b, -1 | \hat{H}_0(t_1) | a, 0 \rangle \int_{\tau_1}^{t_1} dt_2 \langle a, 0 | \hat{V}(t_2) | b, 1 \rangle \langle b, 1 | \hat{U}_0(t_2, \tau_1) | \psi(t_1) \rangle, \\ |\psi(t_1)\rangle = C_p^a(t_1) |a, 0\rangle + C_{p+\hbar k_e}^b(t_1) |b, 1\rangle$$

which is of second order in the perturbative parameter ( $\hat{V}(t_2)$  is integrated twice). In synthesis, the excitation of perturbative amplitudes can only be performed first in a resonant coupling and then in a detuned coupling, but not in the inverse order (Eq. (50)).

- (4) The populations in the three states after the second pulse remains approximately constant in the case  $\mu \gg 1$ , that is to say, when the Rabi frequency is much smaller than the recoil frequency. This can be explained in the light of the Fig. (2.10), because this means that the detuning is so large compared with the Rabi frequency that the transitions between the adjacent states to those connected resonantly through the frequency chirping  $\alpha_{\pm}(t)$  have very low probability to be excited.

As a consequence of these observations, we also conclude that the visibility of the fringes when we close the Mach-Zehnder interferometer is maximized in the situations when we use the special Rabi frequencies (Fig. (4.8)) because it constitutes a mechanism to control the transitions to spurious states (that is to mean, states different than  $|a, 0\rangle$ ,  $|b, 1\rangle$  and  $|a, 2\rangle$ ).<sup>2</sup>

## 2. Phases due to gravitational interaction.

The Fig. (3.3) shows that between the second and the third pulses there is a time  $T$  in which the phase-modulated laser is turned off. Equivalently, between the fifth and sixth pulses there is another dark time of duration  $T$ . Is through these dark times that the wave-functions of the internal states of the atom can acquire different phases due to the gravitational field with which the atoms interact. We introduce a different approach in the experiment, since we use the Galilean transformation to work in the atomic reference frame. From an experimental viewpoint, we use the frequency chirping to compensate the phases due to Doppler shifts in the internal atomic states. We can consider the Eqs. (57), where we have the time-translated equations of the dynamics of the amplitude probabilities. As an example, we can consider the transition from the second pulse to the third pulse. From the Eqs. (57), if the modulated laser is turned off, then  $\Omega_+ = \Omega_- = 0$ , which implies that there is no dynamics for the different internal states of the atom in the different momentum states  $|a, 0\rangle$  and  $|a, 2\rangle$ . This implies that the initial populations at the beginning of the third pulse are the final populations at the end of the second pulse.

Nevertheless, when the laser again is turned on, the Raman frequencies acquire a determined phase, since we are in the atomic reference frame. The transformation of the Raman frequencies, for the chirping  $\alpha_+(t)$ , in orange, and  $\alpha_-(t)$  in purple, are:

$$\Omega_+^a(n, t) \rightarrow \Omega_+ e^{-\frac{i}{2} k_e \gamma t^2 - 2i(\beta+n\mu)(\Omega t)} \quad (61)$$

$$\Omega_+^b(n, t) \rightarrow \Omega_+ e^{\frac{i}{2} k_e \gamma t^2 + 2i[\beta+(n-1)\mu](\Omega t)} \quad (62)$$

$$\Omega_-^a(n, t) \rightarrow \Omega_- e^{\frac{i}{2} k_e \gamma t^2 + 2i[\beta+(n-2)\mu](\Omega t)} \quad (63)$$

$$\Omega_-^b(n, t) \rightarrow \Omega_- e^{-\frac{i}{2} k_e \gamma t^2 - 2i[\beta+(n-1)\mu](\Omega t)} \quad (64)$$

---

<sup>2</sup>Los programas utilizados para ésta subsección se encuentran en la carpeta `Second_Pulse`.



with,

$$\gamma = g - g' \quad (65)$$

is the difference between the gravitational acceleration with the acceleration given by the ramp. Specifically,

$$g' = \mp \frac{1}{2k_e} \partial_t^2 \alpha_{\pm}(t). \quad (66)$$

We can perform the corresponding Raman frequency recalibrations evaluating the Raman frequencies at times:

$$\begin{aligned} t_1 &= \tau_1, \\ t_2 &= \tau_1 + \tau_2, \\ t_{3A} &= \tau_1 + \tau_2 + T, \\ t_{3D} &= \tau_1 + \tau_2 + T + \tau_3, \\ t_4 &= \tau_1 + \tau_2 + T + \tau_3 + \tau_4, \\ t_5 &= \tau_1 + \tau_2 + T + \tau_3 + \tau_4 + \tau_5, \\ t_{6A} &= \tau_1 + \tau_2 + T + \tau_3 + \tau_4 + \tau_5 + T, \\ t_{6D} &= \tau_1 + \tau_2 + T + \tau_3 + \tau_4 + \tau_5 + T + \tau_6, \\ t_7 &= \tau_1 + \tau_2 + T + \tau_3 + \tau_4 + \tau_5 + T + \tau_6 + \tau_7, \end{aligned} \quad (67)$$

where  $\tau_{1,7} = \pi/4\Omega$  ( $\pi/2$ -pulses) and  $\tau_{2,3,4,5,6} = \pi/2\Omega$  ( $\pi$ -pulses). We use  $t_1$  to recalibrate the second pulse,  $t_{3A}$  to recalibrate the third pulse,  $t_{3D}$  to recalibrate the fourth pulse,  $t_4$  to recalibrate the fifth pulse,  $t_{6A}$  to recalibrate the sixth pulse and  $t_{6D}$  to recalibrate the seventh pulse.

From the Eqs. (61), (62), for the third pulse, we can verify that for the states  $|a, 0\rangle$  and  $|b, 1\rangle$  the unique transformation of phase is due to the gravitational transformation. Nevertheless, for the state  $|b, 3\rangle$  the phase of the Raman phase is proportional to the dark time  $T$ :

$$\Omega_+^b(3, t_{3A}) = \Omega_+ e^{\frac{i}{2} k_e \gamma (\tau_1 + \tau_2 + T)^2 + 2i(\beta + 2\mu)[\Omega(\tau_1 + \tau_2 + T)]}.$$

The Fig. (4.10) shows the argument of the numerical and analytical solutions of the state  $|b, 3\rangle$  at the time  $\tilde{t} = t_{3A} + \tau_3/3$  as a function of the dark time  $T$ . From such figure we can visualize the direct proportionality between the argument and  $T$ , with a slope of value  $\pi/\mu$ . Let us consider the equation that determines the dynamics of this state in this pulse (Appendix C):

$$\begin{aligned} C_{p+3\hbar k_e}^b(\tilde{t}) &= e^{i(\beta+2\mu)(\Omega\tau_3/3)} \left\{ \frac{(-i) \arg [\Omega_b^+(3, t_{3A})]}{\sqrt{1+(2\mu)^2}} \sin\left(\frac{\Omega\tau_3}{3} \sqrt{1+(2\mu)^2}\right) C_{p+2\hbar k_e}^a(t_2) \right. \\ &\quad \left. + \left[ \cos\left(\frac{\Omega\tau_3}{3} \sqrt{1+(2\mu)^2}\right) + \frac{i(2\mu)}{\sqrt{1+(2\mu)^2}} \sin\left(\frac{\Omega\tau_3}{3} \sqrt{1+(2\mu)^2}\right) \right] C_{p+3\hbar k_e}^b(t_2) \right\}, \end{aligned}$$

in this case,  $\Omega\tau_3/3 = \pi/6$  and we took  $\mu = \sqrt{3}/2$ , from which this expression becomes:

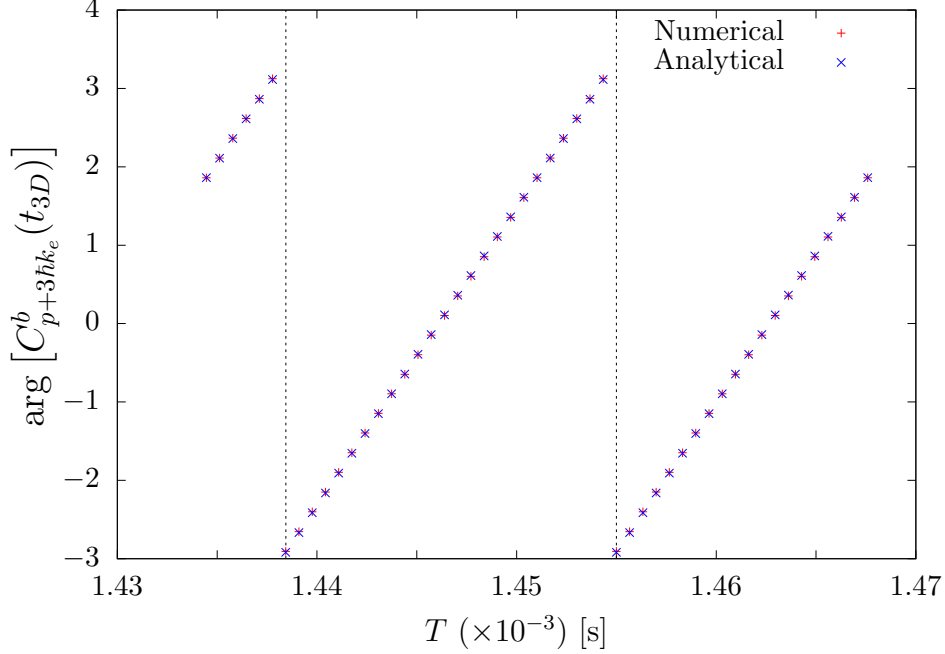


FIGURE 4.10. Argument of the numerical solution and the analytical solution of the state  $|b, 3\rangle$  at the time  $t_{3A} + \tau_3/3$  as a function of the dark time  $T$ . The range of the horizontal axis goes from  $100\tau_2$  to  $100\tau_2 + \pi/(\mu\Omega)$ .

$$C_{p+3hk_e}^b(t_{3D}) = e^{i(\beta+\sqrt{3})(\pi/6)} \left\{ \frac{(-i) \arg [\Omega_b^+(3, t_{3A})]}{2} \sin\left(\frac{\pi}{3}\right) C_{p+2hk_e}^a(t_2) + \left[ \cos\left(\frac{\pi}{3}\right) + i\frac{\sqrt{3}}{2} \sin\left(\frac{\pi}{3}\right) \right] C_{p+3hk_e}^b(t_2) \right\},$$

given that from the second pulse:

$$C_{p+3hk_e}^b(t_2) \ll C_{p+2hk_e}^a(t_2),$$

then,

$$C_{p+3hk_e}^b(\tilde{t}) \sim e^{i(\beta+\sqrt{3})(\pi/6)} \frac{(-i)}{2} \arg [\Omega_b^+(3, t_{3A})] \sin\left(\frac{\pi}{3}\right) C_{p+2hk_e}^a(t_2),$$

from which the  $T$ -dependent phase  $\arg [\Omega_b^+(3, t_{3A})]$  becomes proportional to  $C_{p+3hk_e}^b(\tilde{t})$ , this is the reason why this phase is codified in this state. The contrary is true also for the state  $|a, 2\rangle$ . This state is insensible to changes of dark time  $T$ , because in this case, the phase is proportional mainly to the amplitude

$$C_{p+2hk_e}^a(t_3) \sim e^{-i(\beta+\sqrt{3})(\pi/6)} \left[ \cos\left(\frac{\pi}{3}\right) + i\frac{\sqrt{3}}{2} \sin\left(\frac{\pi}{3}\right) \right] C_{p+2hk_e}^b(t_2).$$

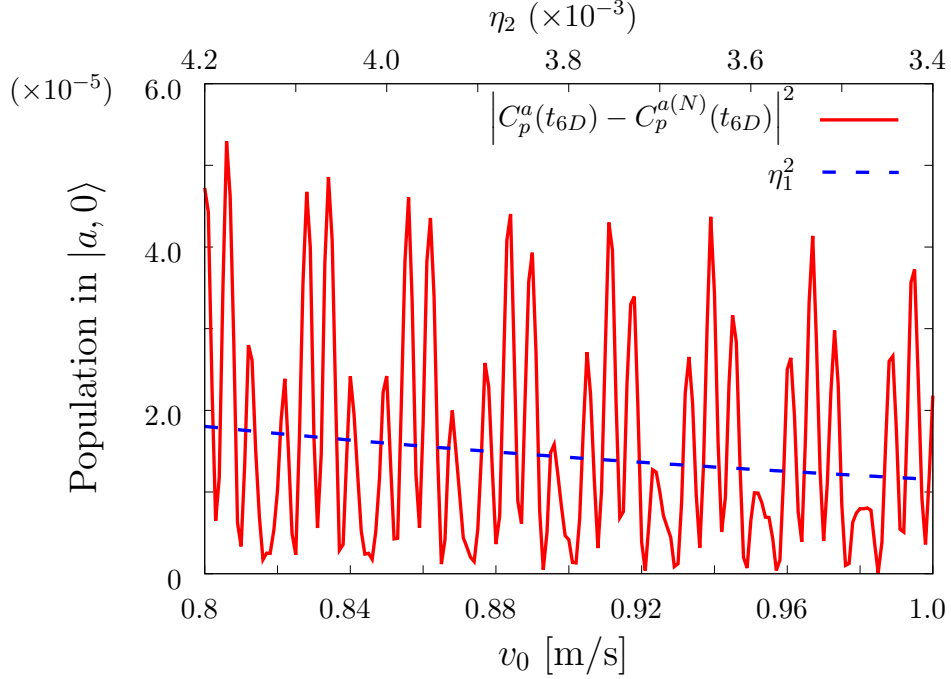


FIGURE 4.11. Error in amplitude of state  $|a, 0\rangle$  as a function of the initial velocity for the sixth pulse. The red-solid line represents the difference between the analytical and numerical ( $N$ ) solutions at the time  $t_{6D}$  (Eq. (67)). The blue-dashed line corresponds to the perturbative parameter  $\eta_1^2$ .

It is worth to say that this is a direct consequence from our perturbative method, because we predict the existence of amplitude at the state  $|b, 3\rangle$  at the end of the second pulse, so it is to this state that the phase proportional to the dark time  $T$  is imprinted.

Nevertheless, by the design of the interferometer, the phase of the state  $|b, 3\rangle$  does not influence the final interferometric fringes. At the end of the third pulse. we have that (Appendix C):

$$C_{p+hk_e}^b(t_{3D}) \sim e^{i\beta(\Omega\tau_3)}(-i) \frac{\Omega_b^+(1, t_{3A})}{|\Omega_b^+(1, t_{3A})|} \sin(\Omega\tau_3) C_p^a(t_2).$$

This means that in spite of  $|a, 0\rangle$  does not acquire a phase dependent on  $\gamma$  (a gravitational phase), the state  $|b, 1\rangle$  does acquire it at the end of the third pulse.<sup>3</sup>

Using the Eqs. (61), (62), (63) and (64), we can transform the Raman frequencies to account for the gravitational phase accumulation. This allows us to obtain the interference fringes as a function of the parameter  $\gamma$  when we close the interferometric sequence of seven steps, as is shown in the next section.

**2.1. Sixth pulse.** The Figs. (4.11) and (4.12) represent the errors of the non-perturbative states  $|a, 0\rangle$  and  $|b, 1\rangle$  at the end of the sixth pulse at time  $t_{6D}$  (Eq. (67)). The successive perturbative amplitudes involved are calculated for the interferometer at Appendix C. In general, from these figures we can deduce that the errors for the states of interest,  $|a, 0\rangle$  and  $|b, 1\rangle$  are well-bounded by the

<sup>3</sup>Los programas utilizado para ésta subsección se encuentran en la carpeta `Third.Pulse`.

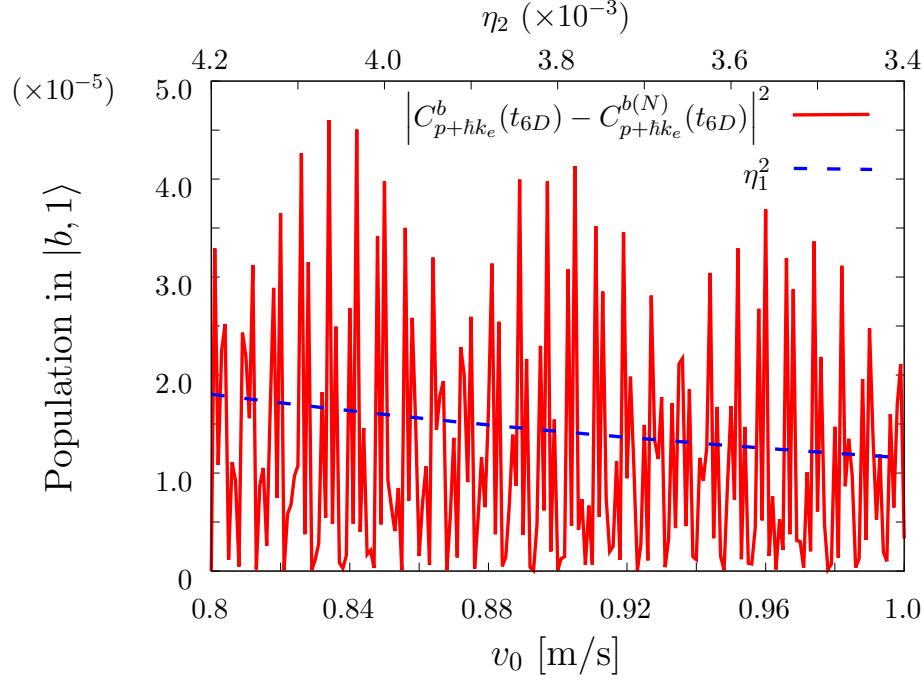


FIGURE 4.12. Error in amplitude of state  $|b, 1\rangle$  as a function of the initial velocity for the sixth pulse. The red-solid line represents the difference between the analytical and numerical ( $N$ ) solutions at the time  $t_{6D}$  (Eq. (67)). The blue-dashed line corresponds to the perturbative parameter  $\eta_1^2$ .

first order perturbative parameter  $\eta_1^2$ , which validates our approach. The cumulative errors are due to the fact that we just considered five states, and we neglected couplings to higher values of momentum states.<sup>4</sup>

### 3. Interferometric Fringes.

For the interferometric sequence of seven pulses, illustrated at Fig. (3.3) we made the following calculations:

- (1) We follow the resonant dynamics of the states  $|a, 0\rangle$  and  $|b, 1\rangle$  (Appendix C), until first order in  $\beta$ , using the first special parameter  $\mu = \sqrt{3}/2$  (Eq. (35)).
- (2) For each of the seven steps, we deduced the appearance of perturbative amplitudes at the states  $|a, 0\rangle$ ,  $|b, 1\rangle$  and  $|a, 2\rangle$ , at first order in the perturbative parameters  $\eta_i$ ,  $i = 1, \dots, 6$ , these appear at Appendix C.

**3.1. Populations of the states  $|a, 0\rangle$  and  $|b, 1\rangle$ .** In a formal sense, to account for the final populations at the internal states  $|a\rangle$  and  $|b\rangle$  we should add up all the corresponding populations, for instance, for the internal state  $|a\rangle$  the population should be:

<sup>4</sup>Los programas utilizados para ésta subsección se encuentran en la carpeta `Sixth_Pulse`.

$$|\langle a|\psi_F\rangle|^2 = \sum_{n=-\infty}^{\infty} |\langle a, n|\psi_F\rangle|^2,$$

where  $|\psi_F\rangle$  is the final state at the end of the seven pulses. Nevertheless, the amplitudes of the states  $|a, n\rangle$  with  $n \neq 0$  are of the first order of perturbation, then its populations  $|\langle a, n|\psi_F\rangle|^2$  are of second order of perturbation. From here, as we want to account for the first order, we neglect all contributions from these states. A similar argument applies to take into account just the state  $|b, 1\rangle$  in the population of the internal state  $|b\rangle$ .

Under this consideration, the respective populations of the states  $|a, 0\rangle$  and  $|b, 1\rangle$  are given by the following expressions:

$$\begin{aligned} |\langle a|\psi_F\rangle|^2 &= a_0 + a_0^\beta \beta + a_2 \eta_2 + a_3 \eta_3 + a_5 \eta_5 + a_6 \eta_6, \\ |\langle b|\psi_F\rangle|^2 &= b_0 + b_0^\beta \beta + b_2 \eta_2 + b_3 \eta_3 + b_5 \eta_5 + b_6 \eta_6, \end{aligned} \quad (68)$$

where the zeroth order solutions are

$$\begin{aligned} a_0 &= \frac{1}{2} \left[ 1 + \cos \left( 2k_e \gamma \left[ (T + 5\tau_1)^2 - \frac{5\tau_1^2}{4} \right] \right) \right], \\ b_0 &= \frac{1}{2} \left[ 1 - \cos \left( 2k_e \gamma \left[ (T + 5\tau_1)^2 - \frac{5\tau_1^2}{4} \right] \right) \right], \end{aligned} \quad (69)$$

with  $\gamma$  defined at Eq. (65). The Eqs. (69) gives us the ideal result, that is to mean, if we do not take into account the contributions of the non-resonant Raman pairs along the interferometric performance. There is a difference of 2 with respect of the reported fringes in the literature [21], due to the enhanced momentum separation in the superposition of momentum states, since the gravitational phase accumulation occurs between the states  $|a, 0\rangle$  and  $|a, 2\rangle$ , with twice the momentum recoil compared with the traditional gravitational phase accumulation between the states  $|a, 0\rangle$  and  $|b, 1\rangle$  [1].

The other coefficients for the states  $|a\rangle$  and  $|b\rangle$  are:

$$\begin{aligned} a_0^\beta &= 0, \\ b_0^\beta &= 0, \\ a_2 &= -\cos(\Phi_g) \sin(\phi_2), \\ b_2 &= -\sin(\Phi_g) \cos(\phi_2), \\ a_3 &= -\cos(\Phi_g) [\sin(\phi_x) + \sin(\phi_y) - \sin(\phi_z)] \\ b_3 &= \sin(\Phi_g) [\cos(\phi_x) + \cos(\phi_y) - \cos(\phi_z)], \\ a_5 &= \cos(\Phi_g) \sin(\phi_5), \\ b_5 &= -\sin(\Phi_g) \cos(\phi_5), \\ a_6 &= \cos(\Phi_g) \sin(\phi_6), \end{aligned}$$

$$b_6 = -\sin(\Phi_g) \cos(\phi_6),$$

with

$$\phi_x = \Phi_g \xi_x + 2k_e v_0 T \Lambda_x + k_e g T^2 \Lambda_x^2 + \frac{\mu}{2}(5\pi + 4\Omega T),$$

$$\phi_y = \Phi_g \xi_y + 2k_e v_0 T \Lambda_y + k_e g T^2 \Lambda_y^2 + \mu(\pi + 2\Omega T),$$

$$\phi_z = \Phi_g \xi_z + 2k_e v_0 T \Lambda_z + k_e g T^2 \Lambda_z^2 + \frac{\mu}{2}(5\pi + 4\Omega T),$$

$$\phi_2 = \Phi_g + 2k_e v_0 \tau_1 + k_e g \tau_1^2,$$

$$\phi_5 = \Phi_g \xi_5 - 2k_e v_0 T \Lambda_5 - k_e g T^2 \Lambda_5^2 - 2\mu(2\pi + \Omega T),$$

$$\phi_6 = \Phi_g \xi_6 - 4k_e v_0 T \Lambda_6 - 4k_e g T^2 \Lambda_6^2 - \mu(5\pi + 4\Omega T),$$

where the dimensionless numbers are given by

$$\xi_x = \frac{3}{2} \left( 1 + \frac{26}{3} \frac{\tau_1}{T} + \frac{111}{6} \frac{\tau_1^2}{T^2} \right),$$

$$\xi_y = \xi_x,$$

$$\xi_z = \frac{3}{2} \left( 1 + \frac{20}{3} \frac{\tau_1}{T} + \frac{31}{2} \frac{\tau_1^2}{T^2} \right),$$

$$\xi_5 = \frac{5}{2} \left( 1 + \frac{46}{5} \frac{\tau_1}{T} + \frac{211}{10} \frac{\tau_1^2}{T^2} \right),$$

$$\xi_6 = \left( 1 + 12 \frac{\tau_1}{T} + \frac{147}{4} \frac{\tau_1^2}{T^2} \right),$$

$$\Lambda_x = 1 + 5 \frac{\tau_1}{T},$$

$$\Lambda_y = 1 + 3 \frac{\tau_1}{T},$$

$$\Lambda_z = \Lambda_x,$$

$$\Lambda_5 = 1 + 7 \frac{\tau_1}{T},$$

$$\Lambda_6 = 1 + \frac{9}{2} \frac{\tau_1}{T}.$$

We have defined,

$$\Phi_g = k_e \gamma T^2, \tag{70}$$

and  $\gamma$  as in Eq. (65).

The parameters  $\eta_1$ ,  $\eta_4$  and  $\eta_7$  do not contribute to the interferometric fringes because from the resonant evolution, when we close the interferometer after the seven steps proposed, its amplitudes remain in

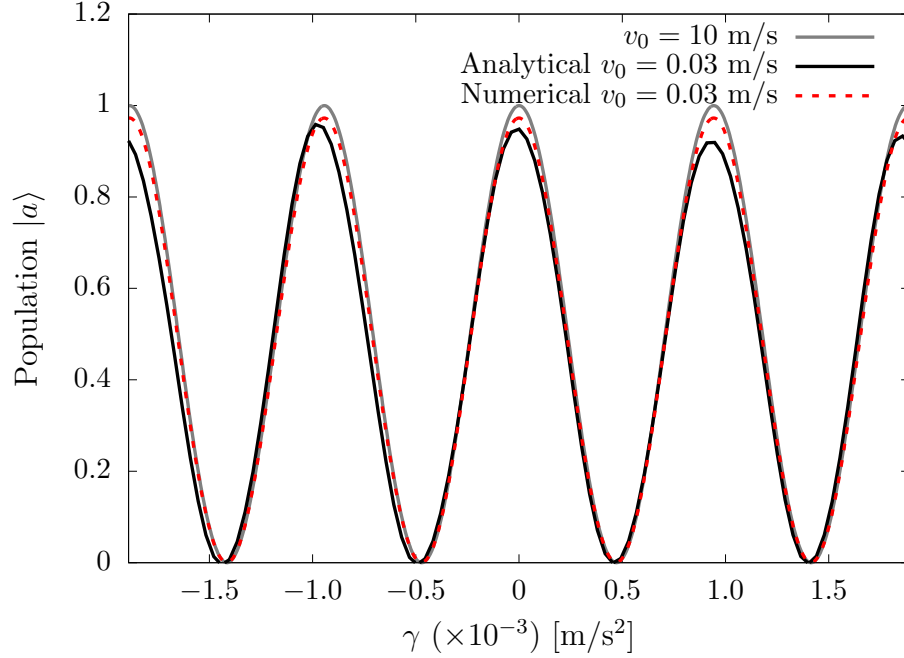


FIGURE 4.13. Interferometric fringes obtained for the population at the state  $|a\rangle$  as a function of the parameter  $\gamma$ . The light gray line shows the case when we have an initial velocity of the atom cloud of  $v_0 = 10$  m/s. The dashed red line shows the numerical case when we have an initial velocity of  $v_0 = 0.03$  m/s while the black line is the analytical first order approximation to these fringes through the perturbative method introduced in the Chapter 3 and the present one.

states  $|b, -1\rangle$  or  $|a, 2\rangle$  or  $|b, 3\rangle$ , which are not taken into account, because these are contributions of second order in the populations of the internal states.

The Fig. (4.13) shows a comparison between the numerical and the analytical results when we have a relatively low initial velocity of the atomic cloud. The criteria to define this is through the corresponding value of  $\eta_1$ , which in this case is of value  $\eta_1 = 0.11$ . From the figure, we can deduce a loss of visibility due to the fact that the detuning due to Doppler effect Eq. (39) increases, allowing population transfer into spurious states. Nevertheless, from the figure we also deduce that our perturbative analytic method can account for this loss of visibility, showing that our method also is useful in determining the error in contrast due to Doppler detunings. For this election of initial velocity, then we got errors approximated to 10% of the fringes, which is a good estimate from the figure.

**3.2. Variation of the parameter  $\beta$ .** The parameter  $\beta$  is a measure of the initial temperature of the atomic cloud at state  $|a, 0\rangle$ . We suppose that we have a momentum distribution given by a gaussian function with average  $p = 0$  and standard deviation  $\sigma_p$ :

$$P(\sigma_p) = \frac{1}{\sigma_p \sqrt{2\pi}} \exp \left[ -\frac{1}{2} \left( \frac{p}{\sigma_p} \right)^2 \right] \quad (71)$$

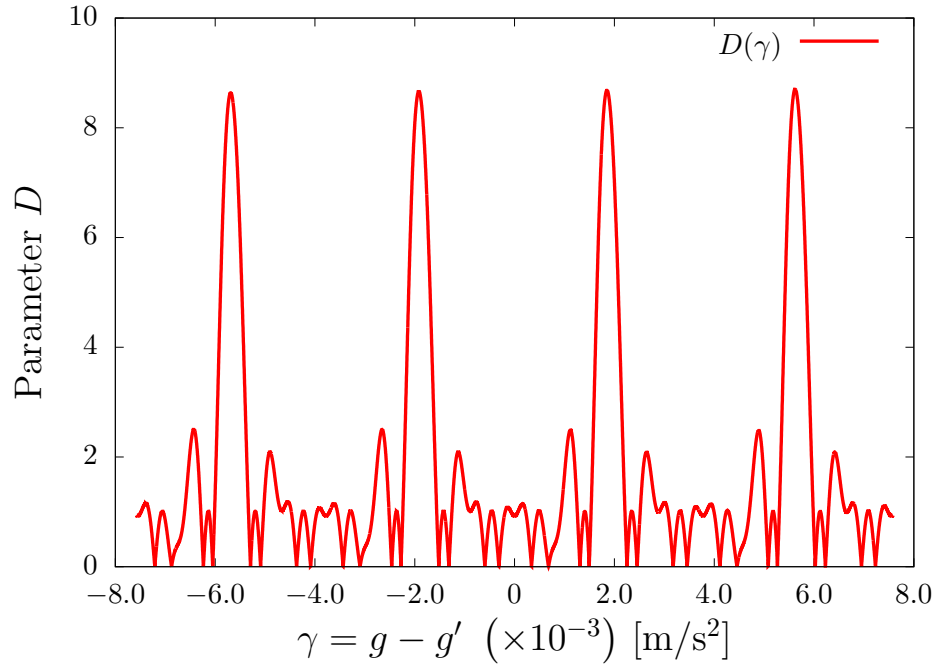


FIGURE 4.14. Parameter  $a_2^\beta$  (Appendix D) as function of  $\gamma = g - g'$ .

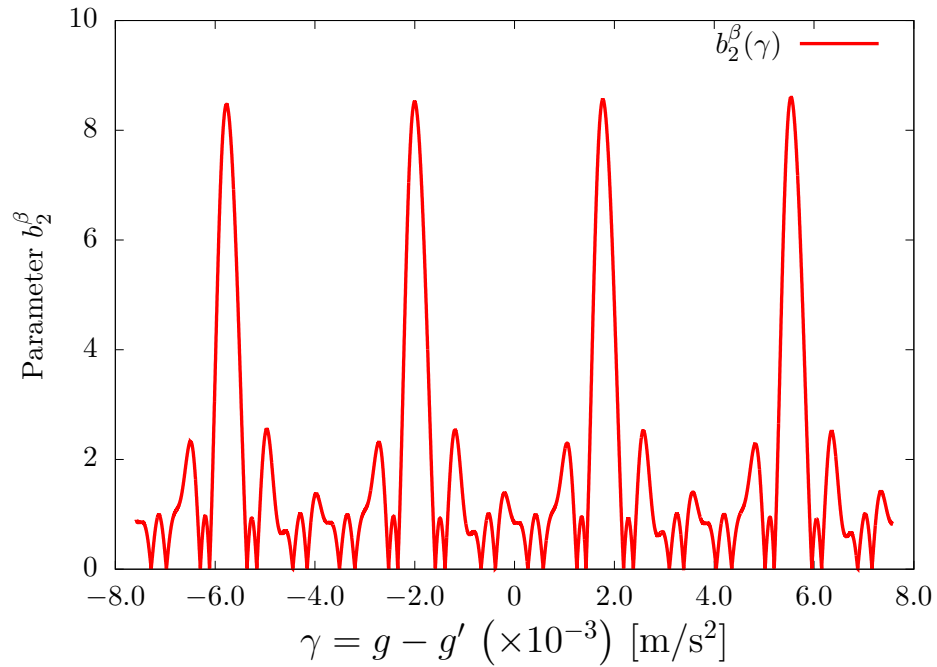


FIGURE 4.15. Parameter  $b_2^\beta$  (Appendix D) as function of  $\gamma = g - g'$ .



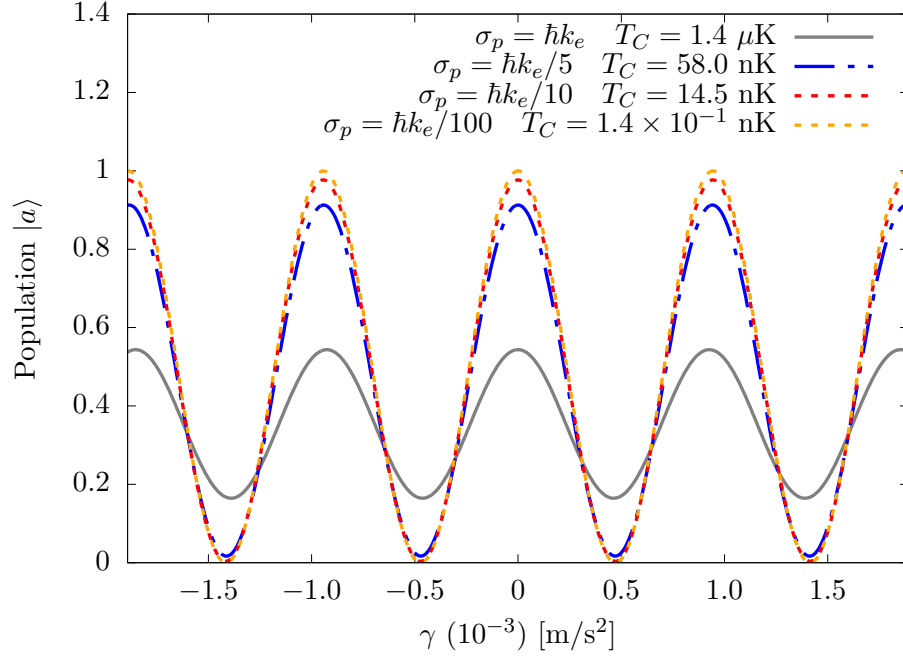


FIGURE 4.16. Interference fringes as a function of  $\gamma = g - g'$  with a variation of the standard deviation  $\sigma_p$  of the momentum initial distribution of the state  $|a, 0\rangle$ , showing that the increase of this deviation reduces the visibility of the fringes.

In the Eq. (68) the term proportional to  $\beta$  is equal to zero, and we would have corrections of second order in  $\beta$  that depend on  $\sigma_p$ .

We estimate the size of these corrections by extending the expansion to the second-order term in  $\beta$  (Appendix D). Equation (68) is valid as long as this second-order correction is small, that is

$$\begin{aligned} D\beta^2(\sigma_p) &< 1 \\ \frac{Dk_e^2\sigma_p^2}{(2m\Omega)^2} &< 1, \end{aligned} \quad (72)$$

where  $D$  is the dimensionless second-order coefficient in the  $\beta$  expansion of Eq. (68), that has an upper value of  $D \leq 8.7$  (Fig. (4.14)). Relating the momentum width ( $\sigma_p$ ) to the temperature ( $T_C$ ) through  $\sigma_p = \sqrt{mk_B T_C}$ , with  $k_B$  the Boltzmann constant, gives a temperature for the validity of our approach

$$T_C < \frac{4m\Omega^2}{Dk_B k_e^2}, \quad (73)$$

that for the case of Rb<sup>87</sup> gives  $T_C < 0.22\mu\text{K}$ . This is a temperature that is possible to achieve experimentally.

Even when the analytical solutions would not work well at higher temperatures, the numerical solution shows that there is still reasonable visibility at  $T_C = 1.45\mu\text{K}$ , as is illustrated at Fig. (4.16).<sup>5</sup>

<sup>5</sup>Los programas utilizados para ésta sección se encuentran en la carpeta **Fringes**.

## Conclusions.

In this thesis work, we present an atomic interferometric scheme applied to gravimetry that prepares a superposition of two momentum states in the same internal level. This superposition becomes much less sensitive to external electromagnetic fluctuations that can potentially introduce systematic errors in the measurement of the gravitational acceleration.

From the work developed along this work, we can deduce the following general remarks:

- We demonstrate a perturbative approach to the solution of the time-dependent Schrödinger's equation that allows us to identify a hierarchy in the couplings and transitions between levels.
- We identify three perturbative parameters that determine the size of the corrections to the signal. The parameter  $\eta$  is related to transitions having the opposite Doppler shift. The parameter  $\mu$  is related to the ratio of the Rabi frequency with respect to four times the recoil frequency and quantifies the detuning for off-resonant transitions with the same sign of the Doppler shift. Finally, the parameter  $\beta$  is related to the initial temperature of the atomic cloud at the beginning of the interferometric sequence, and affects the visibility of the interferometric fringes.
- We find special values of the Rabi frequency that minimize the contribution from the parameter  $\mu$  and improve the visibility of the interference fringes. Its deduction is based on the fact that we can perform  $2\pi$ -transitions in the adjacent pair of states to those that we have resonant through the use of the correct value of the Rabi frequency.
- We provide analytical expressions to calculate the effect of the undesired transitions coming from additional frequencies of the modulation process. It is easy to estimate the order of magnitude of the corrections based on the perturbative parameters. The scheme presented can be used to decide over experimental parameters required to reach a particular precision in gravitational measurements.
- Neighboring levels from the transition used for the gravimetry are coupled to first order, like in the case of the transition  $|a, 0\rangle \leftrightarrow |b, -1\rangle$  having the transition  $|a, 0\rangle \leftrightarrow |b, 1\rangle$  resonant, but also there is a non-adjacent coupling  $|a, 0\rangle \leftrightarrow |a, 2\rangle$  to first order. Subsequent levels are coupled to higher orders.
- The Galilean transformation performed can be considered a generalization of the interaction picture, in the sense that allows us to eliminate the potential energy potential  $mgz$  from the Hamiltonian, introducing the Doppler phase dependence in the amplitude equations.
- The amplitude equations deduced have a temporal symmetry that allows us to deduce the gravitational phase printed in the Rabi frequencies after the dark times in the interferometric scheme.

The perturbative method that we introduce in this work in general solves coupled differential equations in the case when there is a term that evolves with a high frequency compared to the other involved. This is the typical case when it is applied the rotating wave approximation in Quantum Optics. That is to mean, we can now solve this problem at any perturbative order or, through this method, give a

quantification of the error involved when the approximation is used. Additionally, the way we order the Dyson series that was performed not only accounts for the causal solution of the problem, but also now gives a hierarchy of the strength of couplings in an infinite levels problem.

## APPENDIX A

### The Galilean Transformation.

In the present appendix we perform a change of the involved states with the aim to consider the system in the center of mass reference frame of the atom.

The Eqs. (27) and (28) can be gather into the Hamiltonian:

$$\hat{H} = \hat{H}_0 + \hat{H}_I,$$

where:

$$\begin{aligned}\hat{H}_0 &= \frac{\hat{p}_z^2}{2m} + mg\hat{z} \\ \hat{H}_I &= \left( \hbar\Omega_- e^{-ik_e\hat{z}} + \hbar\Omega_+ e^{ik_e\hat{z}} \right) e^{i\alpha(t)} \hat{\sigma}_+ + h.c.\end{aligned}$$

where *h.c.* stands for hermitian conjugate. Let's consider the next operator:

$$\hat{G} = \exp\left(i \int \frac{L_c}{\hbar} dt\right) \exp\left(-i \frac{\hat{p}_z z_c}{\hbar}\right) \exp\left(i \frac{p_c \hat{z}}{\hbar}\right), \quad (74)$$

where  $L_c$  is the classical Lagrangian of the atom,  $z_c$  is the position of the center of mass of the atom and  $p_c$  its momentum all of them as function of time. If we transform the state  $|\psi\rangle$  under the operator Eq. (74) according to the next transformation:

$$|\psi\rangle = \hat{G} |\phi_{CM}\rangle.$$

From here, we have:

$$\begin{aligned}\partial_t |\psi\rangle &= \left(\partial_t \hat{G}\right) |\phi_{CM}\rangle + \hat{G} \partial_t |\phi_{CM}\rangle \\ \hat{G} \partial_t |\phi_{CM}\rangle &= \partial_t |\psi\rangle - \left(\partial_t \hat{G}\right) |\phi_{CM}\rangle \\ \partial_t |\phi_{CM}\rangle &= \hat{G}^\dagger \partial_t |\psi\rangle - \hat{G}^\dagger \left(\partial_t \hat{G}\right) |\phi_{CM}\rangle,\end{aligned}$$

but from the Schrödinger's Equation:

$$i\hbar \partial_t |\psi\rangle = \left(\hat{H}_0 + \hat{H}_I\right) |\psi\rangle, \quad (75)$$

we got that:

$$\begin{aligned}\partial_t |\phi_{CM}\rangle &= \frac{1}{i\hbar} \hat{G}^\dagger \left(\hat{H}_0 + \hat{H}_I\right) |\psi\rangle - \hat{G}^\dagger \left(\partial_t \hat{G}\right) |\phi_{CM}\rangle, \\ i\hbar \partial_t |\phi_{CM}\rangle &= \hat{G}^\dagger \left(\hat{H}_0 + \hat{H}_I\right) \hat{G} |\phi_{CM}\rangle - i\hbar \hat{G}^\dagger \left(\partial_t \hat{G}\right) |\phi_{CM}\rangle.\end{aligned} \quad (76)$$

Now, We have that:

$$\begin{aligned}
\hat{G}^\dagger \left( \partial_t \hat{G} \right) &= \exp \left( -i \frac{p_c \hat{z}}{\hbar} \right) \exp \left( i \frac{\hat{p}_z z_c}{\hbar} \right) \exp \left( -i \int \frac{L_c}{\hbar} dt \right) \\
&\quad \left[ \left( i \frac{L_c}{\hbar} \right) \exp \left( i \int \frac{L_c}{\hbar} dt \right) \exp \left( -i \frac{\hat{p}_z z_c}{\hbar} \right) \exp \left( i \frac{p_c \hat{z}}{\hbar} \right) \right. \\
&\quad + \left( -i \frac{\hat{p}_z \dot{z}_c}{\hbar} \right) \exp \left( i \int \frac{L_c}{\hbar} dt \right) \exp \left( -i \frac{\hat{p}_z z_c}{\hbar} \right) \exp \left( i \frac{p_c \hat{z}}{\hbar} \right) \\
&\quad \left. + \exp \left( i \int \frac{L_c}{\hbar} dt \right) \exp \left( -i \frac{\hat{p}_z z_c}{\hbar} \right) \left( i \frac{\dot{p}_c \hat{z}}{\hbar} \right) \exp \left( i \frac{p_c \hat{z}}{\hbar} \right) \right]
\end{aligned} \tag{77}$$

By the Eq. (2.3.47) [13] (*Baker-Hausdorff* lemma) we have:

$$\begin{aligned}
\exp \left( -i \frac{p_c \hat{z}}{\hbar} \right) \left( -i \frac{\hat{p}_z \dot{z}_c}{\hbar} \right) \exp \left( i \frac{p_c \hat{z}}{\hbar} \right) &= -i \frac{\hat{p}_z \dot{z}_c}{\hbar} - \frac{p_c \dot{z}_c}{\hbar^2} [\hat{z}, \hat{p}_z] \\
&= -i \frac{\hat{p}_z \dot{z}_c}{\hbar} - i \frac{p_c \dot{z}_c}{\hbar}
\end{aligned}$$

If we take the last line of the Eq. (77):

$$\begin{aligned}
\exp \left( -i \frac{\hat{p}_z z_c}{\hbar} \right) \left( i \frac{\dot{p}_c \hat{z}}{\hbar} \right) &= \exp \left( -i \frac{\hat{p}_z z_c}{\hbar} \right) \left( i \frac{\dot{p}_c \hat{z}}{\hbar} \right) \exp \left( i \frac{\hat{p}_z z_c}{\hbar} \right) \exp \left( -i \frac{\hat{p}_z z_c}{\hbar} \right) \\
\exp \left( -i \frac{\hat{p}_z z_c}{\hbar} \right) \left( i \frac{\dot{p}_c \hat{z}}{\hbar} \right) \exp \left( i \frac{\hat{p}_z z_c}{\hbar} \right) &= i \frac{\dot{p}_c \hat{z}}{\hbar} - \frac{\dot{p}_c z_c}{\hbar^2} [\hat{z}, \hat{p}_z] \\
&= i \frac{\dot{p}_c \hat{z}}{\hbar} - i \frac{\dot{p}_c z_c}{\hbar}
\end{aligned}$$

Then we have:

$$\begin{aligned}
&\exp \left( -i \frac{p_c \hat{z}}{\hbar} \right) \exp \left( i \frac{\hat{p}_z z_c}{\hbar} \right) \left( i \frac{\dot{p}_c \hat{z}}{\hbar} - i \frac{\dot{p}_c z_c}{\hbar} \right) \exp \left( -i \frac{\hat{p}_z z_c}{\hbar} \right) \exp \left( i \frac{p_c \hat{z}}{\hbar} \right) \\
&= \exp \left( -i \frac{p_c \hat{z}}{\hbar} \right) \exp \left( i \frac{\hat{p}_z z_c}{\hbar} \right) \left( i \frac{\dot{p}_c \hat{z}}{\hbar} \right) \exp \left( -i \frac{\hat{p}_z z_c}{\hbar} \right) \exp \left( i \frac{p_c \hat{z}}{\hbar} \right) - i \frac{\dot{p}_c z_c}{\hbar} \\
&= \exp \left( -i \frac{p_c \hat{z}}{\hbar} \right) \left( i \frac{\dot{p}_c \hat{z}}{\hbar} + i \frac{\dot{p}_c z_c}{\hbar} \right) \exp \left( i \frac{p_c \hat{z}}{\hbar} \right) - i \frac{\dot{p}_c z_c}{\hbar} \\
&= i \frac{\dot{p}_c \hat{z}}{\hbar}
\end{aligned}$$

Replacing this into the Eq. (77) we obtain:

$$i \hbar \hat{G}^\dagger \left( \partial_t \hat{G} \right) = -L_c + \hat{p}_z \dot{z}_c + p_c \dot{z}_c - \dot{p}_c \hat{z} \tag{78}$$

Also, for  $\hat{H}_0$  we have [22]:

$$\hat{G}^\dagger \hat{H}_0 \hat{G} = \frac{(\hat{p}_z + p_c)^2}{2m} + mg(\hat{z} + z_c) \tag{79}$$

Finally, with the aim to determine the transformation for  $\hat{H}_I$  we have:

$$\hat{G}^\dagger \hat{H}_I \hat{G} = \left( \hbar\Omega_- e^{-ik_e(\hat{z}+z_c)} + \hbar\Omega_+ e^{ik_e(\hat{z}+z_c)} \right) e^{i\alpha(t)} \hat{\sigma}_+ + h.c. \quad (80)$$

Replacing Eqs. (78), (79) and (80) into Eq. (76), we get that:

$$\begin{aligned} i\hbar\partial_t |\phi_{CM}\rangle &= \left[ \frac{\hat{p}_z^2}{2m} + \left( \frac{p_c^2}{2m} + mgz_c + L_c - p_c \dot{z}_c \right) + \left( \frac{p_c}{m} - \dot{z}_c \right) \hat{p}_z + (mg + \dot{p}_c) \hat{z} \right] |\phi_{CM}\rangle \\ &+ \hat{G}^\dagger \hat{H}_I \hat{G} |\phi_{CM}\rangle \end{aligned}$$

If we assume that  $z_c$ ,  $p_c$  and  $L_c$  are the classical position, momentum and Lagrangian of the center of mass of the atom, that is to say:

$$\begin{aligned} \dot{z}_c &= \frac{p_c}{m} \\ \dot{p}_c &= -mg \\ L_c &= p_c \dot{z}_c - \left( \frac{p_c^2}{2m} + mgz_c \right) \end{aligned}$$

We obtained that:

$$i\hbar\partial_t |\phi_{CM}\rangle = \left[ \frac{\hat{p}_z^2}{2m} + \left( \hbar\Omega_- e^{-ik_e(\hat{z}+z_c)} + \hbar\Omega_+ e^{ik_e(\hat{z}+z_c)} \right) e^{i\alpha(t)} \hat{\sigma}_+ + h.c. \right] |\phi_{CM}\rangle \quad (81)$$

We expand the state  $|\phi_{CM}\rangle$  as a continuous superposition of momentum states of the center of mass of the atom:

$$|\phi_{CM}\rangle = \int dp \exp\left(-i\frac{p^2}{2m\hbar}t\right) \left[ C_p^a(t) |a\rangle + C_p^b(t) |b\rangle \right] |p\rangle \quad (82)$$

We have:

$$\begin{aligned} \partial_t |\phi_{CM}\rangle &= \int dp \left( -i\frac{p^2}{2m\hbar} \right) \exp\left(-i\frac{p^2}{2m\hbar}t\right) \left[ C_p^a(t) |a\rangle + C_p^b(t) |b\rangle \right] |p\rangle \\ &+ \int dp \exp\left(-i\frac{p^2}{2m\hbar}t\right) \left[ \dot{C}_p^a(t) |a\rangle + \dot{C}_p^b(t) |b\rangle \right] |p\rangle \end{aligned} \quad (83)$$

As we have that:

$$\hat{H}_0 |\phi_{CM}\rangle = \int dp \left( \frac{p^2}{2m} \right) \exp\left(-i\frac{p^2}{2m\hbar}t\right) \left[ C_p^a(t) + C_p^b(t) \right] |p\rangle \quad (84)$$

Replacing the Eqs. (83) and (84) into Eq. (82) we got:

$$\begin{aligned} &\int dp \exp\left(-i\frac{p^2}{2m\hbar}t\right) i\hbar \left[ \dot{C}_p^a(t) |a\rangle + \dot{C}_p^b(t) |b\rangle \right] |p\rangle \\ &= \int dp \exp\left(-i\frac{p^2}{2m\hbar}t\right) \hat{H}_I \left[ C_p^a(t) |a\rangle + C_p^b(t) |b\rangle \right] |p\rangle \end{aligned} \quad (85)$$

With the aim that the Eq. (85) be correct, we state that:

$$i\hbar \left[ \dot{C}_p^a(t) |a\rangle + C_p^b(t) |b\rangle \right] |p\rangle = \hat{H}_I \left[ C_p^a(t) |a\rangle + C_p^b(t) |b\rangle \right] |p\rangle$$

If we project onto the internal atomic state  $|b\rangle$ , we have:

$$\begin{aligned} i\hbar \dot{C}_p^b(t) |p\rangle &= C_p^a(t) \langle b | \hat{H}_I |a\rangle |p\rangle + C_p^b(t) \langle b | \hat{H}_I |b\rangle |p\rangle \\ i\hbar \dot{C}_p^b(t) |p\rangle &= C_p^a(t) \langle b | \hat{H}_I |a\rangle |p\rangle \\ i\hbar \dot{C}_p^b(t) |p\rangle &= C_p^a(t) \left[ \hbar\Omega_- e^{-ik_e z_c} e^{-ik_e \hat{z}} |p\rangle + \hbar\Omega_+ e^{ik_e z_c} e^{ik_e \hat{z}} |p\rangle \right] e^{i\alpha(t)} \langle b | \hat{\sigma}_+ |a\rangle \end{aligned}$$

Also, as we have that [23]:

$$\exp(\mp ik_e \hat{z}) = \int dp |p\rangle \langle p \pm \hbar k_e|,$$

then we have that:

$$\begin{aligned} e^{\mp ik_e \hat{z}} |p\rangle &= \int dp' |p'\rangle \langle p' \pm \hbar k_e | p\rangle \\ &= \int dp' |p'\rangle \delta(p' \pm \hbar k_e - p) \\ &= \int dp' |p'\rangle \delta[p' - (p \mp \hbar k_e)] \\ &= |p \mp \hbar k_e\rangle \end{aligned}$$

As also  $\hat{\sigma}_+ = |b\rangle \langle a|$  then  $\langle b | \hat{\sigma}_+ |a\rangle = 1$ . We have then:

$$i\hbar \dot{C}_p^b(t) |p\rangle = C_p^a(t) \left[ \hbar\Omega_- e^{-ik_e z_c} |p - \hbar k_e\rangle + \hbar\Omega_+ e^{ik_e z_c} |p + \hbar k_e\rangle \right] e^{i\alpha(t)}$$

Integrating this equation with the weight function as is indicated in Eq. (82) we have:

$$i\hbar \int dp e^{-i\frac{p^2}{2m\hbar}t} C_p^b(t) |p\rangle = \int dp e^{-i\frac{p^2}{2m\hbar}t} C_p^a(t) \left[ \hbar\Omega_- e^{-ik_e z_c} |p - \hbar k_e\rangle + \hbar\Omega_+ e^{ik_e z_c} |p + \hbar k_e\rangle \right] e^{i\alpha(t)}.$$

Projecting this equation onto the state  $|p'\rangle$  we got:

$$\begin{aligned} i\hbar \int dp e^{-i\frac{p^2}{2m\hbar}t} C_p^b(t) \langle p' | p\rangle &= \int dp e^{-i\frac{p^2}{2m\hbar}t} C_p^a(t) \left[ \hbar\Omega_- e^{-ik_e z_c} \langle p' | p - \hbar k_e\rangle + \hbar\Omega_+ e^{ik_e z_c} \langle p' | p + \hbar k_e\rangle \right] e^{i\alpha(t)} \\ i\hbar e^{-i\frac{p'^2}{2m\hbar}t} \dot{C}_{p'}^b(t) &= \left[ e^{-i\frac{(p'+\hbar k_e)^2}{2m\hbar}t} \hbar\Omega_- e^{-ik_e z_c} C_{p'+\hbar k_e}^a(t) + e^{-i\frac{(p'-\hbar k_e)^2}{2m\hbar}t} \hbar\Omega_+ e^{ik_e z_c} C_{p'-\hbar k_e}^a(t) \right] e^{i\alpha(t)} \end{aligned}$$

$$i\hbar \dot{C}_{p'}^b(t) = \left[ \hbar\Omega_- e^{-ik_e z_c(t) - i\frac{k_e p'}{m}t - i\frac{\hbar k_e^2}{2m}t} C_{p'+\hbar k_e}^a(t) + \hbar\Omega_+ e^{ik_e z_c(t) + i\frac{k_e p'}{m}t - i\frac{\hbar k_e^2}{2m}t} C_{p'-\hbar k_e}^a(t) \right] e^{i\alpha(t)}$$

If we follow a similar treatment for the state  $a$ , we got the equations for the amplitudes of probability:

$$\begin{aligned}
i\dot{C}_p^b(t) &= \left[ \Omega_+ e^{ik_e z_c(t) + i(2\beta - \mu)(\Omega t)} C_{p - \hbar k_e}^a(t) + \Omega_- e^{-ik_e z_c(t) - i(2\beta + \mu)(\Omega t)} C_{p + \hbar k_e}^a(t) \right] e^{i\alpha(t)} \\
i\dot{C}_p^a(t) &= \left[ \Omega_+^* e^{-ik_e z_c(t) - i(2\beta + \mu)(\Omega t)} C_{p + \hbar k_e}^b(t) + \Omega_-^* e^{ik_e z_c(t) + i(2\beta - \mu)(\Omega t)} C_{p - \hbar k_e}^b(t) \right] e^{-i\alpha(t)}
\end{aligned} \tag{86}$$

where we have defined,

$$\beta = \frac{k_e p}{2m\Omega} \tag{87}$$

$$\mu = \frac{\hbar k_e^2}{2m\Omega} \tag{88}$$





## APPENDIX B

### Numerical solutions of the Differential Equations.

In the present Appendix we present The Mathematica script was used to obtain the numerical solutions of the Eqs. (57). The code used has the following features:

- The numerical method to solve such equations is the Runge-kutta method  
`Method -> "ExplicitRungeKutta"`
- The different integration times are decomposed in the different times:  
`ti = 0;`  
`tf = \[Tau]/2 + \[Tau];`  
 for the first and second pulses,  
`ti = \[Tau]/2 + \[Tau] + T;`  
`tf = \[Tau]/2 + \[Tau] + T + \[Tau] + \[Tau] + \[Tau];`  
 for the third, fourth and five pulses, and  
`ti = \[Tau]/2 + \[Tau] + T + \[Tau] + \[Tau] + \[Tau] + T;`  
`tf = \[Tau]/2 + \[Tau] + T + \[Tau] + \[Tau] + \[Tau] + T + \[Tau] + \[Tau]/2;`  
 for the sixth and seventh pulses.
- This has the advantage that we can change the time integration step depending on the Doppler phase at the end of each time. This is given by the command  
`StartingStepSize -> (2 \[Pi])/(ke v[tf]) 1/100,`
- The initial conditions for all the states are given by the commands:  
`Cap0[ti] == CaOp0,`  
`Cbp1[ti] == CbOp1Mas,`

```
ti = 0;
tf = \[Tau]/2 + \[Tau];

{Cam6sI, Cam4sI, Cam2sI, Cap0sI, Cap2sI, Cap4sI, Cap6sI, Cbm5sI,
Cbm3sI, Cbm1sI, Cbp1sI, Cbp3sI, Cbp5sI, Cbp7sI} = NDSolveValue[
I Derivative[1][Cam6][t] == Cbm5[t] \[CapitalOmega]pa[-11, t],
I Derivative[1][Cam4][t] ==
Cbm5[t] \[CapitalOmega]ma[-9, t] +
Cbm3[t] \[CapitalOmega]pa[-7, t],
I Derivative[1][Cam2][t] ==
Cbm3[t] \[CapitalOmega]ma[-5, t] +
Cbm1[t] \[CapitalOmega]pa[-3, t],
I Derivative[1][Cap0][t] ==
Cbm1[t] \[CapitalOmega]ma[-1, t] + Cbp1[t] \[CapitalOmega]pa[1, t],
I Derivative[1][Cap2][t] ==
Cbp1[t] \[CapitalOmega]ma[3, t] + Cbp3[t] \[CapitalOmega]pa[5, t],
I Derivative[1][Cap4][t] ==
```

```

Cbp3[t] \[CapitalOmega]ma[7, t] + Cbp5[t] \[CapitalOmega]pa[9, t],
I Derivative[1][Cap6][t] ==
Cbp5[t] \[CapitalOmega]ma[11, t] +
Cbp7[t] \[CapitalOmega]pa[13, t],
I Derivative[1][Cbm5][t] ==
Cam4[t] \[CapitalOmega]m[-9, t] + Cam6[t] \[CapitalOmega]p[-11, t],
I Derivative[1][Cbm3][t] ==
Cam2[t] \[CapitalOmega]m[-5, t] + Cam4[t] \[CapitalOmega]p[-7, t],
I Derivative[1][Cbm1][t] ==
Cap0[t] \[CapitalOmega]m[-1, t] + Cam2[t] \[CapitalOmega]p[-3, t],
I Derivative[1][Cbp1][t] ==
Cap2[t] \[CapitalOmega]m[3, t] + Cap0[t] \[CapitalOmega]p[1, t],
I Derivative[1][Cbp3][t] ==
Cap4[t] \[CapitalOmega]m[7, t] + Cap2[t] \[CapitalOmega]p[5, t],
I Derivative[1][Cbp5][t] ==
Cap6[t] \[CapitalOmega]m[11, t] + Cap4[t] \[CapitalOmega]p[9, t],
I Derivative[1][Cbp7][t] == Cap6[t] \[CapitalOmega]p[13, t],

Cam6[ti] == 0,
Cam4[ti] == 0,
Cam2[ti] == 0,
Cap0[ti] == CaOp0,
Cap2[ti] == 0,
Cap4[ti] == 0,
Cap6[ti] == 0,
Cbm5[ti] == 0,
Cbm3[ti] == 0,
Cbm1[ti] == 0,
Cbp1[ti] == CbOp1Mas,
Cbp3[ti] == 0,
Cbp5[ti] == 0,
Cbp7[ti] == 0,
{Cam6, Cam4, Cam2, Cap0, Cap2, Cap4, Cap6, Cbm5, Cbm3, Cbm1, Cbp1,
Cbp3, Cbp5, Cbp7}, {t, ti, tf},
StartingStepSize -> (2 \[Pi])/(ke v[tf]) 1/100,
MaxSteps -> \[Infinity],
Method -> "FixedStep", Method -> "ExplicitRungeKutta";

```

The functions that are involved in the Runge-Kutta code are the following:

```

\[Delta][n_] := \[CapitalOmega] (2 \[Beta] + n*\[Mu]);
\[Alpha]p[t_] := -ke (z0 + v0*t + (\[Gamma] + g)/2 t^2) - \[Mu]*(\[CapitalOmega] t);
\[Alpha]m[t_] := ke (z0 + v0*t + (\[Gamma] + g)/2 t^2) + 3 \[Mu]*(\[CapitalOmega] t);
\[Alpha][t_] :=
Piecewise[{{\[Alpha]p[t], t <= \[Tau]/2}, {\[Alpha]m[t],
t <= \[Tau]/2 + \[Tau]}, {0,

```

```

t <= \[Tau]/2 + \[Tau] + T}, {\[Alpha]p[t],
t <= \[Tau]/2 + \[Tau] + T + \[Tau]}, {\[Alpha]m[t],
t <= \[Tau]/2 + \[Tau] + T + \[Tau] + \[Tau]}, {\[Alpha]p[t],
t <= \[Tau]/2 + \[Tau] + T + \[Tau] + \[Tau] + \[Tau]}, {0,
t <= \[Tau]/2 + \[Tau] + T + \[Tau] + \[Tau] + \[Tau] +
T}, {\[Alpha]m[t],
t <= \[Tau]/2 + \[Tau] + T + \[Tau] + \[Tau] + \[Tau] +
T + \[Tau]}, {\[Alpha]p[t],
t <= \[Tau]/2 + \[Tau] + T + \[Tau] + \[Tau] + \[Tau] +
T + \[Tau] + \[Tau]/2}}};
\[CapitalOmega]t[t_] :=
Piecewise[{{\[CapitalOmega], t <= \[Tau]/2 + \[Tau]}, {0,
t <= \[Tau]/2 + \[Tau] + T}, {\[CapitalOmega],
t <= \[Tau]/2 + \[Tau] + T + \[Tau] + \[Tau] + \[Tau]}, {0,
t <= \[Tau]/2 + \[Tau] + T + \[Tau] + \[Tau] + \[Tau] +
T}, {\[CapitalOmega],
t <= \[Tau]/2 + \[Tau] + T + \[Tau] + \[Tau] + \[Tau] +
T + \[Tau] + \[Tau]/2}}];
\[CapitalTheta]p[t_] := \[Alpha][t] + ke (z0 + v0*t + g/2 t^2);
\[CapitalTheta]m[t_] := \[Alpha][t] - ke (z0 + v0*t + g/2 t^2);
\[CapitalOmega]p[n_, t_] := \[CapitalOmega]t[t]*
Exp[I*\[CapitalTheta]p[t]]*Exp[I (\[Delta][n]*t)];
\[CapitalOmega]pa[n_, t_] := \[CapitalOmega]t[t]*
Exp[-I*\[CapitalTheta]p[t]]*Exp[-I (\[Delta][n]*t)];
\[CapitalOmega]m[n_, t_] := \[CapitalOmega]t[t]*
Exp[I*\[CapitalTheta]m[t]]*Exp[-I (\[Delta][n]*t)];
\[CapitalOmega]ma[n_, t_] := \[CapitalOmega]t[t]*
Exp[-I*\[CapitalTheta]m[t]]*Exp[I (\[Delta][n]*t)];

```

- These functions represent the different phases due to Doppler effect and the chirping frequency to compensate in the commands:

```

\[CapitalTheta]p[t_] := \[Alpha][t] + ke (z0 + v0*t + g/2 t^2);
\[CapitalTheta]m[t_] := \[Alpha][t] - ke (z0 + v0*t + g/2 t^2);

```

With the aim to check the convergence of the numerical method we changed the number of the sampling in the time integration domain:

```

StartingStepSize -> (2 \[Pi])/(ke v[tf]) 1/10,
StartingStepSize -> (2 \[Pi])/(ke v[tf]) 1/100,
StartingStepSize -> (2 \[Pi])/(ke v[tf]) 1/1000,

```

The numerical results for the probability amplitudes do not change in the digits inside the precision of the variable used for the blue number in the last command. This means that for minimum, we need to sample ten times in an uniform way in one cycle of the Doppler phase  $ke v[tf]$  to guarantee the convergence of the method.



## APPENDIX C

### Perturbative Solutions of the seven steps Interferometer.

In the present Appendix we present the detailed calculations of the probability amplitudes of the seven step interferometer described in Fig. (3.3), as an illustration of the application of the perturbative method found in Chapter 3.

**Resonant Solution with ramp  $\alpha_+$ .**

$$\begin{aligned} C_a(p, t) &= e^{-i\beta(\Omega t)} \left\{ [\cos(\Omega t) + i\beta \sin(\Omega t)] C_a(p, 0) - i \frac{\Omega_+^a(n, t_i)}{|\Omega_+^a(n, t_i)|} \sin(\Omega t) C_b(p + \hbar k_e, 0) \right\} \\ C_b(p + \hbar k_e, t) &= e^{i\beta(\Omega t)} \left\{ -i \frac{\Omega_+^b(n, t_i)}{|\Omega_+^b(n, t_i)|} \sin(\Omega t) C_a(p, 0) + [\cos(\Omega t) - i\beta \sin(\Omega t)] C_b(p + \hbar k_e, 0) \right\} \end{aligned}$$

**Resonant Solution with ramp  $\alpha_-$ .**

$$\begin{aligned} C_a(p + 2\hbar k_e, t) &= e^{i\beta(\Omega t)} \left\{ [\cos(\Omega t) - i\beta \sin(\Omega t)] C_a(p + 2\hbar k_e, 0) - i \frac{\Omega_-^a(n, t_i)}{|\Omega_-^a(n, t_i)|} \sin(\Omega t) C_b(p + \hbar k_e, 0) \right\} \\ C_b(p + \hbar k_e, t) &= e^{-i\beta(\Omega t)} \left\{ -i \frac{\Omega_-^b(n, t_i)}{|\Omega_-^b(n, t_i)|} \sin(\Omega t) C_a(p + 2\hbar k_e, 0) + [\cos(\Omega t) + i\beta \sin(\Omega t)] C_b(p + \hbar k_e, 0) \right\} \end{aligned}$$

We fix the notation:

$$\begin{aligned} F_+^a(n, t_i) &= \frac{\Omega_+^a(n, t_i)}{|\Omega_+^a(n, t_i)|} = e^{-\frac{i}{2}k_e\gamma t_i^2 - 2i(\beta+n\mu)(\Omega t_i)} \\ F_+^b(n, t_i) &= \frac{\Omega_+^b(n, t_i)}{|\Omega_+^b(n, t_i)|} = e^{\frac{i}{2}k_e\gamma t_i^2 + 2i[\beta+(n-1)\mu](\Omega t_i)} \\ F_-^a(n, t_i) &= \frac{\Omega_-^a(n, t_i)}{|\Omega_-^a(n, t_i)|} = e^{\frac{i}{2}k_e\gamma t_i^2 + 2i[\beta+(n-2)\mu](\Omega t_i)} \\ F_-^b(n, t_i) &= \frac{\Omega_-^b(n, t_i)}{|\Omega_-^b(n, t_i)|} = e^{-\frac{i}{2}k_e\gamma t_i^2 - 2i[\beta+(n-1)\mu](\Omega t_i)} \end{aligned}$$

From these solutions, we can write:

$$\begin{aligned} \langle a, 0 | \hat{U}_0(t) &= e^{-i\beta(\Omega t)} \left\{ [\cos(\Omega t) + i\beta \sin(\Omega t)] \langle a, 0 | + (-i)F_+^a(0, t_i) \sin(\Omega t) \langle b, 1 | \right\} \\ \langle b, 1 | \hat{U}_0(t) &= e^{i\beta(\Omega t)} \left\{ (-i)F_+^b(1, t_i) \sin(\Omega t) \langle a, 0 | + [\cos(\Omega t) - i\beta \sin(\Omega t)] \langle b, 1 | \right\} \\ \langle a, 2 | \hat{U}_0(t) &= e^{i\beta(\Omega t)} \left\{ [\cos(\Omega t) - i\beta \sin(\Omega t)] \langle a, 2 | + (-i)F_-^a(2, t_i) \sin(\Omega t) \langle b, 1 | \right\} \\ \langle b, 1 | \hat{U}_0(t) &= e^{-i\beta(\Omega t)} \left\{ (-i)F_-^b(1, t_i) \sin(\Omega t) \langle a, 2 | + [\cos(\Omega t) + i\beta \sin(\Omega t)] \langle b, 1 | \right\} \end{aligned}$$

In an analogous way, we obtain the solutions for non-resonant transitions:

**Non-resonant solution with ramp  $\alpha_+$ .**

$$\begin{aligned}
\langle a, -2 | \hat{U}_0(t) &= e^{-i(\beta-2\mu)(\Omega t)} \left\{ \left[ \cos \left( \Omega t \sqrt{1 + (2\mu)^2} \right) + \frac{(-i)(2\mu)}{\sqrt{1 + (2\mu)^2}} \sin \left( \Omega t \sqrt{1 + (2\mu)^2} \right) \right] \langle a, -2 | \right. \\
&\quad \left. + \frac{(-i)F_a^+(-2, t_i)}{\sqrt{1 + (2\mu)^2}} \sin \left( \Omega t \sqrt{1 + (2\mu)^2} \right) \langle b, 3 | \right\} \\
\langle b, -1 | \hat{U}_0(t) &= e^{i(\beta-2\mu)(\Omega t)} \left\{ \frac{(-i)F_b^+(-1, t_i)}{\sqrt{1 + (2\mu)^2}} \sin \left( \Omega t \sqrt{1 + (2\mu)^2} \right) \langle a, -2 | \right. \\
&\quad \left. + \left[ \cos \left( \Omega t \sqrt{1 + (2\mu)^2} \right) + \frac{i(2\mu)}{\sqrt{1 + \mu^2}} \sin \left( \Omega t \sqrt{1 + (2\mu)^2} \right) \right] \langle b, -1 | \right\} \\
\langle a, 2 | \hat{U}_0(t) &= e^{-i(\beta+2\mu)(\Omega t)} \left\{ \left[ \cos \left( \Omega t \sqrt{1 + (2\mu)^2} \right) + \frac{i(2\mu)}{\sqrt{1 + (2\mu)^2}} \sin \left( \Omega t \sqrt{1 + (2\mu)^2} \right) \right] \langle a, 2 | \right. \\
&\quad \left. + \frac{(-i)F_a^+(2, t_i)}{\sqrt{1 + (2\mu)^2}} \sin \left( \Omega t \sqrt{1 + (2\mu)^2} \right) \langle b, 3 | \right\} \\
\langle b, 3 | \hat{U}_0(t) &= e^{i(\beta+2\mu)(\Omega t)} \left\{ \frac{(-i)F_b^+(3, t_i)}{\sqrt{1 + (2\mu)^2}} \sin \left( \Omega t \sqrt{1 + (2\mu)^2} \right) \langle a, 2 | \right. \\
&\quad \left. + \left[ \cos \left( \Omega t \sqrt{1 + (2\mu)^2} \right) + \frac{(-i)(2\mu)}{\sqrt{1 + \mu^2}} \sin \left( \Omega t \sqrt{1 + (2\mu)^2} \right) \right] \langle b, 3 | \right\}
\end{aligned}$$

**Non-resonant solution with ramp  $\alpha_-$ .**

$$\begin{aligned}
\langle a, 0 | \hat{U}_0(t) &= e^{i(\beta-(2\mu))(\Omega t)} \left\{ \left[ \cos \left( \Omega t \sqrt{1 + (2\mu)^2} \right) + \frac{i(2\mu)}{\sqrt{1 + (2\mu)^2}} \sin \left[ \Omega t \sqrt{1 + (2\mu)^2} \right] \right] \langle a, 0 | \right. \\
&\quad \left. + \frac{(-i)F_a^-(0, t_i)}{\sqrt{1 + (2\mu)^2}} \sin \left[ \Omega t \sqrt{1 + (2\mu)^2} \right] \langle b, -1 | \right\} \\
\langle b, -1 | \hat{U}_0(t) &= e^{-i(\beta-(2\mu))(\Omega t)} \left\{ \frac{(-i)F_b^-(-1, t_i)}{\sqrt{1 + (2\mu)^2}} \sin \left[ \Omega t \sqrt{1 + (2\mu)^2} \right] \langle a, 0 | \right. \\
&\quad \left. + \left[ \cos \left( \Omega t \sqrt{1 + (2\mu)^2} \right) + \frac{(-i)(2\mu)}{\sqrt{1 + (2\mu)^2}} \sin \left[ \Omega t \sqrt{1 + (2\mu)^2} \right] \right] \langle b, -1 | \right\} \\
\langle a, 4 | \hat{U}_0(t) &= e^{i(\beta+(2\mu))(\Omega t)} \left\{ \left[ \cos \left( \Omega t \sqrt{1 + (2\mu)^2} \right) + \frac{(-i)(2\mu)}{\sqrt{1 + (2\mu)^2}} \sin \left[ \Omega t \sqrt{1 + (2\mu)^2} \right] \right] \langle a, 4 | \right. \\
&\quad \left. + \frac{(-i)F_a^-(4, t_i)}{\sqrt{1 + (2\mu)^2}} \sin \left[ \Omega t \sqrt{1 + (2\mu)^2} \right] \langle b, 3 | \right\}
\end{aligned}$$

$$\begin{aligned} \langle b, 3 | \hat{U}_0(t) = & e^{-i(\beta+(2\mu))(\Omega t)} \left\{ \frac{(-i)F_b^-(3, t_i)}{\sqrt{1+(2\mu)^2}} \sin \left[ \Omega t \sqrt{1+(2\mu)^2} \right] \langle a, 4 | \right. \\ & \left. + \left[ \cos \left( \Omega t \sqrt{1+(2\mu)^2} \right) + \frac{i(2\mu)}{\sqrt{1+(2\mu)^2}} \sin \left[ \Omega t \sqrt{1+(2\mu)^2} \right] \right] \langle b, 3 | \right\} \end{aligned}$$

We can now take the solutions of any step of the interferometer.

### 1. Second Pulse.

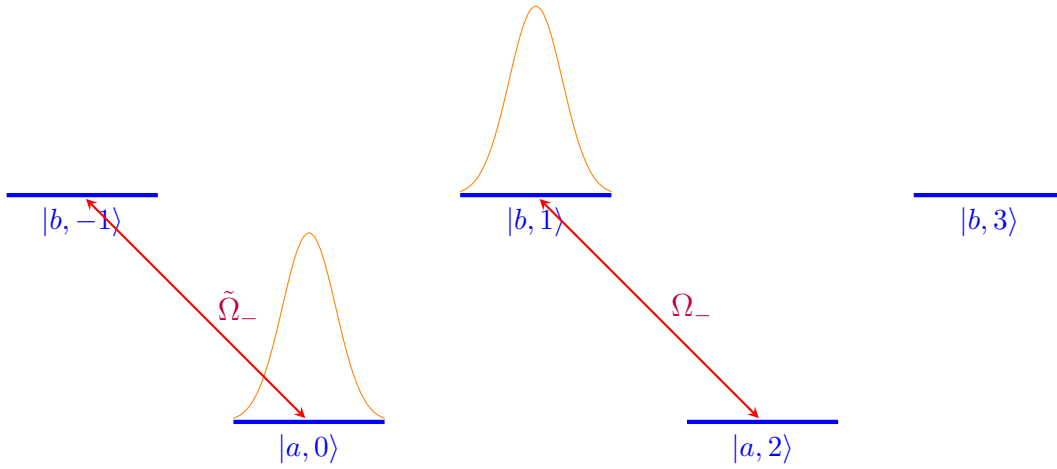


FIGURE C.1. Initial configuration of the probability amplitude of the states before the second pulse is applied.

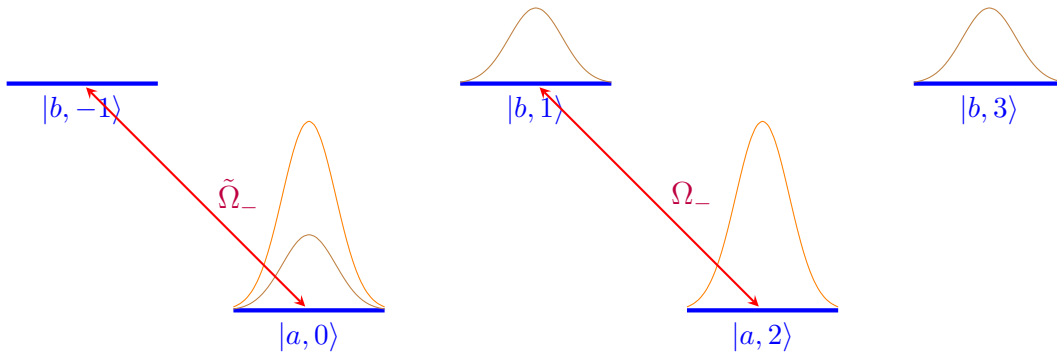


FIGURE C.2. Final configuration of the probability amplitudes of the states after the second pulse.



**1.1. State  $|a, 0\rangle$ .**

$$\begin{aligned}
C_p^a(t_2) &= \langle a, 0 | \hat{U}(t_1, t_2) | \psi(t_1) \rangle \\
&= (-i) \int_{t_1}^{t_2} dt' \langle a, 0 | \hat{V}(t') \hat{U}_0(t_1, t') | \psi(t_1) \rangle \\
&= (-i) \int_{t_1}^{t_2} dt' \langle a, 0 | \hat{V}(t') | b, 1 \rangle \langle b, 1 | \hat{U}_0(t_1, t') | \psi(t_1) \rangle \\
&= (-i) \int_{t_1}^{t_2} dt' R_0(t') \langle b, 1 | \hat{U}_0(t_1, t') | \psi(t_1) \rangle \\
&= (-i) \int_{t_1}^{t_2} dt' \Omega_+^* e^{-2ik_e z_c(t') - 2i(\beta+2\mu)(\Omega t')} \langle b, 1 | \hat{U}_0(t_1, t') | \psi(t_1) \rangle \\
&= (-i) \Omega_+^* e^{-2ik_e z_c(v_0, t_1) - 2i(\beta+2\mu)(\Omega t_1)} \\
&\quad \int_0^{t_2-t_1} dt' e^{-2ik_e z_c(v_0+gt_1, t') - 2i(\beta+2\mu)(\Omega t')} \langle b, 1 | \hat{U}_0(t' - t_1) | \psi(t_1) \rangle
\end{aligned}$$

$$\begin{aligned}
C_p^a(t_2) &= (-i) \Omega_+^* e^{-2ik_e z_c(v_0, t_1) - 2i(\beta+2\mu)(\Omega t_1)} \\
&\quad \int_0^{t_2-t_1} dt' e^{-2ik_e z_c(v_0+gt_1, t') - 2i(\beta+2\mu)(\Omega t')} e^{-i\beta(\Omega t')} [\cos(\Omega t') + i\beta \sin(\Omega t')] C_{p+hk_e}^b(t_1) \\
&= (-i) \Omega_+^* e^{-2ik_e z_c(v_0, t_1) - 2i(\beta+2\mu)(\Omega t_1)} \\
&\quad \int_0^{t_2-t_1} dt' e^{-2ik_e z_c(v_0+gt_1, t') - i(3\beta+4\mu)(\Omega t')} [\cos(\Omega t') + i\beta \sin(\Omega t')] C_{p+hk_e}^b(t_1) \\
&= \eta(t_2) C_{p+hk_e}^b(t_1) e^{-i\phi_+} e^{-2ik_e z_c(v_0, t_1) - 2i(\beta+2\mu)(\Omega t_1)} \\
&\quad \left\{ e^{-2ik_e z_c(v_0+gt_1, \tau_2) - i(3\beta+4\mu)(\Omega \tau_2)} \cos(\Omega \tau_2) - 1 \right\}
\end{aligned}$$

**1.2. State  $|b, 1\rangle$ .**

$$\begin{aligned}
C_{p+hk_e}^b(t_2) &= \langle b, 1 | \hat{U}(t_1, t_2) | \psi(t_1) \rangle \\
&= (-i) \int_{t_1}^{t_2} dt' \langle b, 1 | \hat{V}(t') \hat{U}_0(t_1, t') | \psi(t_1) \rangle \\
&= (-i) \int_{t_1}^{t_2} dt' \langle b, 1 | \hat{V}(t') | a, 0 \rangle \langle a, 0 | \hat{U}_0(t_1, t') | \psi(t_1) \rangle \\
&= (-i) \int_{t_1}^{t_2} dt' R_0^*(t') \langle a, 0 | \hat{U}_0(t_1, t') | \psi(t_1) \rangle \\
&= (-i) \int_{t_1}^{t_2} dt' \Omega_+ e^{2ik_e z_c(t') + 2i(\beta+2\mu)(\Omega t')} \langle a, 0 | \hat{U}_0(t_1, t') | \psi(t_1) \rangle \\
&= (-i) \Omega_+ e^{2ik_e z_c(v_0, t_1) + 2i(\beta+2\mu)(\Omega t_1)} \\
&\quad \int_0^{t_2-t_1} dt' e^{2ik_e z_c(v_0+gt_1, t') + 2i(\beta+2\mu)(\Omega t')} \langle a, 0 | \hat{U}_0(t' - t_1) | \psi(t_1) \rangle
\end{aligned}$$

$$\begin{aligned}
C_{p+\hbar k_e}^b(t_2) &= (-i)\Omega_+ e^{2ik_e z_c(v_0, t_1) + 2i(\beta+2\mu)(\Omega t_1)} \\
&\int_0^{t_2-t_1} dt' e^{2ik_e z_c(v_0+gt_1, t') + 2i(\beta+2\mu)(\Omega t')} \\
&e^{i(\beta-2\mu)(\Omega t')} \left[ \cos\left(\Omega t' \sqrt{1+(2\mu)^2}\right) + \frac{i(2\mu)}{\sqrt{1+(2\mu)^2}} \sin\left(\Omega t' \sqrt{1+(2\mu)^2}\right) \right] C_p^a(t_1) \\
= &(-i)\Omega_+ e^{2ik_e z_c(v_0, t_1) + 2i(\beta+2\mu)(\Omega t_1)} \\
&\int_0^{t_2-t_1} dt' e^{2ik_e z_c(v_0+gt_1, t') + i(3\beta+2\mu)(\Omega t')} \left[ \cos\left(\Omega t' \sqrt{1+(2\mu)^2}\right) + \frac{i(2\mu)}{\sqrt{1+(2\mu)^2}} \sin\left(\Omega t' \sqrt{1+(2\mu)^2}\right) \right] C_p^a(t_1) \\
= &-\eta(t_2) C_p^a(t_1) e^{i\phi_+} e^{2ik_e z_c(v_0, t_1) + 2i(\beta+2\mu)(\Omega t_1)} \\
&\left\{ e^{2ik_e z_c(v_0+gt_1, \tau_2) + i(3\beta+2\mu)(\Omega \tau_2)} \left[ \cos\left(\Omega \tau_2 \sqrt{1+(2\mu)^2}\right) + \frac{i(2\mu)}{\sqrt{1+(2\mu)^2}} \sin\left(\Omega \tau_2 \sqrt{1+(2\mu)^2}\right) \right] - 1 \right\}
\end{aligned}$$

### 1.3. State $|b, 3\rangle$ .

$$\begin{aligned}
C_{p+3\hbar k_e}^b(t_2) &= \langle b, 3 | \hat{U}(t_2) | \psi(t_1) \rangle \\
&= (-i) \int_{t_1}^{t_2} dt' \langle b, 3 | \hat{V}(t') \hat{U}_0(t_1, t') | \psi(t_1) \rangle \\
&= (-i) \int_{t_1}^{t_2} dt' \langle b, 3 | \hat{V}(t') | a, 2 \rangle \langle a, 2 | \hat{U}_0(t_1, t') | \psi(t_1) \rangle
\end{aligned}$$

$$\begin{aligned}
\langle b, 3 | \hat{V}(t') | a, 2 \rangle &= R_2^*(t') \\
&= \Omega_+ e^{2ik_e z_c(t') + 2i(\beta+4\mu)(\Omega t')}
\end{aligned}$$

$$\begin{aligned}
C_{p+3\hbar k_e}^b(t_2) &= (-i)\Omega_+ e^{2ik_e z_c(v_0, t_1) + 2i(\beta+4\mu)(\Omega t_1)} \\
&\int_0^{t_2-t_1} dt' e^{2ik_e z_c(v_0+gt_1, t') + 2i(\beta+4\mu)(\Omega t')} \langle a, 2 | \hat{U}_0(t' - t_1) | \psi(t_1) \rangle
\end{aligned}$$

$$\langle a, 2 | \hat{U}_0(t' - t_1) | \psi(t_1) \rangle = (-i) e^{-i\beta(\Omega t')} F_b^-(1, t_1) \sin(\Omega t') C_{p+\hbar k_e}^b(t_1)$$

$$\begin{aligned}
C_{p+3\hbar k_e}^b(t_2) &= -\Omega_+ F_b^-(1, t_1) C_{p+\hbar k_e}^b(t_1) e^{2ik_e z_c(v_0, t_1) + 2i(\beta+4\mu)(\Omega t_1)} \\
&\int_0^{t_2-t_1} dt' e^{2ik_e z_c(v_0+gt_1, t') + i(\beta+8\mu)(\Omega t')} \sin(\Omega t')
\end{aligned}$$

$$\begin{aligned}
C_{p+3\hbar k_e}^b(t_2) &= i\eta(t_2) F_b^-(1, t_1) C_{p+\hbar k_e}^b(t_1) e^{2ik_e z_c(v_0, t_1) + 2i(\beta+4\mu)(\Omega t_1)} \\
&e^{2ik_e z_c(v_0+gt_1, \tau_2) + i(\beta+8\mu)(\Omega \tau_2)} \sin(\Omega \tau_2)
\end{aligned}$$

## 2. Third Pulse.

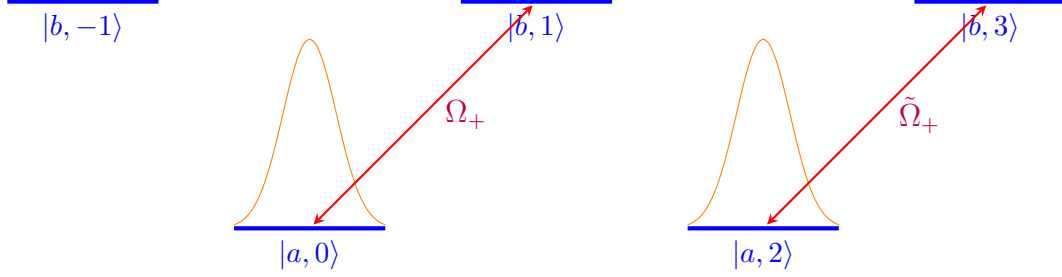


FIGURE C.3. Initial configuration of the probability amplitude of the states before the third pulse.

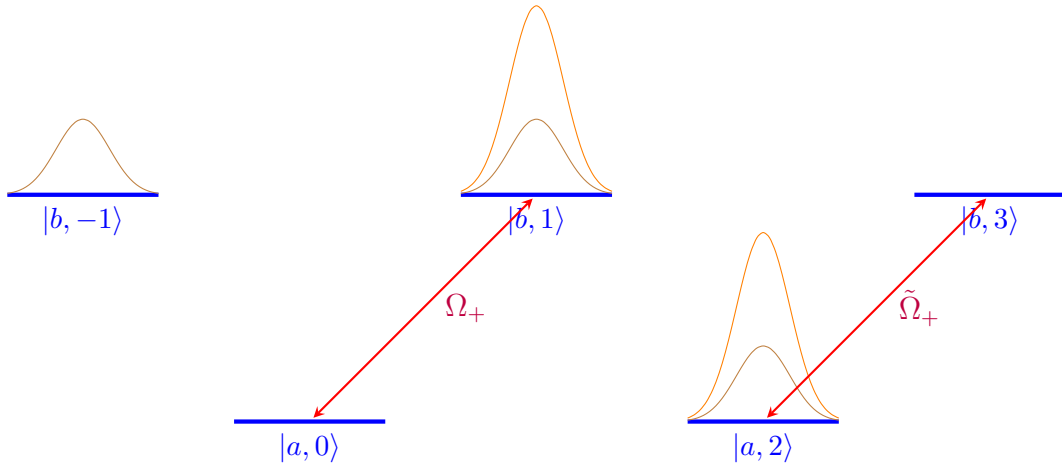


FIGURE C.4. Final configuration of the probability amplitude of the states after the third pulse.

### 2.1. State $|b, -1\rangle$ .

$$\begin{aligned}
 C_{p-\hbar k_e}^b(t_3) &= \langle b, -1 | \hat{U}(t_3) | \psi(t_2) = \psi(t_3) \rangle \\
 &= (-i) \int_{t_{3A}}^{t_{3D}} dt' \langle b, -1 | \hat{V}(t') \hat{U}_0(t_{3A}, t') | \psi(t_2) \rangle \\
 &= (-i) \int_{t_{3A}}^{t_{3D}} dt' \langle b, -1 | \hat{V}(t') | a, 0 \rangle \langle a, 0 | \hat{U}_0(t_{3A}, t') | \psi(t_2) \rangle
 \end{aligned}$$

$$\begin{aligned}
 \langle b, -1 | \hat{V}(t') | a, 0 \rangle &= L_{-2}^*(t') \\
 &= \Omega_- e^{-2ik_e z_e(t') - 2i\beta(\Omega t')}
 \end{aligned}$$

$$C_{p-hk_e}^b(t_3) = (-i)\Omega_- e^{-2ik_e z_c(v_0, t_{3A}) - 2i\beta(\Omega t_{3A})} \int_0^{\tau_3} dt' e^{-2ik_e z_c(v_0 + gt_{3A}, t') - 2i\beta(\Omega t')} \langle a, 0 | \hat{U}_0(t' - t_{3A}) | \psi(t_2) \rangle$$

$$\langle a, 0 | \hat{U}_0(t' - t_{3A}) | \psi(t_1) \rangle = e^{-i\beta(\Omega t')} \{ [\cos(\Omega t') + i\beta \sin(\Omega t')] C_p^a(t_2) \}$$

$$C_{p-hk_e}^b(t_3) = (-i)\Omega_- C_p^a(t_2) e^{-2ik_e z_c(v_0, t_{3A}) - 2i\beta(\Omega t_{3A})} \int_0^{\tau_3} dt' e^{-2ik_e z_c(v_0 + gt_{3A}, t') - 3i\beta(\Omega t')} \cos(\Omega t')$$

$$C_{p-hk_e}^b(t_3) = \eta(t_{3D}) e^{i\phi} C_p^a(t_2) e^{-2ik_e z_c(v_0, t_{3A}) - 2i\beta(\Omega t_{3A})} \left[ e^{-2ik_e z_c(v_0 + gt_{3A}, \tau_3) - 3i\beta(\Omega \tau_3)} \cos(\Omega \tau_3) - 1 \right]$$

## 2.2. State $|b, 1\rangle$ .

$$\begin{aligned} C_{p+hk_e}^b(t_3) &= \langle b, 1 | \hat{U}(t_3) | \psi(t_2) = \psi(t_{3A}) \rangle \\ &= (-i) \int_{t_{3A}}^{t_{3D}} dt' \langle b, 1 | \hat{V}(t') \hat{U}_0(t_{3A}, t') | \psi(t_2) \rangle \\ &= (-i) \int_{t_{3A}}^{t_{3D}} dt' \langle b, 1 | \hat{V}(t') | a, 2 \rangle \langle a, 2 | \hat{U}_0(t_{3A}, t') | \psi(t_2) \rangle \end{aligned}$$

$$\begin{aligned} \langle b, 1 | \hat{V}(t') | a, 2 \rangle &= L_0^*(t') \\ &= \Omega_- e^{-2ik_e z_c(t') - 2i(\beta + 2\mu)(\Omega t')} \end{aligned}$$

$$C_{p-hk_e}^b(t_3) = (-i)\Omega_- e^{-2ik_e z_c(v_0, t_{3A}) - 2i(\beta + 2\mu)(\Omega t_{3A})} \int_0^{\tau_3} dt' e^{-2ik_e z_c(v_0 + gt_{3A}, t') - 2i(\beta + 2\mu)(\Omega t')} \langle a, 2 | \hat{U}_0(t' - t_{3A}) | \psi(t_2) \rangle$$

$$\begin{aligned} \langle a, 2 | \hat{U}_0(t' - t_{3A}) | \psi(t_1) \rangle &= e^{-i(\beta + 2\mu)(\Omega t)} \\ &\left\{ \left[ \cos\left(\Omega t' \sqrt{1 + (2\mu)^2}\right) + \frac{i(2\mu)}{\sqrt{1 + (2\mu)^2}} \sin\left(\Omega t' \sqrt{1 + (2\mu)^2}\right) \right] C_{p+2hk_e}^a(t_2) \right\} \end{aligned}$$

$$\begin{aligned} C_{p-hk_e}^b(t_3) &= (-i)\Omega_- e^{-2ik_e z_c(v_0, t_{3A}) - 2i(\beta + 2\mu)(\Omega t_{3A})} \\ &\int_0^{\tau_3} dt' e^{-2ik_e z_c(v_0 + gt_{3A}, t') - i(3\beta + 6\mu)(\Omega t')} \\ &\left\{ \left[ \cos\left(\Omega t \sqrt{1 + (2\mu)^2}\right) + \frac{i(2\mu)}{\sqrt{1 + (2\mu)^2}} \sin\left(\Omega t \sqrt{1 + (2\mu)^2}\right) \right] C_{p+2hk_e}^a(t_2) \right\} \end{aligned}$$

$$C_{p-hk_e}^b(t_3) = \eta(t_{3D})e^{i\phi} - C_{p+2hk_e}^a(t_2)e^{-2ik_e z_c(v_0, t_{3A}) - 2i(\beta+2\mu)(\Omega t_{3A})} \\ \left\{ e^{-2ik_e z_c(v_0 + gt_{3A}, \tau_3) - i(3\beta+6\mu)(\Omega \tau_3)} \left[ \cos\left(\Omega \tau_3 \sqrt{1 + (2\mu)^2}\right) + \frac{i(2\mu)}{\sqrt{1 + (2\mu)^2}} \sin\left(\Omega \tau_3 \sqrt{1 + (2\mu)^2}\right) \right] - 1 \right\}$$

### 2.3. State $|a, 2\rangle$ .

$$C_{p+2hk_e}^a(t_3) = \langle a, 2 | \hat{U}(t_3) | \psi(t_2) = \psi(t_{3A}) \rangle \\ = (-i) \int_{t_{3A}}^{t_{3D}} dt' \langle a, 2 | \hat{V}(t') \hat{U}_0(t_{3A}, t') | \psi(t_2) \rangle \\ = (-i) \int_{t_{3A}}^{t_{3D}} dt' \langle a, 2 | \hat{V}(t') | b, 1 \rangle \langle b, 1 | \hat{U}_0(t_{3A}, t') | \psi(t_2) \rangle$$

$$\langle a, 2 | \hat{V}(t') | b, 1 \rangle = L_0(t') \\ = \Omega_-^* e^{2ik_e z_c(t') + 2i(\beta+2\mu)(\Omega t')}$$

$$\langle b, 1 | \hat{U}_0(t' - t_{3A}) | \psi(t_1) \rangle = e^{-i\beta(\Omega t')} \{ (-i) F_b^+(1, t_{3A}) \sin(\Omega t') C_p^a(t_2) \}$$

$$C_{p+2hk_e}^a(t_3) = -\Omega_-^* F_b^+(1, t_{3A}) C_p^a(t_2) e^{2ik_e z_c(v_0, t_{3A}) + 2i(\beta+2\mu)(\Omega t_{3A})} \\ \int_0^{\tau_3} dt' e^{2ik_e z_c(v_0 + gt_{3A}, t') + i(\beta+4\mu)(\Omega t')} \sin(\Omega t')$$

$$C_{p+2hk_e}^a(t_3) = i\eta(t_{3D})e^{i\phi} - F_b^+(1, t_{3A}) C_p^a(t_2) e^{2ik_e z_c(v_0, t_{3A}) + 2i(\beta+2\mu)(\Omega t_{3A})} \\ e^{2ik_e z_c(v_0 + gt_{3A}, \tau_3) + i(\beta+4\mu)(\Omega \tau_3)} \sin(\Omega \tau_3)$$

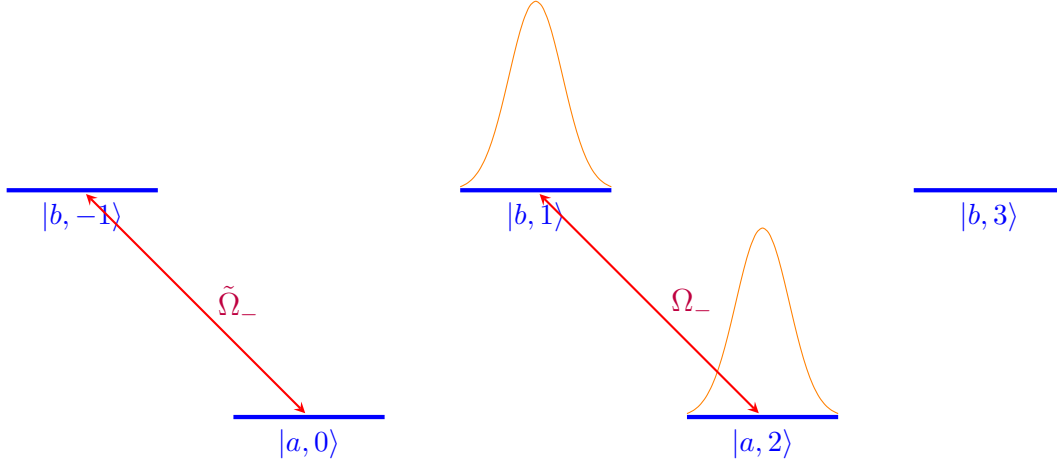
**3. Fourth Pulse.**

FIGURE C.5. Initial configuration of the probability amplitude of the states before the fourth pulse.

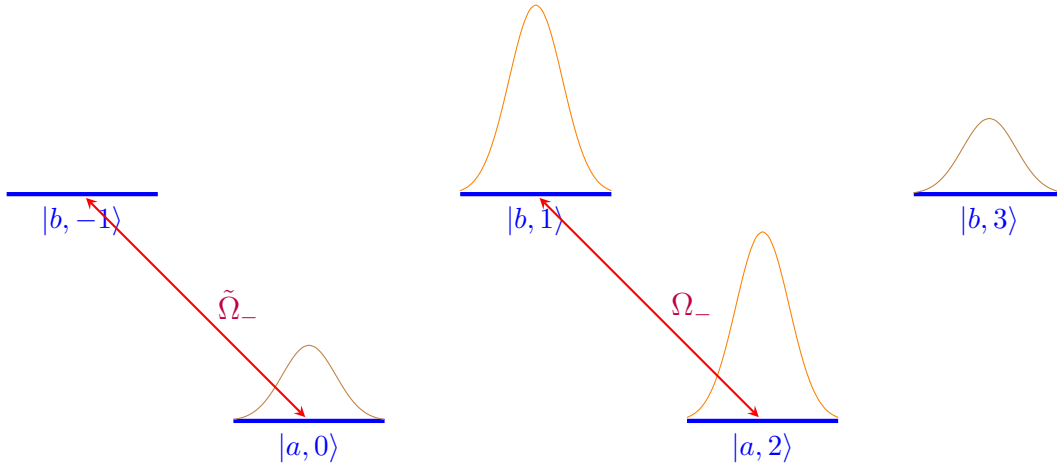


FIGURE C.6. Final configuration of the probability amplitude of the states after the fourth pulse.

**3.1. State  $|a, 0\rangle$ .**

$$\begin{aligned}
 C_p^a(t_4) &= \langle a, 0 | \hat{U}(t) | \psi(t_{3D}) \rangle \\
 &= (-i) \int_{t_{3D}}^{t_4} dt' \langle a, 0 | \hat{V}(t') \hat{U}_0(t_{3D}, t') | \psi(t_{3D}) \rangle \\
 &= (-i) \int_{t_{3D}}^{t_4} dt' \langle a, 0 | \hat{V}(t') | b, 1 \rangle \langle b, 1 | \hat{U}_0(t_{3D}, t') | \psi(t_{3D}) \rangle
 \end{aligned}$$

$$\begin{aligned}\langle a, 0 | \hat{V}(t') | b, 1 \rangle &= R_0(t') \\ &= \Omega_+^* e^{-2ik_e z_c(t') - 2i(\beta+2\mu)(\Omega t')}\end{aligned}$$

$$\begin{aligned}C_p^a(t_4) &= (-i)\Omega_+^* \int_{t_{3D}}^{t_4} dt' e^{-2ik_e z_c(t') - 2i(\beta+2\mu)(\Omega t')} \langle b, 1 | \hat{U}_0(t_{3D}, t') | \psi(t_{3D}) \rangle \\ &= \eta(t_4) e^{-2ik_e z_c(v_0, t_{3D}) - 2i(\beta+2\mu)(\Omega t_{3D})} \int_0^{\tau_4} dt' e^{-2ik_e z_c(v_0 + gt_{3D}, t') - 2i(\beta+2\mu)(\Omega t')} \langle b, 1 | \hat{U}_0(t' - t_{3D}) | \psi(t_{3D}) \rangle\end{aligned}$$

$$\langle b, 1 | \hat{U}_0(t' - t_{3D}) | \psi(t_{3D}) \rangle = e^{-i\beta(\Omega t')} \left[ \cos(\Omega t') C_{p+hk_e}^b(t_{3D}) + (-i)F_b^-(1, t_{3D}) \sin(\Omega t') C_{p+2hk_e}^a(t_{3D}) \right]$$

$$\begin{aligned}C_p^a(t_4) &= (-i)\Omega_+^* e^{-2ik_e z_c(v_0, t_{3D}) - 2i(\beta+2\mu)(\Omega t_{3D})} \\ &\left\{ C_{p+hk_e}^b(t_{3D}) \int_0^{\tau_4} dt' e^{-2ik_e z_c(v_0 + gt_{3D}, t') - i(3\beta+2\mu)(\Omega t')} \cos(\Omega t') \right. \\ &\left. + (-i)F_b^-(1, t_{3D}) C_{p+2hk_e}^a(t_{3D}) \int_0^{\tau_4} dt' e^{-2ik_e z_c(v_0 + gt_{3D}, t') - i(3\beta+4\mu)(\Omega t')} \sin(\Omega t') \right\}\end{aligned}$$

$$\begin{aligned}C_p^a(t_4) &= \eta(t_4) e^{-2ik_e z_c(v_0, t_{3D}) - 2i(\beta+2\mu)(\Omega t_{3D})} \\ &\left\{ C_{p+hk_e}^b(t_{3D}) \left[ e^{-2ik_e z_c(v_0 + gt_{3D}, \tau_4) - i(3\beta+4\mu)(\Omega \tau_4)} \cos(\Omega \tau_4) - 1 \right] \right. \\ &\left. + (-i)F_b^-(1, t_{3D}) C_{p+2hk_e}^a(t_{3D}) e^{-2ik_e z_c(v_0 + gt_{3D}, \tau_4) - i(3\beta+4\mu)(\Omega \tau_4)} \sin(\Omega \tau_4) \right\}\end{aligned}$$

### 3.2. State $|b, 3\rangle$ .

$$\begin{aligned}C_{p+3hk_e}^b(t_4) &= \langle b, 3 | \hat{U}(t) | \psi(t_{3D}) \rangle \\ &= (-i) \int_{t_{3D}}^{t_4} dt' \langle b, 3 | \hat{V}(t') \hat{U}_0(t_{3D}, t') | \psi(t_{3D}) \rangle \\ &= (-i) \int_{t_{3D}}^{t_4} dt' \langle b, 3 | \hat{V}(t') | a, 2 \rangle \langle a, 2 | \hat{U}_0(t_{3D}, t') | \psi(t_{3D}) \rangle\end{aligned}$$

$$\begin{aligned}\langle b, 3 | \hat{V}(t') | a, 2 \rangle &= R_2^*(t') \\ &= \Omega_+ e^{2ik_e z_c(t') + 2i(\beta+4\mu)(\Omega t')}\end{aligned}$$

$$\begin{aligned}C_{p+3hk_e}^b(t_4) &= (-i)\Omega_+ \int_{t_{3D}}^{t_4} dt' e^{2ik_e z_c(t') + 2i(\beta+4\mu)(\Omega t')} \langle a, 2 | \hat{U}_0(t_{3D}, t') | \psi(t_{3D}) \rangle \\ &= (-i)\Omega_+^* e^{2ik_e z_c(v_0, t_{3D}) + 2i(\beta+4\mu)(\Omega t_{3D})} \int_0^{\tau_4} dt' e^{2ik_e z_c(v_0 + gt_{3D}, t') + 2i(\beta+4\mu)(\Omega t')} \langle a, 2 | \hat{U}_0(t' - t_{3D}) | \psi(t_{3D}) \rangle\end{aligned}$$

$$\langle a, 2 | \hat{U}_0(t' - t_{3D}) | \psi(t_{3D}) \rangle = e^{i\beta(\Omega t')} (-i)F_a^-(2, t_{3D}) \sin(\Omega t') C_{p+hk_e}^b(t_{3D}) + e^{i\beta(\Omega t')} \cos(\Omega t') C_{p+2hk_e}^a(t_{3D})$$

$$\begin{aligned}
C_p^a(t_4) &= (-i)\Omega_+^* e^{2ik_e z_c(v_0, t_{3D}) + 2i(\beta + 4\mu)(\Omega t_{3D})} \\
&\left\{ (-i)F_a^-(2, t_{3D})C_{p+\hbar k_e}^b(t_{3D}) \int_0^{\tau_4} dt' e^{2ik_e z_c(v_0 + gt_{3D}, t') + i(3\beta + 8\mu)(\Omega t')} \sin(\Omega t') \right. \\
&\left. + C_{p+2\hbar k_e}^a(t_{3D}) \int_0^{\tau_4} dt' e^{2ik_e z_c(v_0 + gt_{3D}, t') + i(3\beta + 8\mu)(\Omega t')} \cos(\Omega t') \right\}
\end{aligned}$$

$$\begin{aligned}
C_p^a(t_4) &= -\eta(t_4) e^{2ik_e z_c(v_0, t_{3D}) + 2i(\beta + 4\mu)(\Omega t_{3D})} \\
&\left\{ (-i)F_a^-(2, t_{3D})C_{p+\hbar k_e}^b(t_{3D}) e^{2ik_e z_c(v_0 + gt_{3D}, \tau_4) + i(3\beta + 8\mu)(\Omega \tau_4)} \sin(\Omega \tau_4) \right. \\
&\left. + C_{p+2\hbar k_e}^a(t_{3D}) \left[ e^{2ik_e z_c(v_0 + gt_{3D}, \tau_4) + i(3\beta + 8\mu)(\Omega \tau_4)} \cos(\Omega \tau_4) - 1 \right] \right\}
\end{aligned}$$

#### 4. Fifth Pulse.

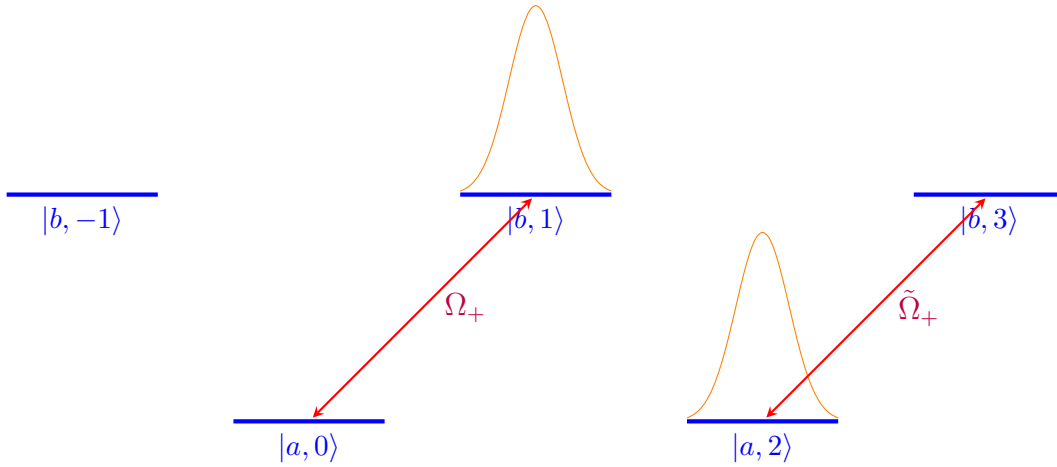


FIGURE C.7. Initial configuration of the probability amplitude of the states before the fifth pulse.



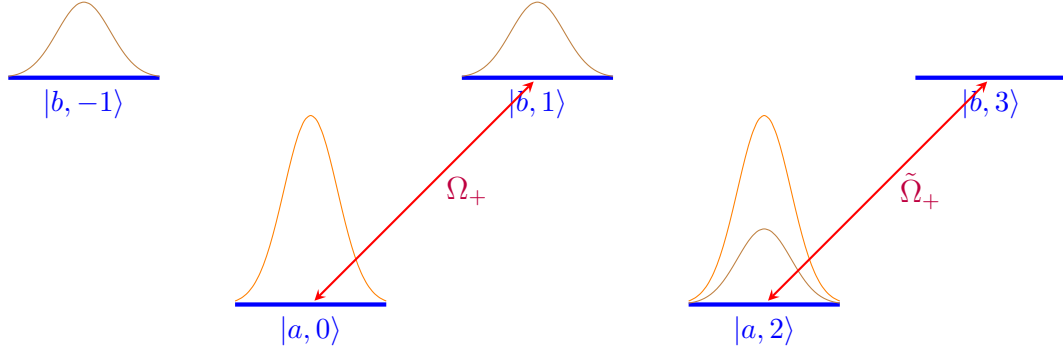


FIGURE C.8. Final configuration of the probability amplitude of the states after the fifth pulse.

#### 4.1. State $|b, -1\rangle$ .

$$\begin{aligned}
 C_{p-\hbar k_e}^b(t_5) &= \langle b, -1 | \hat{U}(t) | \psi(t_4) \rangle \\
 &= (-i) \int_{t_4}^{t_5} dt' \langle b, -1 | \hat{V}(t') \hat{U}_0(t') | \psi(t_4) \rangle \\
 &= (-i) \int_{t_4}^{t_5} dt' \langle b, -1 | \hat{V}(t') | a, 0 \rangle \langle a, 0 | \hat{U}_0(t_4, t') | \psi(t_4) \rangle
 \end{aligned}$$

$$\begin{aligned}
 \langle b, -1 | \hat{V}(t') | a, 0 \rangle &= L_{-2}^*(t') \\
 &= \Omega_- e^{-2ik_e z_c(t') - 2i\beta(\Omega t')}
 \end{aligned}$$

$$\begin{aligned}
 C_{p-\hbar k_e}^b(t_5) &= (-i) \Omega_- \int_{t_4}^{t_5} dt' e^{-2ik_e z_c(t') - 2i\beta(\Omega t')} \langle a, 0 | \hat{U}_0(t_4, t') | \psi(t_4) \rangle \\
 &= (-i) \Omega_- e^{-2ik_e z_c(v_0, t_4) - 2i\beta(\Omega t_4)} \int_0^{\tau_5} dt' e^{-2ik_e z_c(v_0 + gt_4, t') - 2i\beta(\Omega t')} \langle a, 0 | \hat{U}_0(t' - t_4) | \psi(t_4) \rangle
 \end{aligned}$$

$$\langle a, 0 | \hat{U}(t' - t_4) | \psi(t_4) \rangle = e^{-i\beta(\Omega t')} (-i) F_a^+(0, t_4) \sin(\Omega t') C_{p+\hbar k_e}^b(t_4)$$

$$\begin{aligned}
 C_{p-\hbar k_e}^b(t_5) &= -\Omega_- F_a^+(0, t_4) C_{p+\hbar k_e}^b(t_4) e^{-2ik_e z_c(v_0, t_4) - 2i\beta(\Omega t_4)} \\
 &\quad \int_0^{\tau_5} dt' e^{-2ik_e z_c(v_0 + gt_4, t') - 3i\beta(\Omega t')} \sin(\Omega t')
 \end{aligned}$$

$$\begin{aligned}
 C_{p-\hbar k_e}^b(t_5) &= (-i) \eta(t_5) F_a^+(0, t_4) C_{p+\hbar k_e}^b(t_4) e^{-2ik_e z_c(v_0, t_4) - 2i\beta(\Omega t_4)} \\
 &\quad e^{-2ik_e z_c(v_0 + gt_4, \tau_5) - 3i\beta(\Omega \tau_5)} \sin(\Omega \tau_5)
 \end{aligned}$$

**4.2. State  $|b, 1\rangle$ .**

$$\begin{aligned}
C_{p+\hbar k_e}^b(t_5) &= \langle b, 1 | \hat{U}(t) | \psi(t_4) \rangle \\
&= (-i) \int_{t_4}^{t_5} dt' \langle b, 1 | \hat{V}(t') \hat{U}_0(t') | \psi(t_4) \rangle \\
&= (-i) \int_{t_4}^{t_5} dt' \langle b, 1 | \hat{V}(t') | a, 2 \rangle \langle a, 2 | \hat{U}_0(t_4, t') | \psi(t_4) \rangle
\end{aligned}$$

$$\begin{aligned}
\langle b, 1 | \hat{V}(t') | a, 2 \rangle &= L_0^*(t') \\
&= \Omega_- e^{-2ik_e z_c(t') - 2i(\beta+2\mu)(\Omega t')}
\end{aligned}$$

$$\begin{aligned}
C_{p+\hbar k_e}^b(t_5) &= (-i) \Omega_- \int_{t_4}^{t_5} dt' e^{-2ik_e z_c(t') - 2i(\beta+2\mu)(\Omega t')} \langle a, 2 | \hat{U}_0(t_4, t') | \psi(t_4) \rangle \\
&= (-i) \Omega_- e^{-2ik_e z_c(v_0, t_4) - 2i(\beta+2\mu)(\Omega t_4)} \int_0^{\tau_5} dt' e^{-2ik_e z_c(v_0 + gt_4, t') - 2i(\beta+2\mu)(\Omega t')} \langle a, 2 | \hat{U}_0(t' - t_4) | \psi(t_4) \rangle
\end{aligned}$$

$$\begin{aligned}
\langle a, 2 | \hat{U}(t' - t_4) | \psi(t_4) \rangle &= e^{-i(\beta+2\mu)(\Omega t)} \\
&\left[ \cos\left(\Omega t' \sqrt{1 + (2\mu)^2}\right) + \frac{i(2\mu)}{\sqrt{1 + (2\mu)^2}} \sin\left(\Omega t' \sqrt{1 + (2\mu)^2}\right) \right] C_{p+2\hbar k_e}^a(t_4)
\end{aligned}$$

$$\begin{aligned}
C_{p+\hbar k_e}^b(t_5) &= (-i) \Omega_- C_{p+2\hbar k_e}^a(t_4) e^{-2ik_e z_c(v_0, t_4) - 2i(\beta+2\mu)(\Omega t_4)} \\
&\int_0^{\tau_5} dt' e^{-2ik_e z_c(v_0 + gt_4, t') - i(3\beta+6\mu)(\Omega t')} \left[ \cos\left(\Omega t' \sqrt{1 + (2\mu)^2}\right) + \frac{i(2\mu)}{\sqrt{1 + (2\mu)^2}} \sin\left(\Omega t' \sqrt{1 + (2\mu)^2}\right) \right]
\end{aligned}$$

$$\begin{aligned}
C_{p+\hbar k_e}^b(t_5) &= \eta(t_5) C_{p+2\hbar k_e}^a(t_4) e^{-2ik_e z_c(v_0, t_4) - 2i(\beta+2\mu)(\Omega t_4)} \\
&\left\{ e^{-2ik_e z_c(v_0 + gt_4, \tau_5) - i(3\beta+6\mu)(\Omega \tau_5)} \left[ \cos\left(\Omega \tau_5 \sqrt{1 + (2\mu)^2}\right) + \frac{i(2\mu)}{\sqrt{1 + (2\mu)^2}} \sin\left(\Omega \tau_5 \sqrt{1 + (2\mu)^2}\right) \right] - 1 \right\}
\end{aligned}$$

**4.3. State  $|a, 2\rangle$ .**

$$\begin{aligned}
C_{p+2\hbar k_e}^a(t_5) &= \langle a, 2 | \hat{U}(t) | \psi(t_4) \rangle \\
&= (-i) \int_{t_4}^{t_5} dt' \langle a, 2 | \hat{V}(t') \hat{U}_0(t') | \psi(t_4) \rangle \\
&= (-i) \int_{t_4}^{t_5} dt' \langle a, 2 | \hat{V}(t') | b, 1 \rangle \langle b, 1 | \hat{U}_0(t_4, t') | \psi(t_4) \rangle
\end{aligned}$$

$$\begin{aligned}
\langle a, 2 | \hat{V}(t') | b, 1 \rangle &= L_0(t') \\
&= \Omega_-^* e^{2ik_e z_c(t') + 2i(\beta+2\mu)(\Omega t')}
\end{aligned}$$

$$\begin{aligned}
C_{p+2\hbar k_e}^a(t_5) &= (-i)\Omega_-^* \int_{t_4}^{t_5} dt' e^{2ik_e z_c(t')} 2i(\beta+2\mu)(\Omega t') \langle b, 1 | \hat{U}_0(t_4, t') | \psi(t_4) \rangle \\
&= (-i)\Omega_-^* e^{2ik_e z_c(v_0, t_4) + 2i(\beta+2\mu)(\Omega t_4)} \int_0^{\tau_5} dt' e^{2ik_e z_c(v_0 + gt_4, t') + 2i(\beta+2\mu)(\Omega t')} \langle b, 1 | \hat{U}_0(t' - t_4) | \psi(t_4) \rangle
\end{aligned}$$

$$\langle b, 1 | \hat{U}(t' - t_4) | \psi(t_4) \rangle = e^{i\beta(\Omega t')} \cos(\Omega t') C_{p+\hbar k_e}^b(t_4)$$

$$\begin{aligned}
C_{p+2\hbar k_e}^b(t_5) &= (-i)\Omega_-^* C_{p+\hbar k_e}^b(t_4) e^{2ik_e z_c(v_0, t_4) + 2i(\beta+2\mu)(\Omega t_4)} \\
&\quad \int_0^{\tau_5} dt' e^{2ik_e z_c(v_0 + gt_4, t') + i(3\beta+4\mu)(\Omega t')} \cos(\Omega t')
\end{aligned}$$

$$\begin{aligned}
C_{p+2\hbar k_e}^b(t_5) &= -\eta(t_5) C_{p+\hbar k_e}^b(t_4) e^{2ik_e z_c(v_0, t_4) + 2i(\beta+2\mu)(\Omega t_4)} \\
&\quad \left[ e^{2ik_e z_c(v_0 + gt_4, \tau_5) + i(3\beta+4\mu)(\Omega \tau_5)} \cos(\Omega \tau_5) - 1 \right]
\end{aligned}$$

### 5. Sixth Pulse.

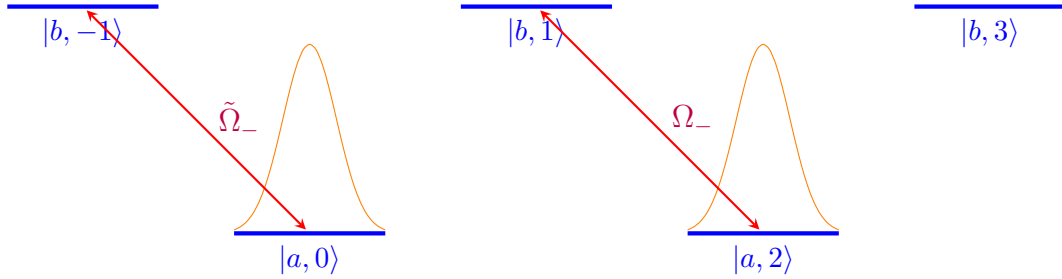


FIGURE C.9. Initial configuration of the probability amplitude of the states before the sixth pulse.

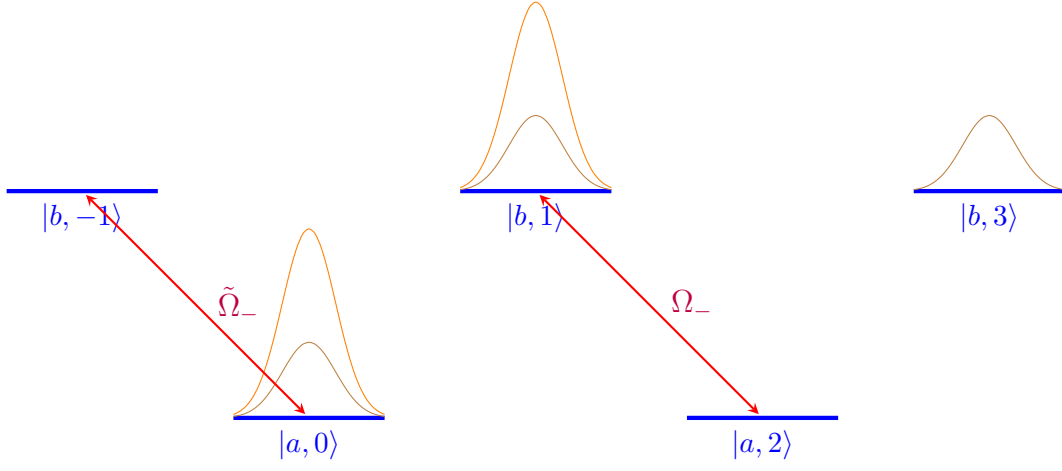


FIGURE C.10. Final configuration of the probability amplitude of the states after the sixth pulse.

### 5.1. State $|a, 0\rangle$ .

$$\begin{aligned}
 C_p^a(t_6) &= \langle a, 0 | \hat{U}(t) | \psi(t_5) \rangle \\
 &= (-i) \int_{t_5}^{t_6} dt' \langle a, 0 | \hat{V}(t') \hat{U}_0(t') | \psi(t_5) \rangle \\
 &= (-i) \int_{t_5}^{t_6} dt' \langle a, 0 | \hat{V}(t') | b, 1 \rangle \langle b, 1 | \hat{U}_0(t_5, t') | \psi(t_5) \rangle
 \end{aligned}$$

$$\begin{aligned}
 \langle a, 0 | \hat{V}(t') | b, 1 \rangle &= R_0(t') \\
 &= \Omega_+^* e^{-2ik_e z_c(t) - 2i(\beta + 2\mu)(\Omega t')}
 \end{aligned}$$

$$\begin{aligned}
 C_p^a(t_6) &= (-i) \Omega_+^* \int_{t_5}^{t_6} dt' e^{-2ik_e z_c(t') - 2i(\beta + 2\mu)(\Omega t')} \langle b, 1 | \hat{U}_0(t_5, t') | \psi(t_5) \rangle \\
 &= (-i) \Omega_+^* e^{-2ik_e z_c(v_0, t_{6A}) - 2i(\beta + 2\mu)(\Omega t_{6A})} \int_0^{\tau_6} dt' e^{-2ik_e z_c(v_0 + gt_{6A}, t') - 2i(\beta + 2\mu)(\Omega t')} \langle b, 1 | \hat{U}_0(t' - t_{6A}) | \psi(t_5) \rangle
 \end{aligned}$$

$$\langle b, 1 | \hat{U}_0(t' - t_{6A}) | \psi(t_5) \rangle = (-i) e^{-i\beta(\Omega t')} F_b^-(1, t_{6A}) \sin(\Omega t') C_{p+2hk_e}^a(t_5)$$

$$\begin{aligned}
 C_p^a(t_6) &= -\Omega_+^* F_b^-(1, t_{6A}) C_{p+2hk_e}^a(t_5) e^{-2ik_e z_c(v_0, t_{6A}) - 2i(\beta + 2\mu)(\Omega t_{6A})} \\
 &\quad \int_0^{\tau_6} dt' e^{-2ik_e z_c(v_0 + gt_{6A}, t') - i(3\beta + 4\mu)(\Omega t')} \sin(\Omega t')
 \end{aligned}$$

$$\begin{aligned}
 C_p^a(t_6) &= (-i) \eta(t_6) F_b^-(1, t_{6A}) C_{p+2hk_e}^a(t_5) e^{-2ik_e z_c(v_0, t_{6A}) - 2i(\beta + 2\mu)(\Omega t_{6A})} \\
 &\quad e^{-2ik_e z_c(v_0 + gt_{6A}, \tau_6) - i(3\beta + 4\mu)(\Omega \tau_6)} \sin(\Omega \tau_6)
 \end{aligned}$$

### 5.2. State $|b, 1\rangle$ .

$$\begin{aligned}
C_p^a(t_6) &= \langle b, 1 | \hat{U}(t) | \psi(t_5) \rangle \\
&= (-i) \int_{t_5}^{t_6} dt' \langle b, 1 | \hat{V}(t') \hat{U}_0(t') | \psi(t_5) \rangle \\
&= (-i) \int_{t_5}^{t_6} dt' \langle b, 1 | \hat{V}(t') | a, 0 \rangle \langle a, 0 | \hat{U}_0(t_5, t') | \psi(t_5) \rangle
\end{aligned}$$

$$\begin{aligned}
\langle b, 1 | \hat{V}(t') | a, 0 \rangle &= R_0^*(t') \\
&= \Omega_+ e^{2ik_e z_c(t) + 2i(\beta + 2\mu)(\Omega t')}
\end{aligned}$$

$$\begin{aligned}
C_p^a(t_6) &= (-i) \Omega_+ \int_{t_5}^{t_6} dt' e^{2ik_e z_c(t') + 2i(\beta + 2\mu)(\Omega t')} \langle a, 0 | \hat{U}_0(t_5, t') | \psi(t_5) \rangle \\
&= (-i) \Omega_+^* e^{2ik_e z_c(v_0, t_{6A}) + 2i(\beta + 2\mu)(\Omega t_{6A})} \int_0^{\tau_6} dt' e^{2ik_e z_c(v_0 + gt_{6A}, t') + 2i(\beta + 2\mu)(\Omega t')} \langle a, 0 | \hat{U}_0(t' - t_{6A}) | \psi(t_5) \rangle
\end{aligned}$$

$$\langle a, 0 | \hat{U}_0(t' - t_{6A}) | \psi(t_5) \rangle = e^{i(\beta - (2\mu))(\Omega t')} \left[ \cos \left( \Omega t' \sqrt{1 + (2\mu)^2} \right) + \frac{i(2\mu)}{\sqrt{1 + (2\mu)^2}} \sin \left[ \Omega t' \sqrt{1 + (2\mu)^2} \right] \right] C_p^a(t_5)$$

$$\begin{aligned}
C_p^a(t_6) &= (-i) \Omega_+ C_p^a(t_5) e^{2ik_e z_c(v_0, t_{6A}) + 2i(\beta + 2\mu)(\Omega t_{6A})} \\
&\int_0^{\tau_6} dt' e^{2ik_e z_c(v_0 + gt_{6A}, t') + i(3\beta + 2\mu)(\Omega t')} \left[ \cos \left( \Omega t' \sqrt{1 + (2\mu)^2} \right) + \frac{i(2\mu)}{\sqrt{1 + (2\mu)^2}} \sin \left[ \Omega t' \sqrt{1 + (2\mu)^2} \right] \right]
\end{aligned}$$

$$\begin{aligned}
C_p^a(t_6) &= -\eta(t_6) C_p^a(t_5) e^{2ik_e z_c(v_0, t_{6A}) + 2i(\beta + 2\mu)(\Omega t_{6A})} \\
&\left\{ e^{2ik_e z_c(v_0 + gt_{6A}, \tau_6) + i(3\beta + 2\mu)(\Omega \tau_6)} \left[ \cos \left( \Omega \tau_6 \sqrt{1 + (2\mu)^2} \right) + \frac{i(2\mu)}{\sqrt{1 + (2\mu)^2}} \sin \left[ \Omega \tau_6 \sqrt{1 + (2\mu)^2} \right] \right] - 1 \right\}
\end{aligned}$$

### 5.3. State $|b, 3\rangle$ .

$$\begin{aligned}
C_{p+3\hbar k_e}^b(t_6) &= \langle b, 3 | \hat{U}(t) | \psi(t_5) \rangle \\
&= (-i) \int_{t_5}^{t_6} dt' \langle b, 3 | \hat{V}(t') \hat{U}_0(t') | \psi(t_5) \rangle \\
&= (-i) \int_{t_5}^{t_6} dt' \langle b, 3 | \hat{V}(t') | a, 2 \rangle \langle a, 2 | \hat{U}_0(t_5, t') | \psi(t_5) \rangle
\end{aligned}$$

$$\begin{aligned}
\langle b, 3 | \hat{V}(t') | a, 2 \rangle &= R_2^*(t') \\
&= \Omega_+ e^{2ik_e z_c(t) + 2i(\beta + 4\mu)(\Omega t')}
\end{aligned}$$

$$\begin{aligned}
C_{p+3\hbar k_e}^b(t_6) &= (-i)\Omega_+^* \int_{t_5}^{t_6} dt' e^{2ik_e z_c(t') + 2i(\beta+4\mu)(\Omega t')} \langle a, 2 | \hat{U}_0(t_5, t') | \psi(t_5) \rangle \\
&= (-i)\Omega_+^* e^{2ik_e z_c(v_0, t_{6A}) + 2i(\beta+4\mu)(\Omega t_{6A})} \int_0^{\tau_6} dt' e^{2ik_e z_c(v_0 + gt_{6A}, t') + 2i(\beta+4\mu)(\Omega t')} \langle a, 2 | \hat{U}_0(t' - t_{6A}) | \psi(t_5) \rangle \\
&\quad \langle a, 2 | \hat{U}_0(t' - t_{6A}) | \psi(t_5) \rangle = e^{i\beta(\Omega t')} \cos(\Omega t') C_{p+2\hbar k_e}^a(t_5) \\
C_{p+3\hbar k_e}^b(t_6) &= (-i)\Omega_+^* C_{p+2\hbar k_e}^a(t_5) e^{2ik_e z_c(v_0, t_{6A}) + 2i(\beta+4\mu)(\Omega t_{6A})} \\
&\quad \int_0^{\tau_6} dt' e^{2ik_e z_c(v_0 + gt_{6A}, t') + i(3\beta+8\mu)(\Omega t')} \cos(\Omega t') \\
C_{p+3\hbar k_e}^b(t_6) &= -\eta(t_6) C_{p+2\hbar k_e}^a(t_5) e^{2ik_e z_c(v_0, t_{6A}) + 2i(\beta+4\mu)(\Omega t_{6A})} \\
&\quad \left[ e^{2ik_e z_c(v_0 + gt_{6A}, \tau_6) + i(3\beta+8\mu)(\Omega \tau_6)} \cos(\Omega \tau_6) - 1 \right]
\end{aligned}$$



## APPENDIX D

### The Second order coefficients.

#### 1. The $a_2^\beta$ coefficient.

The following expression is the second order coefficient for the  $\beta$  expansion of the probability  $|\langle a|\psi_F\rangle|^2$ . The red colored equation has the dominant terms.

$$\begin{aligned}
a_2^\beta &= (-1.46 + 7.10 \times 10^{-15}i) + 4.26 \times 10^{-14}(\Omega T) \\
&- 1.77 \times 10^{-15}(\Omega T)^2 + 0.45 \cos \left[ \frac{1}{2}k_e\gamma \left( T + \frac{3\pi}{4\Omega} \right)^2 \right] + \\
&(-5.32 \times 10^{-15} - 8.88 \times 10^{-16}(\Omega T)) \cos \left[ k_e \left( \gamma T^2 + \frac{33\pi^2\gamma}{32\Omega^2} + \frac{2\pi\gamma T}{\Omega} \right) \right] \\
&- 0.45 \cos \left[ k_e \left( \gamma T^2 + \frac{73\pi^2\gamma}{32\Omega^2} + \frac{3\pi\gamma T}{\Omega} \right) \right] - 1.96 \cos \left[ k_e \left( 2\gamma T^2 + \frac{95\pi^2\gamma}{32\Omega^2} + \frac{5\pi\gamma T}{\Omega} \right) \right] \\
&+(3.55 \times 10^{-14} + 1.77 \times 10^{-15}i)(\Omega T) \cos \left[ k_e \left( 2\gamma T^2 + \frac{95\pi^2\gamma}{32\Omega^2} + \frac{5\pi\gamma T}{\Omega} \right) \right] \\
&- 1.77 \times 10^{-15}(\Omega T)^2 \cos \left[ k_e \left( 2\gamma T^2 + \frac{95\pi^2\gamma}{32\Omega^2} + \frac{5\pi\gamma T}{\Omega} \right) \right] \\
&+ 0.5 \cos \left[ k_e \left( 4\gamma T^2 + \frac{161\pi^2\gamma}{32\Omega^2} + \frac{9\pi\gamma T}{\Omega} \right) \right] - (5.92 \times 10^{-17} \\
&- 1.04 \times 10^{-15}i) \cos \left[ k_e \left( 4\gamma T^2 + \frac{241\pi^2\gamma}{32\Omega^2} + \frac{11\pi\gamma T}{\Omega} \right) \right] \\
&- (1.32 \times 10^{-17} - 2.35 \times 10^{-16}i)(\Omega T) \cos \left[ k_e \left( 4\gamma T^2 + \frac{241\pi^2\gamma}{32\Omega^2} + \frac{11\pi\gamma T}{\Omega} \right) \right] \\
&- (3.31 \times 10^{-18} - 5.87 \times 10^{-17}i) \cos \left[ k_e \left( 7\gamma T^2 + \frac{369\pi^2\gamma}{32\Omega^2} + \frac{18\pi\gamma T}{\Omega} \right) \right] \\
&+ 0.5 \cos \left[ \frac{k_e\gamma (\pi^2 - 24\pi(\Omega T) - 16(\Omega T)^2)}{32\Omega^2} \right] + 0.45 \cos \left[ \frac{3k_e\gamma (3\pi^2 + 5\pi(\Omega T) + 2(\Omega T)^2)}{4\Omega^2} \right] \\
&+ 0.5 \cos \left[ \frac{k_e\gamma (8\pi^2 + 9\pi(\Omega T) + 2(\Omega T)^2)}{4\Omega^2} \right] - 5.32 \times 10^{-15} \cos \left[ \frac{k_e\gamma (4\pi^2 + 7\pi(\Omega T) + 3(\Omega T)^2)}{\Omega^2} \right] \\
&- 8.88 \times 10^{-16}(\Omega T) \cos \left[ \frac{k_e\gamma (4\pi^2 + 7\pi(\Omega T) + 3(\Omega T)^2)}{\Omega^2} \right]
\end{aligned}$$



$$\begin{aligned}
& -0.45 \cos \left[ \frac{k_e \gamma (\pi^2 + 6\pi(\Omega T) + 4(\Omega T)^2)}{4\Omega^2} \right] + 0.5 \cos \left[ \frac{k_e \gamma (12\pi^2 + 17\pi(\Omega T) + 6(\Omega T)^2)}{4\Omega^2} \right] \\
& - (3.31 \times 10^{-18} - 5.87 \times 10^{-17}i) \cos \left[ \frac{k_e \gamma (13\pi^2 + 18\pi(\Omega T) + 6(\Omega T)^2)}{2\Omega^2} \right] \\
& + 0.45 \cos \left[ \frac{k_e \gamma (13\pi^2 + 23\pi(\Omega T) + 10(\Omega T)^2)}{4\Omega^2} \right] - 0.45 \cos \left[ \frac{k_e \gamma (21\pi^2 + 32\pi(\Omega T) + 12(\Omega T)^2)}{4\Omega^2} \right] \\
& - (5.92 \times 10^{-17} - 1.04 \times 10^{-15}i) \cos \left[ \frac{k_e \gamma (21\pi^2 + 32\pi(\Omega T) + 12(\Omega T)^2)}{2\Omega^2} \right] \\
& - (1.32 \times 10^{-17} - 2.35 \times 10^{-16}i)(\Omega T) \cos \left[ \frac{k_e \gamma (21\pi^2 + 32\pi(\Omega T) + 12(\Omega T)^2)}{2\Omega^2} \right] \\
& + 0.45 \cos \left[ \frac{k_e \gamma (23\pi^2 + 40\pi(\Omega T) + 16(\Omega T)^2)}{32\Omega^2} \right] - 0.45 \cos \left[ \frac{k_e \gamma (87\pi^2 + 112\pi(\Omega T) + 32(\Omega T)^2)}{32\Omega^2} \right] \\
& + 0.5 \cos \left[ \frac{k_e \gamma (159\pi^2 + 232\pi(\Omega T) + 80(\Omega T)^2)}{32\Omega^2} \right] - 0.20 \sin \left[ \frac{1}{2} k_e \gamma \left( T + \frac{3\pi}{4\Omega} \right)^2 \right] \\
& - (3.77 \times 10^{-15} - 1.77 \times 10^{-15}i) \sin \left[ k_e \left( \gamma T^2 + \frac{33\pi^2 \gamma}{32\Omega^2} + \frac{2\pi \gamma T}{\Omega} \right) \right] \\
& + 2.61 \times 10^{-16}(\Omega T) \sin \left[ k_e \left( \gamma T^2 + \frac{33\pi^2 \gamma}{32\Omega^2} + \frac{2\pi \gamma T}{\Omega} \right) \right] \\
& + 0.20 \sin \left[ k_e \left( \gamma T^2 + \frac{73\pi^2 \gamma}{32\Omega^2} + \frac{3\pi \gamma T}{\Omega} \right) \right] \\
& - (7.10 \times 10^{-15} + 2.84 \times 10^{-14}i) \sin \left[ k_e \left( 2\gamma T^2 + \frac{95\pi^2 \gamma}{32\Omega^2} + \frac{5\pi \gamma T}{\Omega} \right) \right] \\
& + (8.88 \times 10^{-15} - 7.10 \times 10^{-15}i)(\Omega T) \sin \left[ k_e \left( 2\gamma T^2 + \frac{95\pi^2 \gamma}{32\Omega^2} + \frac{5\pi \gamma T}{\Omega} \right) \right] \\
& + 2.22 \times 10^{-16}(\Omega T)^2 \sin \left[ k_e \left( 2\gamma T^2 + \frac{95\pi^2 \gamma}{32\Omega^2} + \frac{5\pi \gamma T}{\Omega} \right) \right] \\
& + (1.04 \times 10^{-15} + 5.92 \times 10^{-17}i) \sin \left[ k_e \left( 4\gamma T^2 + \frac{241\pi^2 \gamma}{32\Omega^2} + \frac{11\pi \gamma T}{\Omega} \right) \right] \\
& + (2.35 \times 10^{-16} + 1.32 \times 10^{-17}i)(\Omega T) \sin \left[ k_e \left( 4\gamma T^2 + \frac{241\pi^2 \gamma}{32\Omega^2} + \frac{11\pi \gamma T}{\Omega} \right) \right] \\
& + (5.87 \times 10^{-17} + 3.31 \times 10^{-18}i) \sin \left[ k_e \left( 7\gamma T^2 + \frac{369\pi^2 \gamma}{32\Omega^2} + \frac{18\pi \gamma T}{\Omega} \right) \right] \\
& + 2.77 \times 10^{-17} \sin \left[ \frac{k_e \gamma (\pi^2 - 24\pi(\Omega T) - 16(\Omega T)^2)}{32\Omega^2} \right] \\
& - 0.20 \sin \left[ \frac{3k_e \gamma (3\pi^2 + 5\pi(\Omega T) + 2(\Omega T)^2)}{4\Omega^2} \right] + 1.39 \times 10^{-16} \sin \left[ \frac{k_e \gamma (8\pi^2 + 9\pi(\Omega T) + 2(\Omega T)^2)}{4\Omega^2} \right]
\end{aligned}$$

$$\begin{aligned}
& -(5.55 \times 10^{-15} + 1.77 \times 10^{-15}i) \sin \left[ \frac{k_e \gamma (4\pi^2 + 7\pi(\Omega T) + 3(\Omega T)^2)}{\Omega^2} \right] \\
& + 3.94 \times 10^{-17}(\Omega T) \sin \left[ \frac{k_e \gamma (4\pi^2 + 7\pi(\Omega T) + 3(\Omega T)^2)}{\Omega^2} \right] + 0.20 \sin \left[ \frac{k_e \gamma (\pi^2 + 6\pi(\Omega T) + 4(\Omega T)^2)}{4\Omega^2} \right] \\
& + 2.77 \times 10^{-17} \sin \left[ \frac{k_e \gamma (12\pi^2 + 17\pi(\Omega T) + 6(\Omega T)^2)}{4\Omega^2} \right] \\
& + (5.87 \times 10^{-17} + 3.31 \times 10^{-18}i) \sin \left[ \frac{k_e \gamma (13\pi^2 + 18\pi(\Omega T) + 6(\Omega T)^2)}{2\Omega^2} \right] \\
& - 0.20 \sin \left[ \frac{k_e \gamma (13\pi^2 + 23\pi(\Omega T) + 10(\Omega T)^2)}{4\Omega^2} \right] + 0.20 \sin \left[ \frac{k_e \gamma (21\pi^2 + 32\pi(\Omega T) + 12(\Omega T)^2)}{4\Omega^2} \right] \\
& + (1.04 \times 10^{-15} + 5.92 \times 10^{-17}i) \sin \left[ \frac{k_e \gamma (21\pi^2 + 32\pi(\Omega T) + 12(\Omega T)^2)}{2\Omega^2} \right] \\
& + (2.35 \times 10^{-16} + 1.32 \times 10^{-17}i)(\Omega T) \sin \left[ \frac{k_e \gamma (21\pi^2 + 32\pi(\Omega T) + 12(\Omega T)^2)}{2\Omega^2} \right] \\
& + 0.20 \sin \left[ \frac{k_e \gamma (23\pi^2 + 40\pi(\Omega T) + 16(\Omega T)^2)}{32\Omega^2} \right] - 0.20 \sin \left[ \frac{k_e \gamma (87\pi^2 + 112\pi(\Omega T) + 32(\Omega T)^2)}{32\Omega^2} \right] \\
& + 1.38 \times 10^{-16} \sin \left[ \frac{k_e \gamma (159\pi^2 + 232\pi(\Omega T) + 80(\Omega T)^2)}{32\Omega^2} \right]
\end{aligned}$$

$$\begin{aligned}
a_2^\beta \sim & -1.46 + 0.45 \cos \left[ \frac{1}{2} k_e \gamma \left( T + \frac{3\pi}{4\Omega} \right)^2 \right] - 0.45 \cos \left[ k_e \left( \gamma T^2 + \frac{73\pi^2 \gamma}{32\Omega^2} + \frac{3\pi \gamma T}{\Omega} \right) \right] \\
& - 1.96 \cos \left[ k_e \left( 2\gamma T^2 + \frac{95\pi^2 \gamma}{32\Omega^2} + \frac{5\pi \gamma T}{\Omega} \right) \right] + 0.5 \cos \left[ k_e \left( 4\gamma T^2 + \frac{161\pi^2 \gamma}{32\Omega^2} + \frac{9\pi \gamma T}{\Omega} \right) \right] \\
& + 0.5 \cos \left[ \frac{k_e \gamma (\pi^2 - 24\pi(\Omega T) - 16(\Omega T)^2)}{32\Omega^2} \right] + 0.45 \cos \left[ \frac{3k_e \gamma (3\pi^2 + 5\pi(\Omega T) + 2(\Omega T)^2)}{4\Omega^2} \right] \\
& + 0.5 \cos \left[ \frac{k_e \gamma (8\pi^2 + 9\pi(\Omega T) + 2(\Omega T)^2)}{4\Omega^2} \right] - 0.45 \cos \left[ \frac{k_e \gamma (\pi^2 + 6\pi(\Omega T) + 4(\Omega T)^2)}{4\Omega^2} \right] \\
& + 0.5 \cos \left[ \frac{k_e \gamma (12\pi^2 + 17\pi(\Omega T) + 6(\Omega T)^2)}{4\Omega^2} \right] \\
& + 0.45 \cos \left[ \frac{k_e \gamma (13\pi^2 + 23\pi(\Omega T) + 10(\Omega T)^2)}{4\Omega^2} \right] - 0.45 \cos \left[ \frac{k_e \gamma (21\pi^2 + 32\pi(\Omega T) + 12(\Omega T)^2)}{4\Omega^2} \right] \\
& + 0.45 \cos \left[ \frac{k_e \gamma (23\pi^2 + 40\pi(\Omega T) + 16(\Omega T)^2)}{32\Omega^2} \right] - 0.45 \cos \left[ \frac{k_e \gamma (87\pi^2 + 112\pi(\Omega T) + 32(\Omega T)^2)}{32\Omega^2} \right]
\end{aligned}$$

$$\begin{aligned}
& +0.5 \cos \left[ \frac{k_e \gamma (159\pi^2 + 232\pi(\Omega T) + 80(\Omega T)^2)}{32\Omega^2} \right] - 0.20 \sin \left[ \frac{1}{2} k_e \gamma \left( T + \frac{3\pi}{4\Omega} \right)^2 \right] \\
& +0.20 \sin \left[ k_e \left( \gamma T^2 + \frac{73\pi^2 \gamma}{32\Omega^2} + \frac{3\pi \gamma T}{\Omega} \right) \right] - 0.20 \sin \left[ \frac{3k_e \gamma (3\pi^2 + 5\pi(\Omega T) + 2(\Omega T)^2)}{4\Omega^2} \right] \\
& +0.20 \sin \left[ \frac{k_e \gamma (\pi^2 + 6\pi(\Omega T) + 4(\Omega T)^2)}{4\Omega^2} \right] - 0.20 \sin \left[ \frac{k_e \gamma (13\pi^2 + 23\pi(\Omega T) + 10(\Omega T)^2)}{4\Omega^2} \right] \\
& +0.20 \sin \left[ \frac{k_e \gamma (21\pi^2 + 32\pi(\Omega T) + 12(\Omega T)^2)}{4\Omega^2} \right] + 0.20 \sin \left[ \frac{k_e \gamma (23\pi^2 + 40\pi(\Omega T) + 16(\Omega T)^2)}{32\Omega^2} \right] \\
& -0.20 \sin \left[ \frac{k_e \gamma (87\pi^2 + 112\pi(\Omega T) + 32(\Omega T)^2)}{32\Omega^2} \right]
\end{aligned}$$

## 2. The $b_2^\beta$ coefficient.

The following expression is the second order coefficient for the  $\beta$  expansion of the probability  $|\langle b | \psi_F \rangle|^2$ . The red colored equation has the dominant terms.

$$\begin{aligned}
b_2^\beta &= -1.46 + 2.49 \times 10^{-14}(\Omega T) + 2.56 \times 10^{-16}(\Omega T)^2 + 0.45 \cos \left[ \frac{1}{2} k_e \gamma \left( T + \frac{3\pi}{4\Omega} \right)^2 \right] \\
& + (-1.77 \times 10^{-15} - 4.44 \times 10^{-16}(\Omega T)) \cos \left[ k_e \left( \gamma T^2 + \frac{33\pi^2 \gamma}{32\Omega^2} + \frac{2\pi T \gamma}{\Omega} \right) \right] \\
& - 0.45 \cos \left[ k_e \left( \gamma T^2 + \frac{73\pi^2 \gamma}{32\Omega^2} + \frac{3\pi T \gamma}{\Omega} \right) \right] + 1.96 \cos \left[ k_e \left( 2\gamma T^2 + \frac{95\pi^2 \gamma}{32\Omega^2} + \frac{5\pi T \gamma}{\Omega} \right) \right] \\
& - 2.49 \times 10^{-14}(\Omega T) \cos \left[ k_e \left( 2\gamma T^2 + \frac{95\pi^2 \gamma}{32\Omega^2} + \frac{5\pi T \gamma}{\Omega} \right) \right] \\
& - (2.56 \times 10^{-16} - 4.93 \times 10^{-32}i)(\Omega T)^2 \cos \left[ k_e \left( 2\gamma T^2 + \frac{95\pi^2 \gamma}{32\Omega^2} + \frac{5\pi T \gamma}{\Omega} \right) \right] \\
& - 0.5 \cos \left[ k_e \left( 4T^2 \gamma + \frac{161\pi^2 \gamma}{32\Omega^2} + \frac{9\pi T \gamma}{\Omega} \right) \right] - 0.5 \cos \left[ \frac{k_e \gamma (\pi^2 - 24\pi(\Omega T) - 16(\Omega T)^2)}{32\Omega^2} \right] \\
& - 0.45 \cos \left[ \frac{3k_e \gamma (3\pi^2 + 5\pi(\Omega T) + 2(\Omega T)^2)}{4\Omega^2} \right] + 0.5 \cos \left[ \frac{k_e \gamma (8\pi^2 + 9\pi(\Omega T) + 2(\Omega T)^2)}{4\Omega^2} \right] \\
& + 1.77 \times 10^{-15} \cos \left[ \frac{k_e \gamma (4\pi^2 + 7\pi(\Omega T) + 3(\Omega T)^2)}{\Omega^2} \right] \\
& + 4.44 \times 10^{-16}(\Omega T) \cos \left[ \frac{k_e \gamma (4\pi^2 + 7\pi(\Omega T) + 3(\Omega T)^2)}{\Omega^2} \right] \\
& + 0.45 \cos \left[ \frac{k_e \gamma (\pi^2 + 6\pi(\Omega T) + 4(\Omega T)^2)}{4\Omega^2} \right] + 0.5 \cos \left[ \frac{k_e \gamma (12\pi^2 + 17\pi(\Omega T) + 6(\Omega T)^2)}{4\Omega^2} \right]
\end{aligned}$$

$$\begin{aligned}
& -0.45 \cos \left[ \frac{k_e \gamma (13\pi^2 + 23\pi(\Omega T) + 10(\Omega T)^2)}{4\Omega^2} \right] + 0.45 \cos \left[ \frac{k_e \gamma (21\pi^2 + 32\pi(\Omega T) + 12(\Omega T)^2)}{4\Omega^2} \right] \\
& + 0.45 \cos \left[ \frac{k_e \gamma (23\pi^2 + 40\pi(\Omega T) + 16(\Omega T)^2)}{32\Omega^2} \right] - 0.45 \cos \left[ \frac{k_e \gamma (87\pi^2 + 112\pi(\Omega T) + 32(\Omega T)^2)}{32\Omega^2} \right] \\
& - 0.5 \cos \left[ \frac{k_e \gamma (159\pi^2 + 232\pi(\Omega T) + 80(\Omega T)^2)}{32\Omega^2} \right] - 0.20 \sin \left[ \frac{1}{2} k_e \gamma \left( T + \frac{3\pi}{4\Omega} \right)^2 \right] \\
& + 2.93 \times 10^{-15} \sin \left[ k_e \left( \gamma T^2 + \frac{33\pi^2 \gamma}{32\Omega^2} + \frac{2\pi T \gamma}{\Omega} \right) \right] + 5.83 \times 10^{-16} (\Omega T) \sin \left[ k_e \left( \gamma T^2 + \frac{33\pi^2 \gamma}{32\Omega^2} + \frac{2\pi T \gamma}{\Omega} \right) \right] \\
& + 0.20 \sin \left[ k_e \left( \gamma T^2 + \frac{73\pi^2 \gamma}{32\Omega^2} + \frac{3\pi T \gamma}{\Omega} \right) \right] + 6.93 \times 10^{-15} \sin \left[ k_e \left( 2\gamma T^2 + \frac{95\pi^2 \gamma}{32\Omega^2} + \frac{5\pi T \gamma}{\Omega} \right) \right] \\
& - (4.78 \times 10^{-15} + 1.57 \times 10^{-30} i) (\Omega T) \sin \left[ k_e \left( 2\gamma T^2 + \frac{95\pi^2 \gamma}{32\Omega^2} + \frac{5\pi T \gamma}{\Omega} \right) \right] \\
& - (6.33 \times 10^{-16} + 4.93 \times 10^{-32} i) (\Omega T)^2 \sin \left[ k_e \left( 2\gamma T^2 + \frac{95\pi^2 \gamma}{32\Omega^2} + \frac{5\pi T \gamma}{\Omega} \right) \right] \\
& + 8.32 \times 10^{-17} \sin \left[ k_e \left( 4\gamma T^2 + \frac{161\pi^2 \gamma}{32\Omega^2} + \frac{9\pi T \gamma}{\Omega} \right) \right] + 0.20 \sin \left[ \frac{3k_e \gamma (3\pi^2 + 5\pi(\Omega T) + 2(\Omega T)^2)}{4\Omega^2} \right] \\
& + 8.32 \times 10^{-17} \sin \left[ \frac{k_e \gamma (8\pi^2 + 9\pi(\Omega T) + 2(\Omega T)^2)}{4\Omega^2} \right] + 2.93 \times 10^{-15} \sin \left[ \frac{k_e \gamma (4\pi^2 + 7\pi(\Omega T) + 3(\Omega T)^2)}{\Omega^2} \right] \\
& + 1.38 \times 10^{-16} (\Omega T) \sin \left[ \frac{k_e \gamma (4\pi^2 + 7\pi(\Omega T) + 3(\Omega T)^2)}{\Omega^2} \right] - 0.20 \sin \left[ \frac{k_e \gamma (\pi^2 + 6\pi(\Omega T) + 4(\Omega T)^2)}{4\Omega^2} \right] \\
& + 2.77 \times 10^{-17} \sin \left[ \frac{k_e \gamma (12\pi^2 + 17\pi(\Omega T) + 6(\Omega T)^2)}{4\Omega^2} \right] \\
& + 0.20 \sin \left[ \frac{k_e \gamma (13\pi^2 + 23\pi(\Omega T) + 10(\Omega T)^2)}{4\Omega^2} \right] \\
& - 0.20 \sin \left[ \frac{k_e \gamma (21\pi^2 + 32\pi(\Omega T) + 12(\Omega T)^2)}{4\Omega^2} \right] + 2.77 \times 10^{-17} \sin \left[ \frac{k_e \gamma (-\pi^2 + 24\pi(\Omega T) + 16(\Omega T)^2)}{32\Omega^2} \right] \\
& + 0.20 \sin \left[ \frac{k_e \gamma (23\pi^2 + 40\pi(\Omega T) + 16(\Omega T)^2)}{32\Omega^2} \right] - 0.20 \sin \left[ \frac{k_e \gamma (87\pi^2 + 112\pi(\Omega T) + 32\Omega T^2)}{32\Omega^2} \right] \\
& - 8.32 \times 10^{-17} \sin \left[ \frac{k_e \gamma (159\pi^2 + 232\pi(\Omega T) + 80(\Omega T)^2)}{32\Omega^2} \right]
\end{aligned}$$

$$\begin{aligned}
b_2^\beta \sim & -1.46 + +0.45 \cos \left[ \frac{1}{2} k_e \gamma \left( T + \frac{3\pi}{4\Omega} \right)^2 \right] \\
& -0.45 \cos \left[ k_e \left( \gamma T^2 + \frac{73\pi^2 \gamma}{32\Omega^2} + \frac{3\pi T \gamma}{\Omega} \right) \right] + 1.96 \cos \left[ k_e \left( 2\gamma T^2 + \frac{95\pi^2 \gamma}{32\Omega^2} + \frac{5\pi T \gamma}{\Omega} \right) \right] \\
& -0.5 \cos \left[ k_e \left( 4T^2 \gamma + \frac{161\pi^2 \gamma}{32\Omega^2} + \frac{9\pi T \gamma}{\Omega} \right) \right] - 0.5 \cos \left[ \frac{k_e \gamma (\pi^2 - 24\pi(\Omega T) - 16(\Omega T)^2)}{32\Omega^2} \right] \\
& -0.45 \cos \left[ \frac{3k_e \gamma (3\pi^2 + 5\pi(\Omega T) + 2(\Omega T)^2)}{4\Omega^2} \right] + 0.5 \cos \left[ \frac{k_e \gamma (8\pi^2 + 9\pi(\Omega T) + 2(\Omega T)^2)}{4\Omega^2} \right] \\
& +0.45 \cos \left[ \frac{k_e \gamma (\pi^2 + 6\pi(\Omega T) + 4(\Omega T)^2)}{4\Omega^2} \right] + 0.5 \cos \left[ \frac{k_e \gamma (12\pi^2 + 17\pi(\Omega T) + 6(\Omega T)^2)}{4\Omega^2} \right] \\
& -0.45 \cos \left[ \frac{k_e \gamma (13\pi^2 + 23\pi(\Omega T) + 10(\Omega T)^2)}{4\Omega^2} \right] + 0.45 \cos \left[ \frac{k_e \gamma (21\pi^2 + 32\pi(\Omega T) + 12(\Omega T)^2)}{4\Omega^2} \right] \\
& +0.45 \cos \left[ \frac{k_e \gamma (23\pi^2 + 40\pi(\Omega T) + 16(\Omega T)^2)}{32\Omega^2} \right] - 0.45 \cos \left[ \frac{k_e \gamma (87\pi^2 + 112\pi(\Omega T) + 32(\Omega T)^2)}{32\Omega^2} \right] \\
& -0.5 \cos \left[ \frac{k_e \gamma (159\pi^2 + 232\pi(\Omega T) + 80(\Omega T)^2)}{32\Omega^2} \right] - 0.20 \sin \left[ \frac{1}{2} k_e \gamma \left( T + \frac{3\pi}{4\Omega} \right)^2 \right] \\
& +0.20 \sin \left[ k_e \left( \gamma T^2 + \frac{73\pi^2 \gamma}{32\Omega^2} + \frac{3\pi T \gamma}{\Omega} \right) \right] + 0.20 \sin \left[ \frac{3k_e \gamma (3\pi^2 + 5\pi(\Omega T) + 2(\Omega T)^2)}{4\Omega^2} \right] \\
& -0.20 \sin \left[ \frac{k_e \gamma (\pi^2 + 6\pi(\Omega T) + 4(\Omega T)^2)}{4\Omega^2} \right] + 0.20 \sin \left[ \frac{k_e \gamma (13\pi^2 + 23\pi(\Omega T) + 10(\Omega T)^2)}{4\Omega^2} \right] \\
& -0.20 \sin \left[ \frac{k_e \gamma (21\pi^2 + 32\pi(\Omega T) + 12(\Omega T)^2)}{4\Omega^2} \right] + 0.20 \sin \left[ \frac{k_e \gamma (23\pi^2 + 40\pi(\Omega T) + 16(\Omega T)^2)}{32\Omega^2} \right] \\
& -0.20 \sin \left[ \frac{k_e \gamma (87\pi^2 + 112\pi(\Omega T) + 32\Omega^2)}{32\Omega^2} \right]
\end{aligned}$$

## Bibliography

- [1] Lévèque T. Le Gouët J. Chaibi W. Canuel B. Clairon A. Pereira Dos Santos F. Landragin A. Gauguet A. Mehlstäubler. Off-resonant raman transition impact in an atom interferometer. *Phys. Rev. A*. **78**, 043615, 2008.
- [2] Carraz O. Charrière R. Cadoret M. Zahzam N. Bidet Y. Bresson A. Phase shift in an atom interferometer induced by the additional laser lines of a raman laser generated by modulation. *Physical Review A*, 2012.
- [3] Peters A. Chung K. Y. Chu S. High-precision gravity measurements using atom interferometry. *Metrologia* **38**, 25, 2001.
- [4] McGuirk J. M Foster G. T. Fixler J. B. Snadden M. J. Kasevich M. A. Sensitive absolute - gravity gradiometry using atom interferometry. *Phys. Rev. A* **65**, 033608, 2002.
- [5] Gustavson T. L. Landragin A. Kasevich M. A. Rotation sensing with a dual atom-interferometer sagnac gyroscope. *Class. Quantum Grav.* **17** 1, 2000.
- [6] Canuel B. Leduc F. Holleville D. Gauguet A. Fils J. Virdis A. Clairon A. Dimarcq N. Bordé Ch. J. Landragin A. Bouyer P. Six-axis inertial sensor using cold-atom interferometry. *Phys. Rev. Lett.* **97**, 010402, 2006.
- [7] Harms J. Whiting B. Bernard P. Clévéde E. Lognonne P. Montagner J.-P. Juhel K. Barsuglia M. Ampuero J. P. Chassandre-Mottin. Prompt gravity signal induced by the 2011 tohoku-oki earthquake. *Nat. Commun.* **7**, 13349, 2016.
- [8] Rosi G. D'Amico G. Cacciapuoti L. Sorrentino F. Prevedelli M. Zych M. Brukner C. Tino G. M. Quantum test of the equivalence principle for atoms in coherent superposition of internal energy states. *Nat. Commun.* 15529, 2017.
- [9] Berg P. Abend S. Tackmann G. Schubert C. Giese E. Schleich W. P. Narducci F. A. Ertmer W. Rasel E. M. Composite-light-pulse technique for high-precision atom interferometry. *Phys. Rev. Lett.* **114**, 063002, 2015.
- [10] V. Hamzeloui S. Gomez E. Arias, N. Abediyeh. Low phase noise beams for raman transitions with a phase modulator and a highly birefringent crystal. *Optics Express*, Vol. 25, No. 5, 2017.
- [11] D. A. Steck. *Quantum and Atom Optics*. <http://steck.us/teaching> (revisión 0.12.0), 2017.
- [12] H. Goldstein. *Classical Mechanics*. Addison - Wesley, 1980.
- [13] J.J. Sakurai. *Modern Quantum Mechanics*. Addison - Wesley, San Francisco, 2011.
- [14] P. R. Berman. *Atom Interferometry*. Academic Press, 1997.
- [15] L. Li R. Liu M. Zhan M. Wang, J. Zhou. Cold atom interferometers and their applications in precision measurements. *Front. Phys. China*, 4, 2009.
- [16] Berthold-Georg Englert Rui Han, Hui Khoon Ng. Raman transitions without adiabatic elimination: a simple and accurate treatment. *Journal of Modern Optics*, 60:4, 255-265, 2013.
- [17] V. S. Berman, P. R. Malinovsky. *Principles of Laser Spectroscopy and Quantum Optics*. Princeton University Press, 2011.
- [18] N. H. Asmar. *Partial Differential Equations with Fourier Series and Boundary Value Problems*. Pearson Prentice Hall, 2005.
- [19] P. Metcalf, H. J. van der Straten. *Laser Cooling and Trapping*. Springer Science, 1999.
- [20] E. Mandel, L. Wolf. *Optical Coherence and Quantum Optics*. Cambridge University press, 1995.
- [21] Ménoiret V. Vermeulen P. Le Moigne N. Bonvalot S. Bouyer P. Landragin A. Desruelle B. Gravity measurements below  $10^{-9}$  g with transportable absolute quantum gravimeter. *Scientific Reports*, 2018.
- [22] D. M. S. Kasevich M. A. Hogan, J. M. Johnson. Light-pulse atom interferometry. *arXiv:0806.3261v1*, 2008.
- [23] D. S. Kasevich M. Chu S. Moler, K. Weiss. Theoretical analysis of velocity-selective raman transitions. *Physical Review A*, 1992.